Modeling of Fluidized Bed Reactor for Bio Oil Production from Oil Palm Empty Fruit Bunch by Pyrolysis Process

Kyaw Thu

A Thesis Submitted in Fulfillment of the Requirements for the Degree of
Doctor of Philosophy in Chemical Engineering
Prince of Songkla University
2019

Copyright of Prince of Songkla University

Modeling of Fluidized Bed Reactor for Bio Oil Production from Oil Palm Empty Fruit Bunch by Pyrolysis Process

Kyaw Thu

A Thesis Submitted in Fulfillment of the Requirements for the Degree of
Doctor of Philosophy in Chemical Engineering
Prince of Songkla University
2019

Copyright of Prince of Songkla University

Thesis Title	Modeling of Fluidized Bed Reactor for Bio Oil Production from Oil Palm Empty Fruit Bunch by Pyrolysis Process
Author	Mr. Kyaw Thu
Major Program	Chemical Engineering

Major Advisor

……..
(Assoc. Prof. Dr. Chayanoot Sangwichien)

Co-Advisor

……
(Assoc. Prof. Dr. Taweesak Reungpeerakul)

Examining Committee:

……Chairperson
(Asst. Prof. Dr. Wipawee Khamwichit)

……...Committee
(Assoc. Prof. Dr. Chayanoot Sangwichien)

……...Committee
(Assoc. Prof. Dr. Taweesak Reungpeerakul)

……...Committee
(Assoc. Prof. Dr. Ram Yamsaengsung)

……...Committee
(Assoc. Prof. Dr. Supawan Tirawanichakul)

The Graduate School, Prince of Songkla University, has approved this thesis as fulfillment of the requirements for the Doctor of Philosophy Degree in Chemical Engineering.

..……...……

(Prof. Dr. Damrongsak Faroongsarng)
Dean of Graduate School

This is to certify that the work here submitted is the result of the candidate's own investigations. Due acknowledgement has been made of any assistance received.

……..……..Signature
(Assoc. Prof. Dr. Chayanoot Sangwichien)
Major Advisor

…….. Signature
(Mr. Kyaw Thu)
Candidate

I hereby certify that this work has not been accepted in substance for any degree, and is not being currently submitted in candidature for any degree.

…….Signature
(Mr. Kyaw Thu)
Candidate

Thesis Title	Modeling of Fluidized Bed Reactor for Bio Oil Production from Oil Palm Empty Fruit Bunch by Pyrolysis Process
Author	Mr. Kyaw Thu
Major Program	Chemical Engineering
Academic Year	2018

ABSTRACT

This present work aimed to study the modeling of bio oil production from the empty fruit bunch (EFB) biomass by fast pyrolysis. The heat diffusion equation and global chemical kinetic scheme were used to model the heat conduction along the radius of the empty fruit bunch particle and to predict yields of three products (bio oil, gas and char) over the EFB particle size range 150-500 μm at the reaction temperature range of 723-873 K. The heat transfer in solids and chemical reaction engineering module were chosen to predict the effects of reaction parameters by finite element based COMSOL Multiphysics 4.3b software. The results showed that the surface and center reaction temperatures of EFB particles gave a suitable reaction time across the particle sizes. The predicted pyrolysis product yields for various vapor residence times were compared with reported experiment yields. The simulations of heat transfer and product yield for fast pyrolysis of EFB were in a good agreement with reported experimental data.

ACKNOWLEDGEMENT

The completion of this thesis would be quite impossible without the help of many people. I wish to express my gratitude to those who had contribute it the completion of this thesis.

I would like to express the deepest appreciation to my advisor, Assoc. Prof. Dr. Chayanoot Sangwichien and my co-advisor, Assoc. Prof. Dr. Taweesak Reungpeerakul for their supervision, critical reading of manuscript, and tolerance helped in all the time of this thesis. Moreover, their advisory role is greatly acknowledged.

I would like to record specially thanks to Assoc. Prof. Dr. Ram Yamsaengsung, for his helpful comments and suggestions in second manuscript. I would like to extend thanks to the teachers from Chemical Engineering Department, for their help, valuable guidance, kindly permission and suggestion, through the preparation of this thesis. I also would like to thank to all staffs of Chemical Engineering Department for maintain friendly and cordial atmosphere.

I would like to acknowledge the financial support from the Higher Education Research Promotion and the Thailand's Education Hub for Southern Region of ASEAN Countries Project Office of the Higher Education Commission.

Finally, I would like to express my memorable pleasure and thanks to my parents and family for their moral support, patience, understanding and encouragement to attain my destination without any trouble and also would like to thank my classmates and friends who helped me towards the successful completion of this thesis.

Kyaw Thu

Contents

		Page
List of Tables		XI
List of Figures		XII
CHAPTER 1: Introduction		1
1.1	Background	1
1.2	Objectives	2
1.3	Scope of the study	3
1.4	Financial support	3
CHAPTER 2: Literature reviews		4
2.1	Oil palm biomass and its chemical compositions	4
2.1.1	Cellulose	4
2.1.2	Hemicellulose	4
2.1.3	Lignin	5
2.2	Waste products from oil palm mill	5
2.2.1	Empty fruit bunch biomass	5
2.3	Thermochemical conversion of oil palm biomass	6
2.3.1	Pyrolysis	6
2.3.1.1	Slow pyrolysis	6
2.3.1.2	Fast pyrolysis	7
2.3.1.3	Flash pyrolysis	7
2.4	Pyrolysis reactors	7
2.4.1	Fluidized bed reactor	8
2.4.1.1	Bubbling fluidized bed reactor	8
2.4.1.2	Circulating fluidized bed reactor	8
2.5	Reaction parameters	9
2.5.1	Feedstock size	9
2.5.2	Reaction temperature	10
2.5.3	Nitrogen flow rate	10

Contents (Continued)

		Page
2.6	Pyrolysis products	10
2.6.1	Biochar	11
2.6.2	Bio-oil	11
2.6.3	Pyrolysis gas	11
2.7	Reported experiment work for fast pyrolysis of EFB biomass	12
2.8	Previous modeling work for fast pyrolysis of biomass	13
CHAPTER 3:	Materials and methodology	31
3.1	Materials	31
3.1.1	Fluidizing gas	31
3.1.2	Fluidization particle	32
3.2	Heat transfer model	32
3.2.1	Minimum fluidization velocity (U_{mf})	33
3.2.2	Heat transfer coefficient (h)	34
3.2.3	Heat of reaction (ΔH)	35
3.3	Kinetics model of pyrolysis	36
3.3.1	One-stage single reaction model	36
3.3.2	One-stage multiple reaction model	37
3.3.3	Two-stage semi-global model	38
3.3.3.1	Simple kinetics model	38
3.3.3.2	Global kinetics model	39
3.3.3.3	Advanced kinetics model	42
3.4	Simulation model and parameters	43
3.5	COMSOL Multiphysics®	44
CHAPTER 4:	Results and discussion	45
4.1	Parameters estimation	45
4.2	Heat transfer model simulation	45
4.2.1	Effect of minimum fluidization velocity (U_{mf}) on heat transfer model	46
4.2.2	Effect of heat transfer coefficient (h) on heat transfer model	47

Contents (Continued)

	Page
4.2.3 Effect of particle size on heat transfer model	50
4.2.4 Effect of temperature and time on heat transfer model	52
4.3 Kinetics model simulation	54
4.3.1 Effect of reaction temperature on product yields	54
4.3.2 Effect of residence time on product yields	59
4.4 Model validation	61
CHAPTER 5: Conclusion	64
References	66
Appendix A: Parameters estimation for heat transfer model	73
Appendix B: Product yields at different reaction temperature (K) and various residence time (s)	92
Appendix C: Manuscript 1	100
Appendix D: Manuscript 2	118
VITAE	133

List of Tables

Table		Page
2.1.	The differences between bubbling and circulating fluidizing bed reactors	9
2.2.	Bio-oil production from oil palm solid wastes by fluidized bed pyrolysis reactor	14
2.3.	Reported modeling work for various biomass fast pyrolysis	24
3.1.	Properties of nitrogen gas at different temperature (Erik et al., 2012)	32
3.2.	Four correlations proposed for ranges of sand particle diameters (d_s) and densities (ρ_s)	34
3.3.	Two types of correlation for heat transfer coefficient (h) calculation	35
3.4.	Energy required for thermal decomposition of EFB biomass (Asadieraghi et al., 2015)	36
3.5.	Simple kinetics model parameters for fast pyrolysis of lignocellulose biomass	39
3.6.	Kinetics parameters for fast EFB pyrolysis (Diebold, 1994, Miller et al., 1996)	41
3.7.	Simulation parameters	43
4.1.	Estimated U_{mf} by four correlations at 723-873 K	46
4.2.	Estimated heat transfer coefficient (h) at 773 K	48
4.3.	Product yields at temperature 723 K	58
4.4.	Comparison between reported experimental and simulated product yields at the vapor residence time range of 0.79-1.32 s and at the reaction temperature of 773 K	63

List of Figures

Figure		Page
3.1.	Parallel reaction model for biomass pyrolysis	38
3.2.	A simple model for biomass fast pyrolysis	39
3.3.	A global kinetics model for fast pyrolysis of (a) cellulose, (b) hemicellulose and (c) lignin	42
4.1.	Relationship between (a) Re_{mf} vs Ar and (b) U_{mf} vs Temperature	47
4.2.	Effect of heat transfer coefficient on particle size in range of 150-500 μm at temperature in the range 723-873 K with different U_{mf}	49
4.3.	Particle size effect on EFB fast pyrolysis at 723 K and at 1.03 s	51
4.4.	Particle size effect on EFB fast pyrolysis at 773 K and at 1.32 s	51
4.5.	Particle size effect on EFB fast pyrolysis at 873 K and at 1.05 s	52
4.6.	Temperature profiles for particle size in the range of 150-500 μm	53
4.7.	Temperature profiles for particle size in the range of 300-355 μm	54
4.8.	Temperature profiles for particle size in the range of 250-355 μm	54
4.9.	Simulated product compositions of EFB biomass fast pyrolysis at the temperature in the range of 723-873 K and residence time range of 0.2-5 s	56

List of Figures (Continued)

Figure		Page
4.10.	Simulated product yields of EFB biomass fast pyrolysis at the temperature in the range of 723-873 K and residence time range of 0.2-5 s	58
4.11.	Simulated product yields of EFB biomass fast pyrolysis at residence time (a) 0.5 s, (b) 1 s and (c) 2 s at the temperature in the range 723-823 K	59
4.12.	Liquid yield on EFB fast pyrolysis at vapor residence time in the range (a) 0.5-1 s, (b) 1-2 s and (c) 0.5-2 s with temperature range of 723-823 K	61
4.13.	Validation between reported experimental and simulated product yields of (a) liquid, (b) char and (c) gas	62

CHAPTER 1
Introduction

1.1 Background

Palm oil is the most widely cultivated as a source of oil around the world. The world largest cultivation of palm oil is found in the South East Asia countries. Indonesia and Malaysia are first and second largest palm oil plantation accounting for both 70% of the world. Thailand is the world's third-largest country of palm oil plantation. Palm oil plantation is more economic than other trees such as rubber, rice, and popcorn. According to this fact, the increments of palm oil cultivated areas in Thailand have been seen 9% annually over the past decade. The southern part of Thailand is major palm oil plantation areas in the past because of suitable climate. As a result, the amplification of the palm oil industry in Thailand is continuously developing because of not only the consumption of edible oil but also renewable energy production (Silalertruksa et al., 2016).

Renewable energy technologies are friendly with the environment. In the past century, most of the energy is produced from fossil fuels. However, the world energy production from fossil fuel will decline in the past decade. Renewable energy obtained from biomass developed around the world in recent years. In Thailand, most of the renewable energy is produced from biomass and then followed by biogas, solar, municipal solid waste and wind, respectively. Oil palm waste from oil palm mill are chosen as a main source of biomass for production of the renewable energy. In oil palm mills, the two major types of wastes are produced as the solid and liquid wastes. The several forms of solid wastes from the oil palm mills are empty fruit bunches (EFB), palm press fiber (PPF), palm kernel shell (PKS), palm kernel cake (PKC) and sludge cake (SC). Palm oil mill effluent (POME) is the main liquid waste in oil palm mills. The huge amount of both solid and liquid wastes is produced in oil palm mills. In addition, solid wastes are found as the main byproducts of the oil palm mills (Prasentsan et al., 1996).

The large quantity of empty fruit bunch is produced as a by-product in oil palm mills in the Southern Thailand. In the past, solid wastes from palm oil mills are disposed by the landfilling method, which is very difficult to store and costly to

manage. In some factories, these wastes are burnt in the furnaces, which causes air pollution. The conversion of wastes into renewable energy is an effective way to solve this problem. Empty fruit bunches can be converted into using renewable energy. The main two way of biomass into useful alternative energy conversion is the biochemical and thermochemical process. In the thermochemical route, the pyrolysis process takes place in the inert atmosphere. Pyrolysis is the popular thermochemical process for liquid fuel production from biomass. On the other hand, pyrolysis reactors are also mainly played in bio-oil production from biomass. Fluidized bed reactors are widely used in liquid (bio-oil) production from fast pyrolysis of various biomass. The main three products of empty fruit bunch pyrolysis are gas, liquid, and char.

In the last decades, many simulation tools have been widely used to study for reactor design of fast pyrolysis of biomass. Papadikis et al., (2009a, 2009b, 2010) studied the fast pyrolysis of different biomass to predict the pyrolysis product yields using computing fluid dynamics (CFD) with Euler-Euler model in Fluent software. Mabrouki et al., (2015) studied for optimization of the liquid product yields from palm oil residues by fast pyrolysis using SuperPro Designer (SPD) software. Humbird et al., (2017) simulated to optimize the pyrolysis product yields on fast pyrolysis of three biomass (softwood, corn stover, and switchgrass) by Aspen plus process simulation tool. In this research studies the effects of reaction parameters on bio-oil production from EFB biomass by fast pyrolysis in fluidized bed reactor by finite element based COMSOL Multiphysics 4.3b software.

1.2 Objectives

To study one-dimension model of bubbling fluidized bed reactor modeling.

To study the effects of reaction parameters of bubbling fluidized bed reactor modeling for bio-oil production from oil palm empty fruit bunch (OPEFB) using pyrolysis process.

1.3 Scope of the study

Scope1: To simulate heat transfer model and study the effects of minimum fluidization velocity, heat transfer coefficient, particle size, reaction temperature and reaction time parameters on particle heat transfer.

Scope2: To simulate reaction kinetics model and study the effects of reaction temperature and vapor residence time parameters on product yields.

1.4 Financial support

The authors acknowledge the financial support from the Higher Education Research Promotion and the Thailand's Education Hub for Southern Region of Asean Countries Project Office of the Higher Education Commission.

CHAPTER 2

Literature reviews

2.1 Oil palm biomass and its chemical compositions

Biomass is a type of hydrocarbon material which mainly composed of hydrogen, carbon, oxygen, and nitrogen according to Yaman et al., (2004). The two main sources of solid palm oil biomass wastes production are plantations and the extraction mills. The wastes in the oil palm plantations are fronts and trunks. The wastes in the palm oil extraction mills are empty fruit bunch, mesocarp fiber and the kernel shell. In the palm oil mill, 90% biomass is discarded as wastes. The oil palm biomass is a source of raw material for renewable energy production. It can be considered not only as a clean source of energy but also as very sustainable for the environment. The major chemical compositions of oil palm biomass are cellulose, hemicellulose, and lignin (Basu, 2004).

2.1.1 Cellulose

The primary structural component of cell walls in biomass is cellulose that is the most common organic compound on Earth. The generic formula of cellulose is $(C_6H_{10}O_5)_n$ and has a long chain polymer with a high degree of polymerization (~10,000) and a large molecular weight (~500,000). Many glucose molecules of cellulose are produced according to a crystalline structure of thousands of units. Cellulose is primarily composed of d-glucose, which is made of six carbons or hexose sugars. Cellulose is not digestible by humans because of highly insoluble and, though a carbohydrate (Basu, 2004).

2.1.2 Hemicellulose

The main another component of the cell walls in biomass is hemicellulose. The structure of hemicellulose is random, amorphous form with little strength. Hemicellulose has carbohydrates branched chain structure and a lower DP (degree of polymerization). The generic formula of hemicellulose is $(C_5H_8O_4)_n$. The constituents of hemicelluloses are d-xylose, d-glucose, d-galactose, l-ababinose, d-glucurnoic acid, and d-mannose. The branched structures of these constituents in hemicellulose contain 50 to 200 units. According to the including these constituents,

hemicellulose tends to yield more gases and less tar than cellulose in pyrolysis process (Basu, 2004).

2.1.3 Lignin

The secondary structural component of cell walls in biomass is lignin which is a complex highly branched polymer of phenylpropane. The primary polymer of lignin is 4-propenyl phenol, 4-propenyl-2-methoxy phenol, and 4-propenyl-2.5-dimethoxyl phenol and has a three-dimensional structure. Lignin is the hard-cellulose fibers because of benzene rings structure of monomeric units in the polymers. The primarily composed of lignin glued together with adjacent cells or tracheids by the middle lamella. The special feature of Lignin is not insoluble in acid (Basu, 2004).

2.2 Waste products from oil palm mill

The two main types of wastes products in oil palm mill are liquid effluent and solid wastes. In palm oil mill effluent, liquid wastes consist of a mixture of condensate from bunch sterilizing, sludge from clarification centrifuges and water from the hydro-cyclone. The other main waste from oil palm mill is solid wastes. The solid wastes of oil palm mill are empty fruit bunch, decenter cake, solids from effluent ponds, surplus shell, and fiber. Among these solid wastes, the main waste is empty fruit bunch which is the largest amount produced in oil palm mill annually.

2.2.1 Empty fruit bunch biomass

In oil palm mill, the main solid wastes component is the empty fruit bunch. The empty fruit bunches are incinerated for production of its ash which is organic fertilizer in furnaces. But this process causes the air pollution problem. According to the increased of energy demand, empty fruit bunch can be considered as an energy source for production of renewable energy which is environmentally friendly. Empty fruit bunch can be used to produce renewable energy by using thermochemical combustion technologies. The pretreatment process is required to prepare the EFB for efficient combustion.

2.3 Thermochemical conversion of oil palm biomass

The three types of thermochemical conversion are direct combustion, gasification, and pyrolysis (Basu, 2004). The simplest and oldest method is combustion in which biomass can be applied for energy. In palm oil mills, oil palm kernel shell and fibers are ordinarily used to fuel for production of their electricity and steam demand by burning these wastes. Gasification is an indirect combustion process of carbonaceous material which is take place at the higher reaction temperature in the range from 1073 K to 2073 K. All solid wastes from oil palm plantations (such as oil palm trunk, palm kernel shell, empty fruit bunches, mesocarp fiber, and oil palm fiber) can be used to produce energy and hydrogen gas in the gasification process. Finally, pyrolysis is thermal degradation of biomass at an ambient pressure and at the reaction temperature range of 673-873 K that occurs in the inert atmosphere. The main three pyrolysis products are fuel gas, bio-oil, and charcoal. Empty fruit bunch solid wastes from oil palm plantations can be used to produce bio-oil in pyrolysis process.

2.3.1 Pyrolysis

Pyrolysis is a thermochemical process which takes place in the absence of oxygen. It has similar properties like cracking, devolatilization, carbonization, dry distillation, destructive distillation, and thermolysis, but it has different properties with the gasification process. Biomass degraded into gas, liquid, and char products during pyrolysis. The main three types of pyrolysis can be classified according to the operating condition such as slow (conventional), fast and flash pyrolysis (Basu, 2004). The nitrogen flow rate, reaction temperature, heating rate, residence time and particle size are important parameters on the reaction conditions in the pyrolysis process. Reactor types are also mainly role in the pyrolysis process. There are many types of pyrolysis reactor (such as a fixed bed reactor, fluidized bed reactor, microwave reactor and so on) are used to produce renewable energy production.

2.3.1.1 Slow pyrolysis

Slow (conventional) pyrolysis is used to produce of char at low temperatures and low heating rates for a primary goal at thousands of years ago. In this process, the feedstock biomass is heated slowly in the inert atmosphere to a relatively

low temperature (~673 K) over the vapor residence time is too high (5 min to 30 min). Slow pyrolysis involves all three types of pyrolysis product (gas, liquid, and char) but the main goal product of this type is char (Basu, 2004). According to the low temperature and high residence time, condensable vapor can be converted into char and non-condensable gases because of adequate time of reaction. In addition, high residence time and low heat transfer cause the demand for extra energy input.

2.3.1.2 Fast pyrolysis

The principal purpose of fast pyrolysis is to maximize the production of liquid or bio-oil. In the fast pyrolysis process, biomass is rapidly heated to a high temperature within the range of 698 to 873 K in the absence of oxygen. Depending on the using of feedstock, fast pyrolysis typically produces in the ranges of 60–75 wt.% of oily products (oil and other liquids), 15–25 wt.% of solids (mainly biochar) and 10–20 wt.% of gaseous products, respectively (Basu, 2004). The main parameters of the fast pyrolysis process are high heating rate, very short vapor residence time, rapid quenching of vapors and reaction temperature.

2.3.1.3 Flash pyrolysis

The basic characteristic of flash pyrolysis biomass is heated rapidly in an inert atmosphere at high reaction temperatures range over 723-1723 K and very short vapor residence time (less than 1 s) to produce condensable and non-condensable gas (Basu, 2004). The condensable vapor is then condensed into a liquid fuel in cooling step. According to this result, flash pyrolysis causes the reducing of char products. In this process, biomass can be converted up to 75% of the bio-oil yield of the total pyrolysis.

2.4 Pyrolysis reactors

The reactor is very important for any pyrolysis process because it can improve the essential characteristics of operating parameters. With the improvement of pyrolysis technology, several reactor designs have been developed to optimize the pyrolysis performance and to produce high-quality bio-oil. In the pyrolysis process, reactor types are classified according to their specific characteristics, bio-oil yielding

capacity, advantages, and limitations. Based on the gas-solid contacting mode, the most popular fluidized-bed reactors are described in the following sub-sections.

2.4.1 Fluidized bed reactor

The basic feature of the fluidized-bed reactor consists of a fluid-solid mixture that acts turbulent flow of solid particulate substance by the introducing of pressurized fluid from the bottom of the reactor. Fluidized-bed reactors come to be popular reactor type for fast pyrolysis process because they have many benefits such as speedy heat transfer, good control for reaction parameters, and high contact surface area between fluid and solid per unit bed volume (Lv et al., 2004). The main two types of fluidized bed reactor are bubbling and circulating fluidized bed reactor. The advantages of these two types of reactor are shown in Table 2.1.

2.4.1.1 Bubbling fluidized bed reactor

Bubbling fluidized beds are relatively easy to scale up and operate. The main characteristics of bubbling fluidized-beds are good heat transfer, better control for pyrolysis temperature, good solids-to-gas contact and storage capacity. Biomass is fed into a bubbling bed of hot sand which is fluidized materials. This hot sand rapidly heats the biomass in a absent oxygen environment, where it is decomposed into pyrolytic products (liquid, char, and gas). The char products are removed from reactor by using a cyclone separator and stored after the pyrolytic reaction. The condensable vapors are rapidly quenched and condensed into liquid (bio-oil) products and stored. The non-condensable vapors are collected into gas bubble. Bubbling fluidized-bed pyrolysis reactor is very popular due to yield of high-quality liquid (bio-oil) products (Jahirul et al., 2012).

.

2.4.1.2 Circulating fluidized-bed reactor

Circulating fluidized-beds have the same principle as the bubbling fluidized-bed reactors except for shorter residence times for chars and vapors. The major advantages of circulating fluidized bed reactor is easily separated and burnt the char products from the reactor in an external fluidized bed. The main two types of circulating fluidized bed reactors are single circulating and double circulating reactors (Jahirul et al., 2012).

Table 2.1. The differences between bubbling and circulating fluidizing bed reactors

Bubbling Fluidizing Bed reactor	Circulating Fluidizing Bed reactor
Larger particle size	Small particle size
Lower heating value fuels	High temperature
Better temperature control	Thermal inertia
Better Solids-to-gas contact	Shorter residence times for chars and vapors
Better Heat transfer and storage capacity	Easy separation of char entrained from the reactor
High solid density in the bed	Burning of char in an external fluidized bed

2.5 Reaction parameters

Reaction parameters of the reactor design modeling are studied for optimum reaction conditions of EFB by pyrolysis on bio-oil production. The following reaction parameters such as feedstock size, reaction temperature, heating rate, and nitrogen rate are needed to study for prediction of the optimum reactor design of EFB pyrolysis process.

2.5.1 Feedstock size

The size of feedstock has an influence on the product yields of biomass pyrolysis. Small particle sizes offer less resistance to the escape of condensable gases, which causes the minimize of the secondary reaction. But large particle sizes facilitate secondary reactions formation due to the higher resistance. The range of EFB particle sizes in literature used from <150 μm to 500 μm (Abdullah et al., 2008).

2.5.2 Reaction temperature

During pyrolysis, reaction temperature affects not only composition but also yield of the product. The release of various vapor products is changed with different temperatures in the biomass pyrolysis. High reaction temperature prefers to the bio-oil production. Low temperatures intend to obtain more char yield. In literature,

the reaction temperature for bio-oil production of fast pyrolysis used in the range from 673-873 K (Abdullah et al., 2008).

2.5.3 Nitrogen flow rate

The nitrogen flow rate effects the product of pyrolysis product. Slower nitrogen flowrate offers the higher liquid yield, while rapid nitrogen flowrate causes the higher char yield. Mohamed et al., (2013) studied that the effect of various nitrogen flow rates (150, 200, 300, 400 and 500 cm^3/min) for bio-oil production using fixed bed pyrolysis reactor. Ngo et al., (2013) studied that using fluidized bed reactor with nitrogen flowrate from 10 to 15 L/min to produce bio-oil.

2.6 Pyrolysis products

The main three pyrolysis products are solid (mostly char or carbon), liquid (tars, heavier hydrocarbons, and water) and gas (CO_2, H_2O, CO, C_2H_2, C_2H_4, C_2H_6, C_6H_6, etc.). Char, permanent gases, and bio-oil with dark brown viscous liquid are the three primary products from biomass pyrolysis. The maximum yield of desirable products from biomass pyrolysis depend on the reaction parameters. The low temperature and low heating rate pyrolysis process cause the maximum yield of charcoal. The maximum liquid production occurs at high temperature, high heating rate and short gas residence time in the pyrolysis process. High temperature, low heating rate, and long gas residence time pyrolysis process led to the maximum fuel gas production. The water content in the biomass also mainly point for biomass pyrolysis because it produces a high amount of condensate water in the liquid phase (Demirbas et al., 2000).

2.6.1 Biochar

The solid product of biomass pyrolysis is biochar which highly carbonaceous material. The advantages of biochar from biomass pyrolysis are efficient transportation and storage, and flexible in production and marketing. Biochar is mainly used as an alternative energy source in the agricultural industry for carbon sequestration in soils, enhancement of water holding capacity, improvement of soil quality, and nutrient retention. It is to be used as an alternative fuel source because of high carbon

content and low sulfur content. According to the containing over 60% moisture, and lower lignin content of raw empty fruit bunch, a small amount of carbon can be retained in EFB pyrolysis as compared to another woody biomass. Equation (2.1) described the char production obtained during pyrolysis reaction on a weight basis.

$$\text{Char yield} = \frac{\text{mass of char (g)}}{\text{mass of EFB (g)}} \times 100\% \quad (2.1)$$

2.6.2 Bio-oil

The liquid product of pyrolysis is bio-oil which is produced from the condensation of vapor of a pyrolysis reaction by cooling. The bio-oils can be used to substitute for fuel oil because it has heating values of 40%–50% of that of hydrocarbon fuels. The bio-oils are composed of a complex mixture of oxygenated compounds and it consists of various chemical functional groups such as carbonyls; carboxyls and phenolics. Pyrolysis oil contains about 300 to 400 compounds. The bio-oil production obtained during pyrolysis reaction on a weight basis can be calculated by equation (2.2).

$$\text{Bio-oil yield} = \frac{\text{mass of oil (g)}}{\text{mass of EFB (g)}} \times 100\% \quad (2.2)$$

2.6.3 Pyrolysis gas

In pyrolysis, primary decomposition of raw material produces both condensable gases (vapor) and non-condensable gases (primary gas). The condensable gases, which are made of heavier molecules, condense upon cooling, converting to the liquid yield of pyrolysis. Lower-molecular-weight gases such as carbon dioxide, carbon monoxide, methane, ethane, and ethylene are a mixture of non-condensable gases of the pyrolysis process. Secondary non-condensable gases are produced through secondary cracking of the vapor because of the long residence time of pyrolysis process. Non-condensable gases can be passed to the cooling zone. Therefore, the final non-condensable gas product is thus a mixture of both primary and secondary gases. Equation (2.3) shows the gas production obtained during pyrolysis reaction on a weight basis.

Gas yield = 100% – bio-oil yield – char yield (2.3)

2.7 Reported experiment work for fast pyrolysis of EFB biomass

Many authors have been studied the biofuel energy production from fast pyrolysis of empty fruit bunch biomass in fluidized bed reactor. Sulaiman et al., (2011) have studied to maximize for liquids yield from EFB fast pyrolysis using different particle sizes (less than 150 μm, 150-250 μm, 250-300 μm, 355-500 μm) were pyrolyzed in a bench scale fluidized bed system at 723 K reactor temperature and at 1.03 s residence time. Sembiring et al., (2015) worked the empty fruit bunch particle size of 210 μm for highest bio-oil yield at an optimum pyrolysis temperature of 773 K. Kim et al., (2013) studied the average biomass size of 700 μm for the production of pyrolysis oil from Jatropha seed shell cake (JSC), palm kernel shell (PKS) and empty palm fruit bunches (EFB) wastes. Abdullah et al., (2008) studied the maximum pyrolytic liquid and char at the reactor temperature range from 673 to 873 K and vapor residence time of 1.02–1.05 s by using EFB particle size of 250-355 μm. The maximum liquid yields from washed and unwashed EFB was studied using a particle size of 355–500 μm at the reactor temperature range from 698 K to 823 K and vapor residence time of 1.01–1.04 s by Abdullah et al., (2006). According to the above facts, particle size, reaction temperature and time are important parameters on heat transfer mechanisms on EFB biomass fast pyrolysis. Table 2.2 shows the experiment literature reviews for bio-oil production from oil palm solid wastes by fluidized bed pyrolysis reactor.

2.8 Previous modeling work for fast pyrolysis of biomass

With the rapid advancement of computation techniques in last decades, various computational simulation tools were widely employed for understanding inner conditions (such as hydrodynamics, heat transfer and chemical reaction) of the fluidized bed for biomass fast pyrolysis. Euler-Euler and Euler-Lagrangian models with various kinetic mechanism have been used to study the effect of reactor hydrodynamics, product yields and reaction parameters by computational fluid dynamics (CFD) (Eri et al., 2017). Papadikis et al., (2009a, 2009b 2010) chosen two-stage, semi-global model

to predict the product yield of wood biomass pyrolysis using Eulerian CFD method in Fluent software. Many authors (Liu et al., 2017, Dong et al., 2017, Xue et al., 2011, Xue et al., 2012, Xiong et al., 2014a, Xiong et al., 2014b, and Xiong et al., 2014) applied a multi-stage global kinetic mechanism for reaction kinetic on different biomass fast pyrolysis using CFD with Euler-Euler model in Fluent software. Mabrouki et al., (2015) simulated multi-component global mechanism model to maximize the liquid yield from fast pyrolysis of three palm oil residues using SuperPro Designer (SPD) software. Table 2.3 shows the modeling literature reviews for bio-oil production from different biomass solid wastes by using fluidized bed pyrolysis reactor.

Table 2.2. Bio-oil production from oil palm solid wastes by fluidized bed pyrolysis reactor

No.	Paper Name	Authors	Experiment Condition	Material	Products	Remarks
1.	Optimum conditions for maximizing pyrolysis liquids of oil palm empty fruit bunches	Sulaiman et al., 2011	Fluidized bed bench scale fast pyrolysis unit Fluidized bed reactor Diameter = 40 mm Height = 260 mm EFB particle sizes = less than 150 μm, 150-250 μm, 250-300 μm, 355-500 μm Temperature range = 673-773 K N_2 flowrates = 100ml/min	Empty fruit bunch (EFB)	Bio-oil, char, and gas	-The maximum liquid product from fast pyrolysis of EFB was yielded around 55% using particle size range over 300-355 μm at a residence time of 1.03 s and at a reactor temperature of 723 K.
2.	Bio-oil from Fast Pyrolysis of Empty Fruit Bunch	Sembiring et al., 2015	Fluidized bed reactor Stainless steel cylinder Height = 400 mm	Empty Fruit	Bio-oil, char, and gas	-The maximum bio-oil product of 27 % was obtained about 27 % at an optimum pyrolysis

	at Various Temperature		Inner diameter = 50 mm. Sand particle size = between 355 μm and 500 μm The depth of sand = approximately 81 mm Fluidization height = 400 mm Fluidizing gas = Nitrogen Three fast pyrolysis temperatures = 673 K, 773 K and 873 K	Bunches (EFB)		temperature of 773 K with a particle size of 210 μm. -The higher temperature causes lower bio-oil product yields.
3.	Fast pyrolysis of empty fruit bunches	Abdullah et al., 2010	Fluidized Bed Reactor Type 316 stainless steel cylinder Height = 260 mm Internal diameter = 40 mm	Empty Fruit Bunches (EFB)	Bio-oil, char, and gas	-Gas product yields became higher than liquid and char yields at temperatures above 873 K. -Not only to maximize liquid product yield but also to

			Sand particle size = 355-500 μm Depth of sand = approximately 80 mm Fluidization height = 120 mm Vapor residence time =1.02–1.05 s Feedstock particle size = 250–355 μm Temperature range = 673–873 K			minimize char yield was found at a residence time of 1.03 s.
4.	Bio-oil derived from empty fruit bunches	Abdullah et al., 2008	Fluidized bed bench scale fast pyrolysis unit Type 316 stainless steel cylinder Height = 260 mm	Empty Fruit Bunches (EFB)	Bio-oil, char, and gas	-The gas yield increases with temperature, while the char yield decreases.

			Diameter = 40 mm. Sand particle size = 355-500 μm The depth of sand = approximately 80 mm Fluidization height = 120 mm Fluidising gas = nitrogen Vapor residence time = 1.01–1.04 s Feedstock particle size = 355–500 μm Temperature range = 698–823 K			-The higher amount of ash content in the biomass cause the lower liquid yields. -The maximum liquid yields produced from washed EFB and unwashed EFB were up to 72% and under to 50%, respectively.
5.	Production of bio-oil rich in acetic acid and phenol from fast	Jeong et al., 2016	Bench-scale Fast Pyrolysis Fluidized Bed Reactor Internal diameter = 160 mm	Palm residue (palm	Bio-oil, char, and gas	-The bio-oil yields in the range of 63–86 wt.% and 12–36 wt.% were collected from condensers

	pyrolysis of palm residues using a fluidized bed reactor: Influence of activated carbons		Height = 610 mm Particle size = 400-800 μm Temperature = 788 K	kernel shells (PKS), mesocarp fibers (MF))		and impact separators, respectively. -The compositions of carbon monoxide and carbon dioxide gases in the non-condensable gas product are produced more than 80 wt.% during pyrolysis. -The highest carbon content in biochar (a solid fraction) found about 87 wt.%.
6.	Production and detailed characterization of bio-oil from fast pyrolysis of palm kernel shell	Asadullah et al., 2013	Bench-scale fluidized bed reactor stainless steel (grade SS316) Internal diameter = 60 mm Height = 600 mm	Palm kernel shell (PKS)	Bio-oil, char, and gas	-Char yield was decreased, and gas yield was increased when increasing of pyrolysis temperature.

			Fluidizing sand size = 400-500 μm N_2 flow range = 1-2 $Lmin^{-1}$ Feeding rates = 3 -10 $gmin^{-1}$ Maximum Temperature = 823 K			-An increase of liquid yield has occurred when higher feeding rate and nitrogen flow rate.
7.	Bio-oil from the pyrolysis of palm and Jatropha wastes in a fluidized bed	Kim et al., 2013	Stainless steel fluidized bed reactor Internal Diameter = 102 mm Height = 970 mm Temperature range = 653–803 K N2 flow rates = 15–41 L/min Superficial gas velocities = 0.031-0.084 m/s	Jatropha Seedshell cake (JSC), Palm kernel shell (PKS) and Empty	Bio-oil, char, and gas	-The higher char yield occurs at below 673 K because of incomplete pyrolysis reaction as a resulted in lower liquid yield. -The higher temperature happens secondary reactions of char which cause to yield more volatiles.

			Average particles size = 700 μm	fruit bunch (EFB)		
8.	Fast pyrolysis of palm kernel cake using a fluidized bed reactor: Design of experiment and characteristics of bio-oil	Ngo et al., 2013	Fluidized bed reactor Diameter = 36 mm Height = 200 mm Mass of a sample = 100 g N_2 flow rate = from 10 to 15 L/min Temperatures = 673 K and 773 K Residence time range = 0.6–0.9 s	Palm kernel cake (PKC)	Bio-oil, char, and gas	-Neither the short residence time nor the higher flow rate of the fluidizing gas gave an increase of liquid yield. -The maximum liquid product was yielded about 49.5 wt.% with using a particle size of 600 μm at an optimum pyrolysis temperature of 773 K and a short residence time of 0.6 s.

9.	Catalytic pyrolysis of palm kernel shell waste in a fluidized bed	Kim et al., 2014	Stainless steel fluidized bed reactor Internal Diameter = 102 mm Height = 97 mm N_2 flow rates = 2.95 L/min Biomass average particles size = 700 μm Superficial gas velocities = 0.014– 0.015 m/s	Palm kernel shell (PKS)	Bio-oil, char, and gas	-The yield of bio-oil decreased from biomass with catalytic pyrolysis than without catalytic pyrolysis according to the production of primary volatiles from catalytic reaction. -Catalysts pore structure and temperature are mainly affected by the char yields.
10.	Production of bio-based phenolic resin and activated carbon from bio-oil and biochar derived from fast pyrolysis of palm kernel shells	Choi et al., 2015	Fluidized-bed reactor Height = 390 mm Inner diameter =110 mm Temperature range = 752–828 K Feed material = from 300 to 2000 g	Palm kernel shells (PKS)	Bio-oil, char, and gas	-Higher ash content in biomass decrease bio-oil yield. -The higher compositions of carbon monoxide and methane gasses than carbon dioxide gas occurs in non-condensable gas

			Feed rate = 10 g/min Mass of fluidized sand = 2.4 kg			product yield as the reaction temperature increased. -Very higher phenol content in bio-oils (8 wt.%) from fast pyrolysis of palm kernel shells occurred than the wood biomass pyrolysis.
11.	Fast pyrolysis of palm kernel shells: Influence of operation parameters on the bio-oil yield and the yield of phenol and phenolic compounds	Kim et al., 2010	Fluidized-bed reactor Inner diameter = 110 mm Height = 390 mm Temperature range = 703-813 K Mass of feed material = 350 g Mass of fluidized sand = 3.8 kg Residence time = 0.5 s	Palm kernel shells (PKS)	Bio-oil, char, and gas	-The maximum bio-oil product yield was obtained 48.7 wt.% pyrolysis temperature up to 763 K. -The highest char product was yielded at 708 K because of the incomplete reaction of the feedstock material.

						-At 748 K, the large quantities of phenolic and phenol phenolic compounds occur about 70 area percentage in the bio-oil product yield.

Table 2.3. Reported modeling work for various biomass fast pyrolysis

No.	Paper Name	Authors	Method and simulation model	Feedstock	Products	Remarks
1.	Application of CFD to model fast pyrolysis of biomass	Papadikis et al., 2009a	-Lagrangian - Eulerian method -Two-stage, semi-global model -Commercial software (FLUENT 6.2) -Fluidized bed reactor	Wood biomass	Bio-oil, char, and gas	-The reaction mechanism is strongly affected by the particle situation in the reactor. -Temperature distribution along the radius of the particle can determine the exact amount of mass sources.
2.	Computational modeling of the impact of particle size to the heat transfer coefficient between	Papadikis et al., 2010	-Eulerian method -Two-stage, semi-global model	Wood biomass	Bio-oil, char, and gas	-The residence time of the biomass particle in the reactor mainly influence on the final product yields.

	biomass particles and a fluidized bed		-Commercial software (FLUENT 6.2) -Fluidized bed reactor			-Smaller particle sizes gave higher bio-oil yields due to secondary reactions. -Important data for the overall process of fast pyrolysis can be obtained by using computational fluid dynamics. -The residence time of the particle in the reactor affected the final product yields for a various diameter of particles. -Smaller particles gave a good heat transfer mechanism for fast pyrolysis of wood biomass in the fluidized bed.
3.	CFD modeling of the fast pyrolysis of biomass in fluidized bed reactors. Part B Heat, momentum	Papadikis et al., 2009b	-Eulerian method -Two-stage, semi-global model	Wood biomass	Bio-oil, char, and gas	-The heat and momentum transport in the fluidized bed reactor is simulated to predict the temperature gradient of the radial particle and product yields, respectively.

	and mass transport in bubbling fluidized beds		-Commercial software (FLUENT 6.2) -Fluidized bed reactor			-The prediction of the vapors residence time and biomass particle can be performed by using two-stage, semi-global model.
4.	CFD modeling of particle shrinkage in a fluidized bed for biomass fast pyrolysis with quadrature method of moment	Liu et al., 2017	-Eulerian-Eulerian multi-phase CFD model -A multi-stage global reaction mechanism -CFD package FLUENT 16.2 -Fluidized bed reactor	Wood biomass	Bio-oil, char, and gas	- Particle shrinkage unconcerned the yield of bio-oil yield. -When an increase of particles residence time, char yield increases slightly with the degree of particle shrinkage.

5.	Modeling of biomass pyrolysis in a bubbling fluidized bed reactor: Impact of intra-particle heat conduction.	Dong et al., 2017	-Eulerian-Eulerian model -Finite volume method (FVM) -Fluidized bed reactor	Cornstalk	Tar, char, and gas	-The fluidizing superficial gas velocity of fluidizing is one of important design parameters for not only the heating up rate and contacting time between tar and char. -To avoid the secondary cracking of tar, char should be quickly removed from the reactor. - To improve the accuracy of the final product yields, detail reaction mechanisms for fast pyrolysis of biomass need to be proposed in the future work.
6.	A CFD model for biomass fast pyrolysis in fluidized-bed reactors.	Xue et al., 2011	-Euler–Euler multiphase CFD model -Multi-stage kinetic model	cellulose and bagasse	Tar, char, and gas	-CFD model can be used to predict the various parameters for fast pyrolysis of biomass with known constituents in a fluidized-bed reactor.

			-Fluidized bed reactor			- Model validation for fluidized-bed reactors is important to optimize of the not only design but also operating parameters.
7.	Experimental validation and CFD modeling study of biomass fast pyrolysis in fluidized-bed reactors.	Xue et al., 2012	-Euler–Euler multiphase CFD model -Multi-stage kinetic model -Fluidized bed reactor	pure cellulose and red oak	Bio-oil, char, and gas	-The simulated product yields from pure cellulose and red oak were validated with available experimental data. -Operating temperature and hydrodynamic parameters are important to the accurate pyrolysis processes modeling in a fluidized bed reactor.
8.	Modeling effects of interphase transport coefficients on biomass pyrolysis in fluidized beds.	Xiong et al., 2014a	-Multi-fluid model -The multi-component multi-stage kinetic model	Switchgrass	Tar, char, and gas	-The numerically simulated product yields were compared with reported experimental data. -A longer solid biomass residence time with higher gas velocity gave

			-Fluidized bed reactor			higher tar yields and lower gas and char yields.
9.	BIOTC: An open-source CFD code for simulating biomass fast pyrolysis	Xiong et al., 2014b	-Multi-fluid model -The multi-component multi-stage kinetic model -Fluidized bed reactor -BIOTC code	Switchgrass	Tar, char, and gas	-An open-source code, BIOTC, can be applied to simulate for thermochemical conversion of biomass in bubbling fluidized bed reactor.
10.	Comparison of multi-component kinetic relations on bubbling fluidized-bed woody	Matta et al., 2017	-Two multicomponent, multistep kinetic reaction schemes	Hardwood Sawdust and Interior Hog Fines	Bio-oil, char, and gas	-Miller & Bellan (1996) mechanism and Ranzi et al. (2014) mechanism are used to predict the product yields from fast pyrolysis of hardwood

	biomass fast pyrolysis reactor model performance					sawdust (HWS) and interior hog fines (IHF) in a fluidized bed reactor. -The predicted product yields from mechanisms are good in agreement with reported experimental results.
11.	Simulation of biofuel production via fast pyrolysis of palm oil residues	Mabrouki et al., 2015	-Multi-stage kinetic model -Fluidized bed reactor -SuperPro Designer (SPD) software	Palm shell (PS), empty fruit bunch (EFB) and mesocarp fiber (MF)	Bio-oil, char, and gas	-The model validation was performed compared with reported experimental data of wood fast pyrolysis. -The maximum bio-oil product yield gave at 823 K pyrolysis temperature and at 0.5 s residence time.

CHAPTER 3
Materials and methodology

3.1 Materials

The feedstocks of EFB biomass are obtained from palm oil extraction plant. Sulaiman et al., (2011) have studied the properties of empty fruit bunch. The fruit bunches were chopped and shredded to reduce the feedstock size to less than 500 mm by using a Fritsch grinder with a screen size of 500 mm. The hydrolysis method is applied to test for the constituents of biomass, such as, cellulose (59.7 wt.%), hemicellulose (22.1 wt.%), lignin (18.1 wt.%) and extractives (0.1 wt.%). Element analysis of EFB performed to test the compositions of carbon (49.07 wt.%), hydrogen (6.48 wt.%), nitrogen (0.7 wt.%), sulphur (less than 0.1 wt.%), oxygen (38.29 wt.%), and potassium (2 wt.%). The moisture (7.95 wt.%), volatiles (83.86 wt.%), ash (5.36 wt.%), fixed carbon (10.78 wt.%) and higher heating value (19.35 wt.%) in EFB biomass were tested by using proximate analysis. The ash content of EFB was determined using methods of National Renewable Energy Laboratory (NREL). The reduced feedstocks are dried at 105 °C for 24 h (Kim et al., 2013). Before pyrolysis, they are stored within plastic bag at room temperature.

3.1.1 Fluidizing gas

Nitrogen gas was also one of the main parameters in fluidized bed reactor for fast pyrolysis process. It was affected not only fluidization sand and biomass particles but also the carrier of the hot gas in the fast pyrolysis process. Table 3.1 shows the properties of nitrogen gas at the range of reaction temperature over 723-873 K.

Table 3.1. Properties of nitrogen gas at different temperature (Erik et al., 2012)

Temperature (K)	Specific heat capacity (J/kg K)	Viscosity (kg/m s)	Thermal conductivity (W/m K)	Density (kg/m^3)
723	1102.8	3.275×10^{-5}	0.052	0.478
748	1109.2	3.343×10^{-5}	0.054	0.462
773	1115.6	3.411×10^{-5}	0.055	0.445
798	1121.9	3.479×10^{-5}	0.056	0.429
823	1127.9	3.545×10^{-5}	0.057	0.417
848	1133.9	3.611×10^{-5}	0.058	0.405
873	1139.9	3.677×10^{-5}	0.059	0.393

3.1.2 Fluidization particle

Sand is the most commonly used as a fluidization particle for biomass fast pyrolysis in bubbling fluidized bed reactor. The particle size of sand was the main effect on heat transfer of biomass particle. The density of 2500 kg/m^3 and mean particle size (427.5 μm) of inert sand was used for fluidization medium.

3.2 Heat transfer model

The heat transfer in empty fruit bunch particles was simulated with the heat diffusion equation. Equation (3.1) was applied for heat conduction mechanisms along the radius of an isotropic spherical empty fruit bunch particle.

$$\frac{\partial}{\partial t}(\rho Cp_{eff} T) = \frac{1}{r^2}\frac{\partial}{\partial r}(k_{eff} r^2 \frac{\partial T}{\partial r}) + (-\Delta H)(\frac{\partial \rho}{\partial r}) \tag{3.1}$$

where the effective thermal conductivity (k_{eff}) and effective specific heat capacity (Cp_{eff}) are given by equations (3.2) and (3.3),

$$k_{eff} = k_c + |k_b - k_c|\alpha_b \tag{3.2}$$

$$Cp_{eff} = Cp_c + |Cp_b - Cp_c|\alpha_b \quad (3.3)$$

where k_c, k_b, Cp_c, Cp_b and α_b were the char thermal conductivity, biomass thermal conductivity, char specific heat capacity, biomass specific heat capacity and biomass mass fraction.

The boundary conditions on the surface and at the center of the EFB particle were set as follows,

$$-k_{eff}\left.\frac{\partial T}{\partial r}\right|_{r=R} = h(T_i - T_s) \quad (3.4)$$

$$\left.\frac{\partial T}{\partial r}\right|_{r=0} = 0 \quad (3.5)$$

where T_i, T_s, and h are ambient temperature, surface temperature, and the film heat transfer coefficient.

3.2.1 Minimum fluidization velocity (U_{mf})

In the literature, many authors have predicted the minimum fluidization velocity (U_{mf}) for biomass particles in energy extraction by combustion, gasification or pyrolysis. The predictions are based on four approaches, namely pressure drop, dimensional analysis, drag force, and terminal velocity. Using the pressure drop approach, Wen et al., (1966) developed an Ergun equation to estimate the minimum fluidization velocity (U_{mf}) using dimensionless Reynolds (Re_{mf}) and Archimedes (Ar) groups, shown in equations from (3.6) to (3.8). In Table 3.2, four correlations for the Geldart group B were tested to estimate the minimum fluidization velocity (U_{mf}) for fast fluidized bed pyrolysis of EFB.

$$U_{mf} = \frac{Re_{mf} \times \mu_g}{\rho_g \times d_s} \quad (3.6)$$

$$Re_{mf} = (K_1^2 + K_2 Ar)^{0.5} - K_1 \quad (3.7)$$

$$Ar = \frac{(g \times \rho_g \times (\rho_s - \rho_g) \times d_s^3)}{\mu_g{}^2} \quad (3.8)$$

where K_1, K_2, ρ_s, d_s, μ_g, ρ_g, and g are empirical constant 1, and 2, sand particle density, sand particle diameter, the viscosity of the gas, density of gas and gravitational acceleration constant, respectively.

Table 3.2. Four correlations proposed for ranges of sand particle diameters (d_s) and densities (ρ_s)

No.	Authors	Correlation	Diameter d_s (μm)	Density ρ_s (kg/m^3)
1.	Bin et al., 1994	$Re_{mf} = (27.31^2+0.0386Ar)^{0.5}-27.31$	40-2120	1600-7500
2.	Bourgeois et al., 1968	$Re_{mf} = (25.46^2+0.0382Ar)^{0.5}-25.46$	86-25,000	1200-19300
3.	Hilal et al., 2001	$Re_{mf} = (13.07^2+0.0263Ar)^{0.5}-13.07$	80-1230	1228-8900
4.	Vaid et al., 1978	$Re_{mf} = (24.00^2+0.0546Ar)^{0.5}-24.00$	114-1829	1669-4332

3.2.2 Heat transfer coefficient (h)

The heat transfer coefficient of EFB pyrolysis was calculated by well-known two correlations. Collier et al., (2004) studied the calculation for heat transfer coefficient under the condition of biomass particle size (d_p) smaller than sand particle size (d_s). The heat transfer coefficient for sand particle diameter larger than the biomass particle diameter was estimated by Ranz et al., (1952). Table 3.3 shows the two types of correlation for heat transfer coefficient calculation with respects to the biomass and sand particle diameter.

Table 3.3. Two types of correlation for heat transfer coefficient (h) calculation

Case	Correlation	Equation
$d_p < d_s$	Collier et al., 2004	$h = (k_g/d_p) \times (2+0.9Re^{0.62}(d_p/d_s)^{0.2})$
$d_p > d_s$	Ranz et al., 1952	$h = (k_g/d_p) \times (2+0.6Re^{1/2}Pr^{1/3})$

where unitless Reynold number (Re) and Prandtl number were shown in the following equations (3.9) and (3.10),

$$Re = \frac{\rho_g \times U_{mf} \times d_b}{\mu_g} \tag{3.9}$$

$$Pr = \frac{\mu_g \times Cp_g}{k_g} \tag{3.10}$$

3.2.3 Heat of reaction (ΔH)

The main three steps of thermal degradation of EFB biomass are dehydration, slow depolymerization, and complex thermal depolymerization, respectively. A dehydration process performed to remove the moisture content of biomass at the temperature below 423 K. A slow depolymerization process for the dehydrated samples happened in the range over 423–498 K. Then, the complex thermal decomposition reaction occurred in the temperature range of 498–673 K. Lignin components in the biomass are mainly decomposed in this step. STAR^e software (Version 9.20) was used to estimate for the energy requirement of the biomass dehydration process and thermal decomposition process. Table 3.4 shows the calculated energy values for the three steps. The required energy for complex thermal decomposition reaction of biomass samples was higher than the required energy for the evaporation of moisture content in biomass (Asadieraghi et al., 2015).

Table 3.4. Energy required for thermal decomposition of EFB biomass (Asadieraghi et al., 2015)

Feedstock biomass	The energy requirement for dehydration(kJ/kg)	The energy requirement for slow depolymerization (kJ/kg)	Energy requirement complex thermal depolymerization (kJ/kg)	The total energy required (kJ/kg)
EFB	182.6	2.44	225.76	410.80

3.3 Kinetics model of pyrolysis

Kinetics model of pyrolysis plays as the main role for optimizing the operating parameters and maximizing desired product yields. Last decade, many authors have been studied to obtain good data of kinetics rate constants which could be applied in various biomass fast pyrolysis at a transient process. Three types of pyrolysis kinetics models for the lignocellulosic biomass are one-stage single and multiple reaction models, and two-stage semi-global model (Blasi et al., 1993a). A simple one-step pyrolysis reaction mechanism used in one-stage single reaction model. Three parallel kinetics reactions are applied to illustrate the degradation of biomass into tar, char and gas products in one-stage multiple reactions. It can be also used to determine the product yields in a one-stage simplified kinetics model. The primary and secondary reactions are combined as a series model in two-stage semi-global.

3.3.1 One-stage single reaction model

In this reaction model, biomass is decomposed into volatile and char product on a single overall reaction:

$$\text{Biomass} \longrightarrow \text{Volatile} + \text{Char} \tag{3.11}$$

The pyrolysis reaction rate depends on the unreacted mass of the biomass. Therefore, Equation (3.11) can be considered to express the decomposition rate of mass in a single reaction model.

$$\frac{dm_b}{dt} = -k(m_b - m_c) \quad (3.12)$$

Here, m_b = decomposition rate of mass (kg)

m_c = remained mass of char after complete conversion (kg)

k = the reaction rate constant (s^{-1}), and

t = time (s).

The mass fractional conversion of the biomass can be written in nondimensional form as

$$X = \frac{(m_0 - m_b)}{(m_0 - m_c)} \quad (3.13)$$

where X and m_0 are mass fraction conversion of the biomass and the initial mass of the biomass (kg).

Substituting mass fractional conversion of the biomass in equation (3.13),

$$\frac{dX}{dt} = k(1 - X) \quad (3.14)$$

Solving the equation (3.14), we get

$$X=1-Aexp(-kt) \quad (3.15)$$

where A, E, R, and T are pre-exponential coefficient, activation energy (J/mol), gas constant (J/mol.K), temperature (K), respectively.

3.3.2 One-stage multiple-reaction model

Biomass decomposed into tar, char and gas products in one stage multiple reaction models. Figure 3.1 illustrates the pathways of parallel reaction model for biomass pyrolysis.

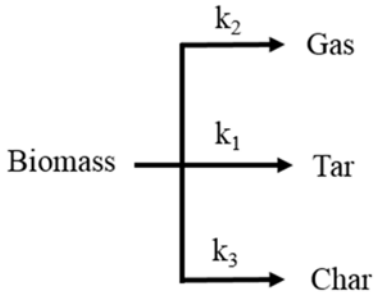

Figure 3.1. Parallel reaction model for biomass pyrolysis

3.3.3 Two-stage semi-global model

Three types of two-stage semi-global kinetics model for prediction of product yields were applied in biomass fast pyrolysis process. They are simple, global and advance models. The main three pyrolytic products were bio-oil, char, and gas. These three pyrolytic products were decomposed at primary and secondary reactions.

3.3.3.1 Simple kinetics model

In the simple kinetics model, biomass decomposed into bio-oil, char and gas in primary reaction and then bio-oil break down into char and gas products in secondary reaction because of long vapor residence time at the elevated reaction temperature. Chan et al., (1985)**,** Liden et al., (1988) and Blasi et al., (1993b) have proposed the kinetics parameters of each reaction in the simple kinetics model. Papadikis et al., (2009a, 2009b, 2010) have studied the bio-oil production from wood biomass fast pyrolysis using a simple kinetics model. Figure 3.2 illustrates the simple kinetics model for biomass pyrolysis process.

Table 3.5. Simple kinetics model parameters for fast pyrolysis of lignocellulose biomass

No.	Pyrolysis reaction	Pre-exponential factor, A (s^{-1})	Activation Energy, E (kJ mol^{-1})	References
1.	Biomass to gas	2.8×10^{8}	140	Chan et al., 1985
2.	Biomass to char	3.2×107	121	Chan et al., 1985
3.	Biomass to tar	1.8×10^{8}	133	Chan et al., 1985
4.	Tar to gas	2.6×10^{6}	108	Liden et al., 1988
5.	Tar to char	1.0×10^{6}	108	Blasi et al., 1993b

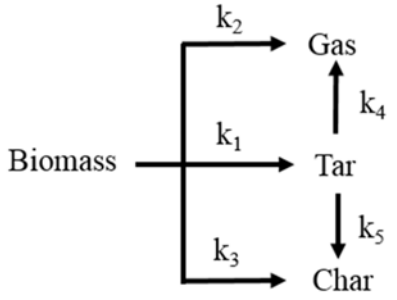

Figure 3.2. A simple model for biomass fast pyrolysis

3.3.3.2 Global kinetics model

A global kinetics model for biomass fast pyrolysis was published by Shafizadeh et al., (1979). They considered the feedstock biomass consists of cellulose, hemicellulose, and lignin. This consideration was mainly different between simple and

global kinetics models. The other main difference step between simple and global model is active material which is a low degree of polymerization (DP) stage. Therefore, constituents of biomass were decomposed into intermediate products in primary reaction and then they break down into bio-oil, char and gas products in the secondary reaction. In fact, primary vapor can be decomposed into non-condensable gas in the secondary reaction. In 1994, the global kinetics model for cellulose fast pyrolysis was published by Diebold, (1994). In his work, cellulose decomposed into active cellulose in the first stage and then they broke down into pyrolytic products in the second stage as shown in Figure 3.3. The kinetic mechanism of these two stages studied by seven reactions pathways. Miller et al., (1996) studied the kinetics mechanisms of hemicellulose and lignin fast pyrolysis using Shafizadeh et al., (1979) pathways. The constituents of biomass allowed to the formation of active material and then they decomposed into three pyrolytic products. The vapor product permitted to convert into the gas produced in a secondary reaction. The Arrhenius equation chosen for each kinetics reaction mechanisms of the cellulose, hemicellulose, and lignin as shown in equation (3.16). The activation energy and preexponential factor for first-order irreversible reactions of the cellulose, hemicellulose, and lignin found from academic works of literature for the global kinetic scheme (Diebold, 1994, Miller et al., 1996). Table 3.6 shows kinetics reaction parameters for the fast pyrolysis of three constituents in a global kinetic scheme. The chemical compositions for three constituents of empty fruit bunch are shown in Table 3.1.

$$K_i = A_i \exp(-E_i / RT) \tag{3.16}$$

Here K_i = rate of reaction (s^{-1}),

A_i = pre-exponential factor (s^{-1}),

E_i = activation energy (J/mol),

R = gas constant (8.314 J/mol K) and

T = reaction temperature (K)

Table 3.6. Kinetics parameters for fast EFB pyrolysis (Diebold, 1994, Miller et al., 1996)

Pyrolysis reaction	Pre-exponential factor, A (s^{-1})	Activation energy, E (kJ/mol)
Cellulose to Active Cellulose	2.80×10^{19}	240.0
Cellulose to 0.6Char + 0.4H_2O	6.70×10^{5}	110.0
Active Cellulose to Gas	3.60×10^{11}	200.0
Active Cellulose to Vapors	6.80×10^{9}	140.0
Active Cellulose to 0.6Char + 0.4H_2O	1.30×10^{10}	150.0
Vapors to Gas	3.60×10^{11}	200.0
Vapors to Tar	1.80×10^{3}	61.0
Hemicellulose to Active Hemicellulose	2.10×10^{16}	186.7
Active Hemicellulose to Vapors	8.75×10^{15}	202.4
Active Hemicellulose to 0.6Char + 0.4Gas	2.60×10^{11}	145.7
Vapors to Gas	4.28×10^{6}	108.0
Lignin to Active Lignin	9.60×10^{8}	107.6
Active Lignin to Vapors	1.50×10^{9}	143.8
Active Lignin to 0.75Char + 0.25Gas	7.70×10^{6}	111.4
Vapors to Gas	4.28×10^{6}	108.0

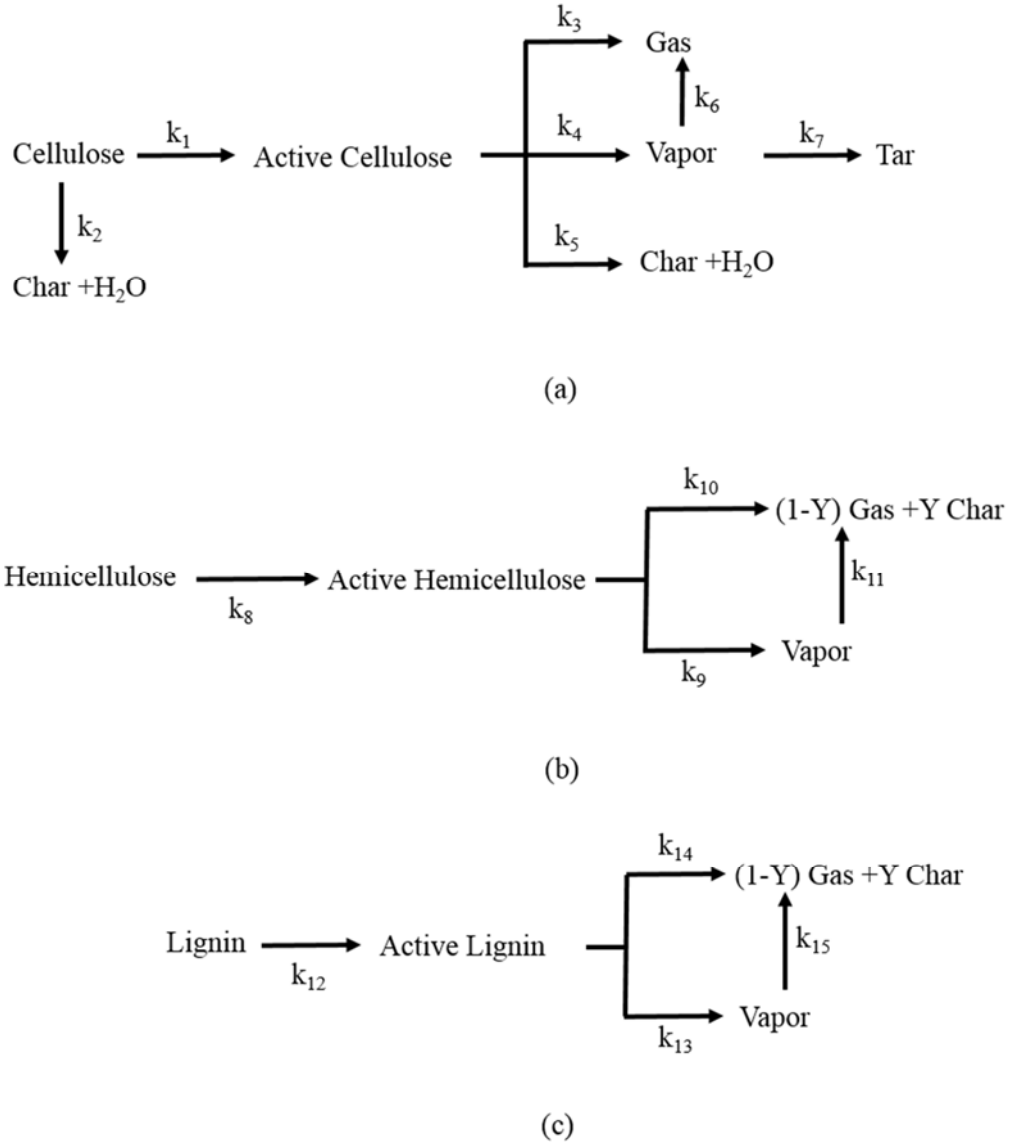

Figure 3.3. A global kinetics model for fast pyrolysis of (a) cellulose, (b) hemicellulose and (c) lignin

3.3.3.3 Advanced kinetics model

The advanced kinetics model studied for the detail reaction mechanisms of biomass fast pyrolysis due to lack of details kinetics reaction mechanism in both simple and global kinetics schemes. The main purpose of the advance model is to predict detail product species from biomass pyrolysis. In 2008, advance reactions mechanism is proposed for the fast pyrolysis of cellulose, hemicellulose, and lignin in

biomass by Ranzi et al., (2008). After six years, they have published upgrade more detail reactions mechanism for an advanced model in which several lumped reactions were mentioned for the feedstock constituent's fast pyrolysis (Ranzi et al., 2014).

3.4 Simulation model and parameters

The simulation utilized heat transfer in solids for heat transfer model and reaction engineering modules for reaction kinetics model in COMSOL Multiphysics 4.3b software. The heat transfer inside a particle was by diffusion from the surface to center. Fifteen reactions is applied to predict product yield from fast pyrolysis of EFB by a global kinetics model. Both heat transfer and kinetics for fast pyrolysis of EFB were considered transient. Empty fruit bunch (EFB) biomass used as feedstock material in this study. The EFB particles assumed to be sphere shaped. In the simulation, the particle size of EFB and reaction temperature are in the range over 150-500 μm, and 673-873 K, respectively. Table 3.7 shows the parameters used in simulation.

Table 3.7. Simulation parameters

No	Name	Symbol	Value	References
1.	Density of EFB	ρ_b	800 kg/m^3	Salema et al., 2015
2.	The thermal conductivity of EFB	k_b	0.03 W/m K	Salema et al., 2015
3.	The specific heat capacity of EFB	C_b	1150 J/kg K	Salema et al., 2015
4.	The specific heat capacity of char	C_{pc}	1004 J/kg K	Dupont et al., 2014
5.	The thermal conductivity of char	k_c	0.062 W/m K	Gupta et al., 2003

3.5 COMSOL Multiphysics®

COMSOL Multiphysics® is a software package which originally known as FEMLAB because it uses the finite element method to analyze and solve complex problems. These applications include AC/DC Module, Acoustics Module, CAD Import Module, Chemical Engineering Module, Earth Science Module, Heat Transfer Module, Material Library, MEMS Module, RF Module, and Structural Mechanics Module. Each module contains modeling tools and equations for the application described. Modeling tools from multiple modules can be coupled together to accurately depict complicated systems and processes. The Chemical Engineering Module contains tools for modeling fluid, heat, and mass transfer, as well as for chemical reactions. These tools can be used for both steady-state and transient analysis. The module can be used to simulate a variety of systems, including batch reactors, separators and scrubbers, filtration, heat exchangers, and packed bed reactors. Models may be created in 1, 2, or 3 dimensions, and use partial differential equations to relate the physics of each aspect of a model. Often topics such as heat and mass transfer are taught separately, but both take place in a chemical reactor and using COMSOL to model these phenomena can make it easier to understand and visualize (COMSOL Group, 2008).

CHAPTER 4

Results and discussion

The four main parts of simulation for EFB biomass pyrolysis such as parameters estimation, heat transfer model simulation, kinetics model simulation, and model validation were discussed in this section.

4.1 Parameters estimation

Four correlations are applied to estimate minimum fluidization velocity for fluidization between biomass particle size in the range 150-500 μm and sand particle size in the range 355-500 μm at reaction temperature range over 723-873 K. The average fluidized bed particle size of 427.5 μm used in minimum fluidization velocity estimation. The calculation of dimensionless Archimedes and Reynold dimensionless number based on the properties of nitrogen fluidization gas at temperature in the range 723-873 K. The Archimedes number in the range of 556.87-998.58 and Reynold number in the range of 0.391-1.11 were calculated by using four correlations. The estimated values of U_{mf} by four correlations are in the range over 0.086-0.153 m/s at temperature in the range 723-873 K. The calculation steps of minimum fluidization parameter are described in Section A.1. of Appendix A. The heat transfer coefficient parameter for particle size in the range 150-500 μm of EFB biomass calculated based on the estimated minimum fluidization velocity. The calculated steps and values of heat transfer coefficient of EFB biomass particles are shown in Section A.2. of Appendix A. The products yield from EFB biomass fast pyrolysis at different reaction temperature and various residence time are shown in Appendix B.

4.2 Heat transfer model simulation

The effect of important parameters for heat transfer model are discussed in this section. They are minimum fluidization velocity, heat transfer coefficient, particle size, temperature and reaction time.

4.2.1 Effect of minimum fluidization velocity (U_{mf}) on heat transfer model

The minimum fluidization velocity is also one of the important design parameters which depend on size, shape, and density of particles. The higher Archimedes number and Reynold number caused the higher minimum fluidization velocity by using four correlations. Figure 4.1. (a) illustrates the relationship between Archimedes and Reynold dimensionless number for four correlations. The higher minimum fluidization velocity happened the higher heat transfer coefficient of biomass smaller particle, but it was lower in large particle. Therefore, particle size was mainly affected for calculation of U_{mf} on fast pyrolysis process. The higher U_{mf} was need to rapid good heat transfer from surface to center of EFB particle heat diffusion at lower reaction temperature. Table 4.1. and Figure 4.1. (b) show the estimated minimum fluidization velocity at different reaction temperature.

Table 4.1. Estimated U_{mf} by four correlations at 723-873 K

Temperature (K)	U_{mf} by Bin Correlation	U_{mf} by Bourgies Correlation	U_{mf} by Hilal Correlation	U_{mf} by Vaid Correlation
723	0.096	0.101	0.133	0.153
748	0.094	0.099	0.131	0.15
773	0.092	0.098	0.129	0.147
798	0.09	0.096	0.126	0.144
823	0.089	0.094	0.124	0.142
848	0.087	0.092	0.122	0.139
873	0.086	0.091	0.119	0.137

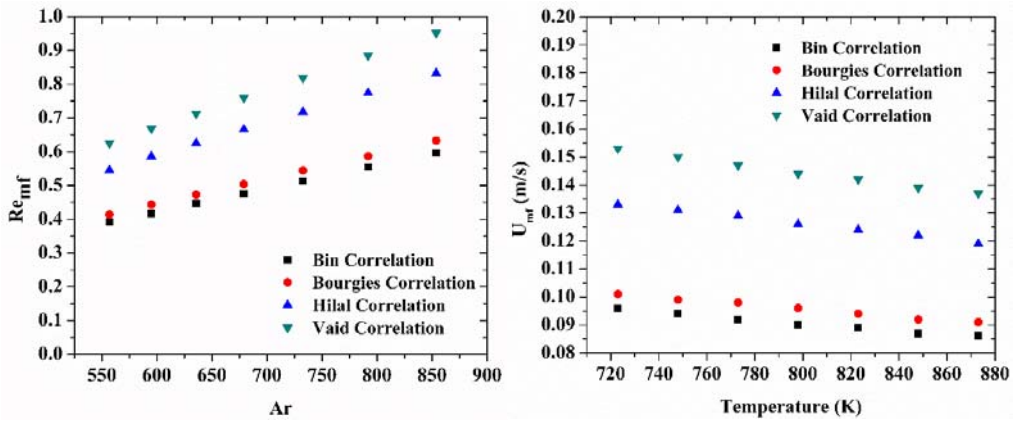

(a) Re_{mf} vs Ar (b) U_{mf} vs Temperature

Figure 4.1. Relationship between (a) Re_{mf} vs Ar and (b) U_{mf} vs Temperature

4.2.2 Effect of heat transfer coefficient (h) on heat transfer model

The heat transfer coefficient was correlated to the important reaction parameters such as particle size, reaction temperature and minimum fluidization velocity (U_{mf}). The maximum heat transfer coefficient for smallest particle size of 150 µm was estimated about 898.96 W/m^{2}K at 873 K. Therefore, smaller particle size was caused higher heat transfer coefficient at higher reaction temperature. When the biomass particle size increase to 500 µm which large than fluidized bed particle size, the minimum heat transfer coefficient was found about 254.28 W/m^{2}K by using Ranz et al., (1952) correlation at 723 K. As a result, the large particle and lower reaction temperature gave lower heat transfer coefficient. As particle size and reaction temperature, minimum fluidization velocity also affected the heat transfer coefficient of particle. The higher minimum fluidization happened the higher heat transfer coefficient. At 873 K, the heat transfer coefficient for particle size of 150 µm increased from 870.76 W/m^{2}K to 898.96 W/m^{2}K when an increase of minimum fluidization velocity from 0.086 m/s to 0.137 m/s. Several hundreds of heat transfer coefficient estimates have been applied in models of fast biomass pyrolysis in a fluidized bed reactor. Papadikis et al., (2009b) used the estimated heat transfer coefficient range 190-475 W/m^{2}K for modeling of spherical wood biomass particles fast pyrolysis at 773 K. Similarly, Velden et al., (2010) used the average heat transfer coefficient about 500 W/m^{2}K for fast pyrolysis of saw dust biomass at 773 K. Table 4.2. shows the estimated heat transfer coefficient at the reaction temperature of 773 K. In this work, the average

heat transfer coefficient of 550, 515 and 460 W/m^{2}K were applied for 150-500 µm, 250-355 µm, and 300-355 µm, respectively, in the heat transfer model simulation at the reaction temperature in the range of 723-873 K. Figure 4.2 shows the estimated heat transfer coefficient for particle size range of 150-500 µm at different reaction temperature and U_{mf}.

Table 4.2. Estimated heat transfer coefficient (h) at 773 K

Particle Size (µm)	h (W/m^{2}K) at 0.092 m/s	h (W/m^{2}K) at 0.098 m/s	h (W/m^{2}K) at 0.129 m/s	h (W/m^{2}K) at 0.147 m/s
150	827.03	830.77	848.88	858.62
250	525.52	528.94	545.39	554.28
300	449.37	452.68	468.66	477.26
355	390.16	393.32	408.85	417.17
500	265.74	267.21	274.14	277.79

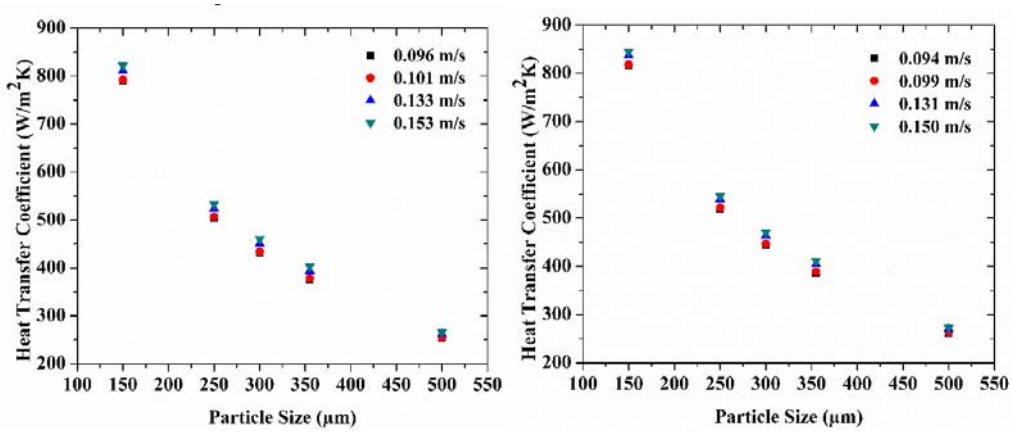

(a) 723 K (b) 748 K

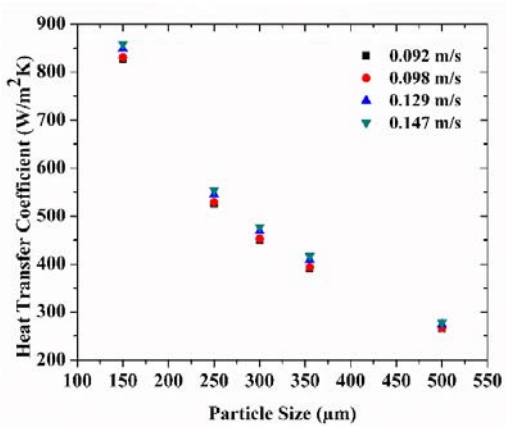

(c) 773 K

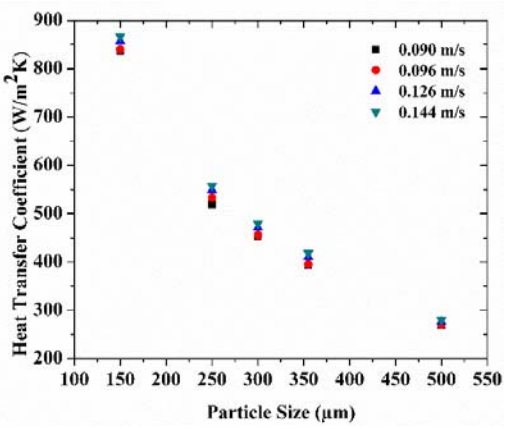

(d) 798 K

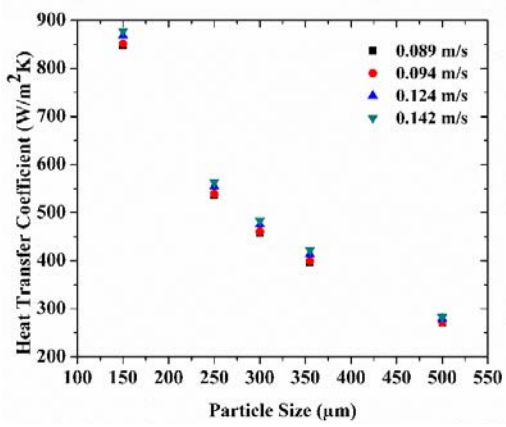

(e) 823 K

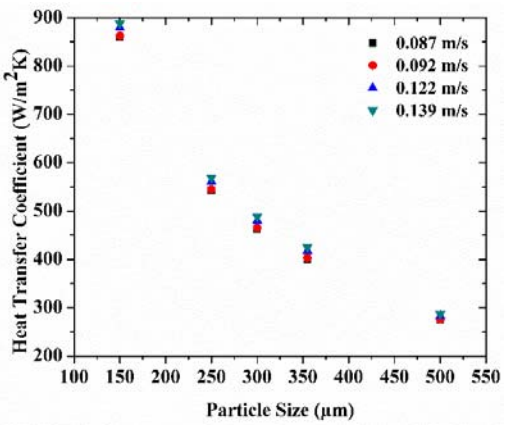

(f) 848 K

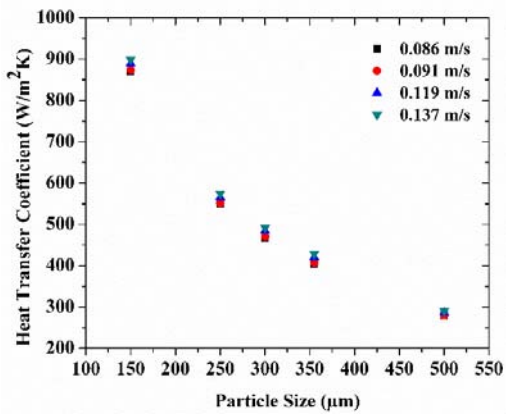

(g) 873 K

Figure 4.2. Effect of heat transfer coefficient on particle size in range of 150-500 µm at temperature in the range 723-873 K with different U_{mf}

4.2.3 Effect of particle size on heat transfer model

Particle size is the one important parameter on biomass fast pyrolysis. In this work, heat transfer of EFB biomass fast pyrolysis were considered particle sizes in the ranges between 150 µm and 500 µm. Due to the surface area of particle, the effective heat transfer on small particle size occurred higher than the large particle size. Figure 4.3 shows the heat transfer coefficient effect on particle size range 150-500 µm at different temperature and U_{mf} by four correlations. The simulated surface and center temperature for small particle size range of 150-300 µm was occurred about 722.84-722.93 K and 722.72-722.91 K, respectively at 1.03 s as shown in Figure 4.3 (a-c). But, the simulated surface and center temperature for large particle size of 500 µm gave about 713.89 K and 701.29 K, respectively at 1.03 s (in Figure 4.3 (e)). Therefore, the large particle size was difficult to reach the desire pyrolysis temperature than small particle size. According to this results, higher reaction temperature or longer vapor residence time were needed to reach the complete heat transfer in large particle size. The following section 4.2.4 was discussed detail about the effect of reaction temperature and vapor residence time on large particle size. The simulated reaction temperature in small particle size was observed closely to the reported experimental reaction temperature of 723 K by Sulaiman et al., (2011). Figure 4.4 and 4.5 show the simulated surface and center reaction temperature of particle size in the range 300-355 µm and 250-355 µm at 1.32 s and at 1.05 s, respectively. The simulated temperature in particle size of 300 µm and 250 µm gave closer to the reported experimental pyrolysis temperature of 773 K and 873 K than particle size of 355 µm.

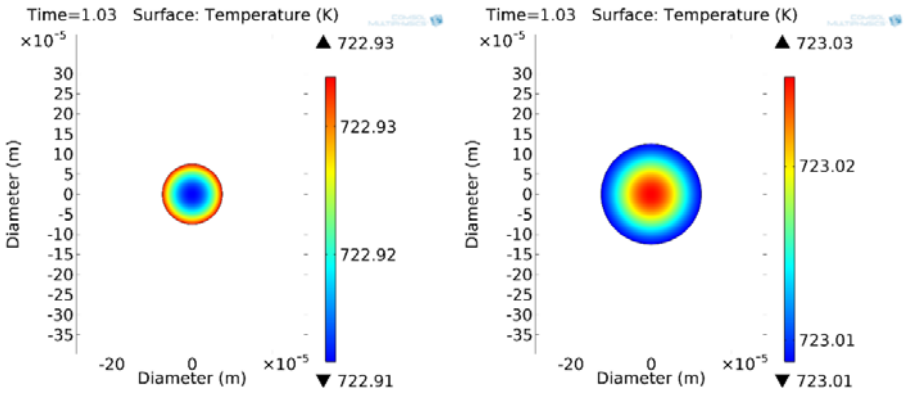

(a) 150 µm (b) 250 µm

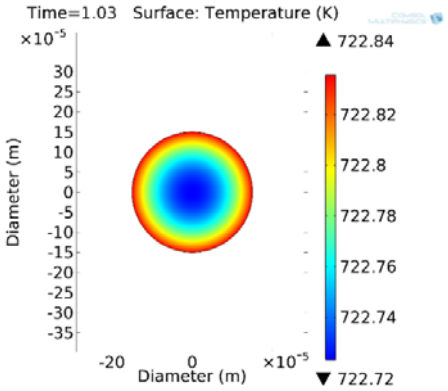

(c) 300 µm

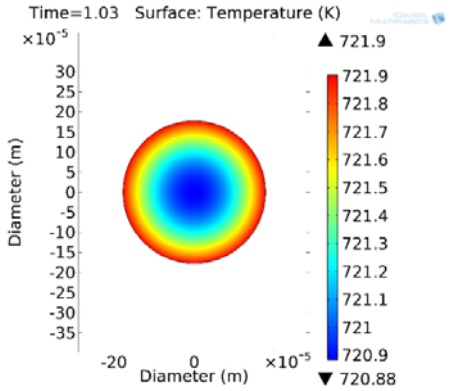

(d) 355 µm

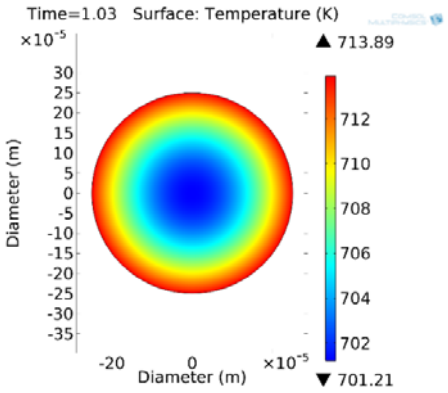

(e) 500 µm

Figure 4.3. Particle size effect on EFB fast pyrolysis at 723 K and at 1.03 s

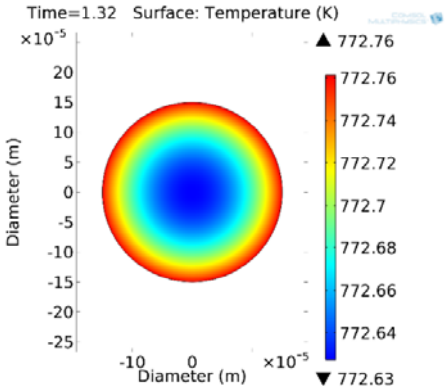

(a) 300 µm

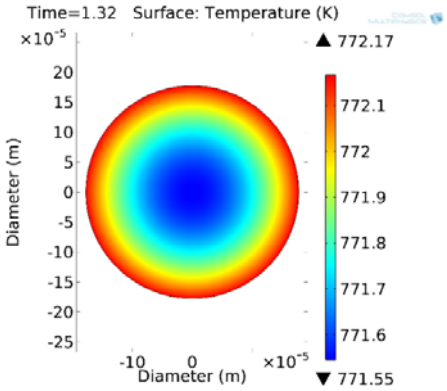

(b) 355 µm

Figure 4.4. Particle size effect on EFB fast pyrolysis at 773 K and at 1.32 s

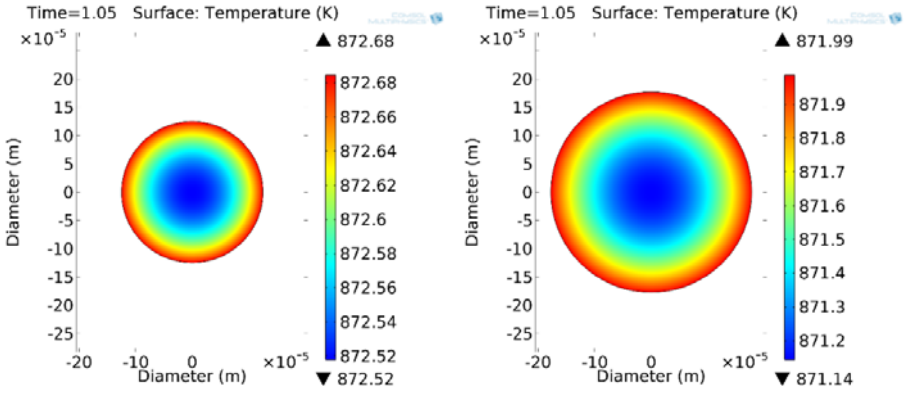

(a) 250 µm (b) 355 µm

Figure 4.5. Particle size effect on EFB fast pyrolysis at 873 K and at 1.05 s

4.2.4 Effect of temperature and time on heat transfer model

The heat transfer of empty fruit bunch particle was simulated at the different temperature by using heat diffusion equation in COMSOL Multiphysics software. The particle sizes range of 150-500 µm simulated to predict the temperature profiles of EFB particles pyrolysis at reaction temperature 723-873 K and at reaction time below of 2 s. For the reaction temperature of 723 K, the simulated complete heat transfer for particle size in the range of 150-300 µm and 355-500 µm are obtained at time of below 1 s and in the range of 1-2 s, respectively (in Figure 4.6). The stable simulated reaction temperature for particle size 150 µm and 500 µm started at 0.6 s and 1.8 s, respectively. Therefore, lower reaction temperature causes the longer reaction time for large particle size. When temperature increase from 723 K to 773 K, the stable temperature profiles for particle size of 300 µm and 355 µm started at time 0.79 s and 1.32 s as, respectively, as shown in Figure 4.7. According to this result, large particle size needs long reaction time to reach pyrolysis temperature than small particle size. At 873 K, the stable highest simulated temperature of particle size 250-355 µm showed at time in the range of 0.6-1 s (in Figure 4.8). Therefore, reaction time was lower in small particle size heat transfer, but it was higher in large particle size heat transfer. In addition, higher reaction temperature and lower time need to reach complete heat transfer for large particle size. The simulated profiles of reaction temperature in the range 723-873 K is in a good agreement compared with reported experimental data of Sulaiman et al., (2011).

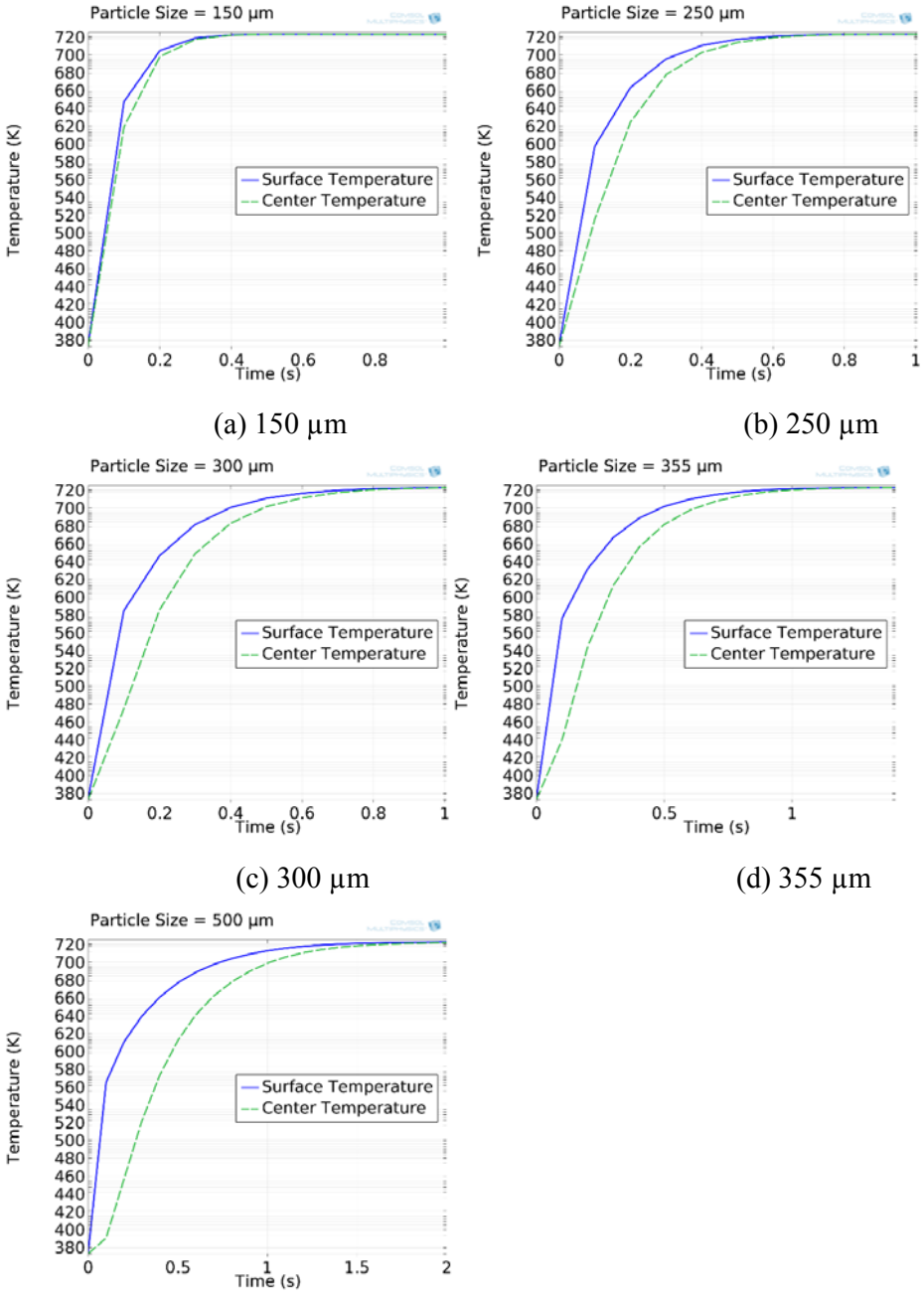

(a) 150 µm (b) 250 µm

(c) 300 µm (d) 355 µm

(e) 500 µm

Figure 4.6. Temperature profiles for particle size in the range of 150-500 µm

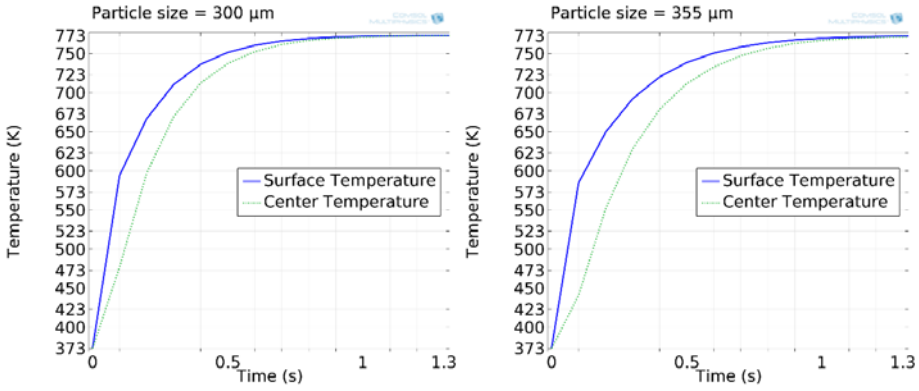

(a) 300 µm (b) 355 µm

Figure 4.7. Temperature profiles for particle size in the range of 300-355 µm

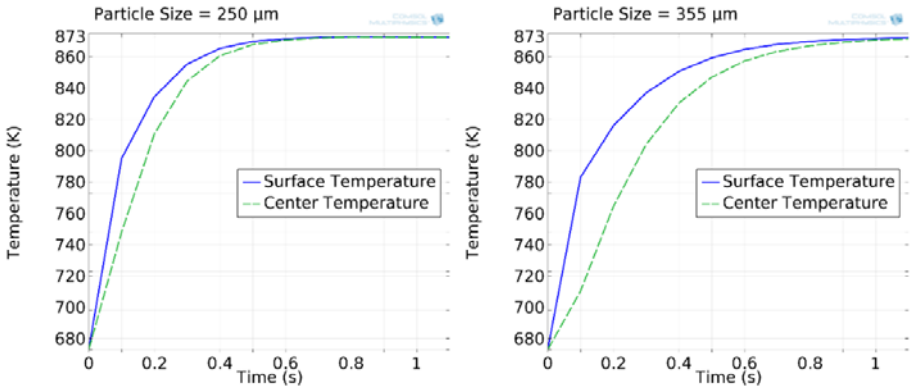

(a) 250 µm (b) 355 µm

Figure 4.8. Temperature profiles for particle size in the range of 250-355 µm

4.3 Kinetics model simulation

4.3.1 Effect of reaction temperature on product yields

Figure 4.9 shows the simulated product yields compositions of EFB fast pyrolysis at reaction temperature range from 723 to 873 K with different vapor residence time. Sulaiman et al., (2011) have studied the effect of reaction temperature on experimental product yield for empty fruit bunch fast pyrolysis temperature in the range 723-873 K. The optimum product yields for fast pyrolysis of EFB biomass predicted at in the range 723-873 K temperature and vapor residence time in the range 0.2-2 s. At 723 K, the optimal liquid yield was obtained about 52.5 wt.% in reported

experimental data and 53.23 wt.% in simulation at vapor residence of 1.05 s and 2 s, respectively. The lower temperature caused the increase of liquid yield at long vapor residence time than short vapor residence time in simulation. But it was also increase of char yield because of incomplete reaction. The gas yield was increased from 6.26 wt.% to 11.56 wt.% when an increase of vapor residence time from 1 s to 2 s at 723 K in Table 4.3. When the temperature increased to 748 K, the simulated liquid and char product yield decreased from 53.23 wt.%, 35.11 wt.% to 51.21 wt.%, 27.25 wt.% but gas yield increased from 11.56 wt.% to 21.44 wt.% at 2 s. Similarly, the simulated liquid yield decreased from 53.14 wt.% to 44.70 wt.% when an temperature increase from 773 K to 798 K at 1 s. The gas yield was highly increased when the temperature increase from 823 K to 873 K at below 0.5 s. The lower temperature need long vapor residence time to obtain higher liquid product yield and to avoid an increase of char product yield. The higher temperature prefers to increase the gas product because of secondary reactions. The optimal reaction temperature of liquid for both reported experimental and simulation was found at the temperature in the range 723-873 K and at vapor residence time below 2 s as shown in Figure 4.10. Therefore, the product yields of EFB fast pyrolysis were mainly depended upon on the reaction temperature and vapor residence time.

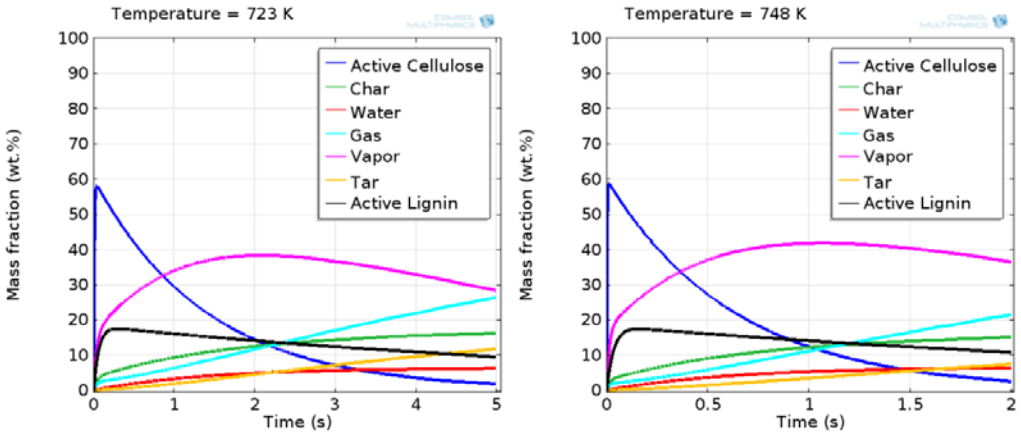

(a) 723 K (b) 748 K

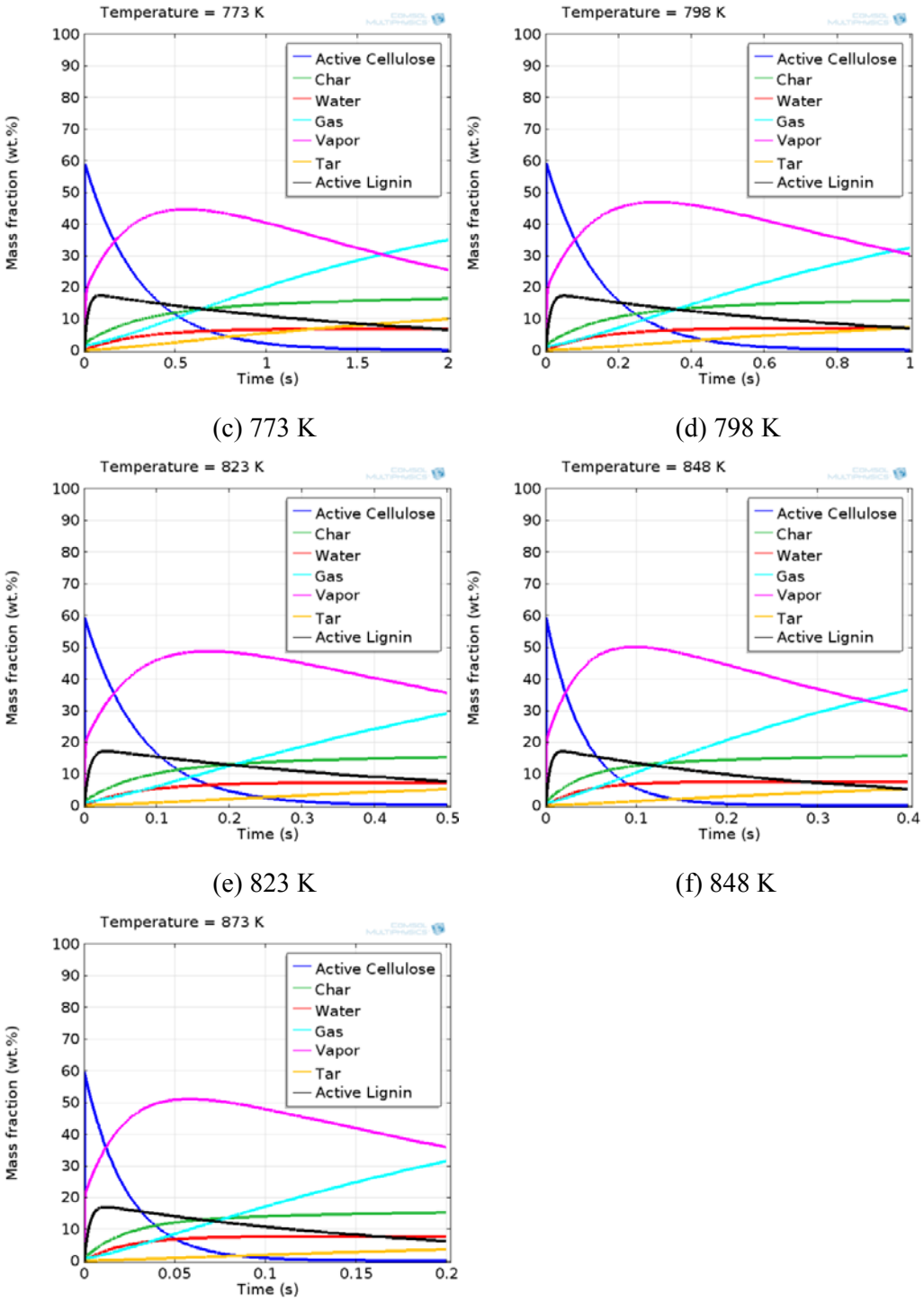

(c) 773 K (d) 798 K

(e) 823 K (f) 848 K

(g) 873 K

Figure 4.9. Simulated product compositions of EFB biomass fast pyrolysis at the temperature in the range of 723-873 K and residence time range of 0.2-5 s

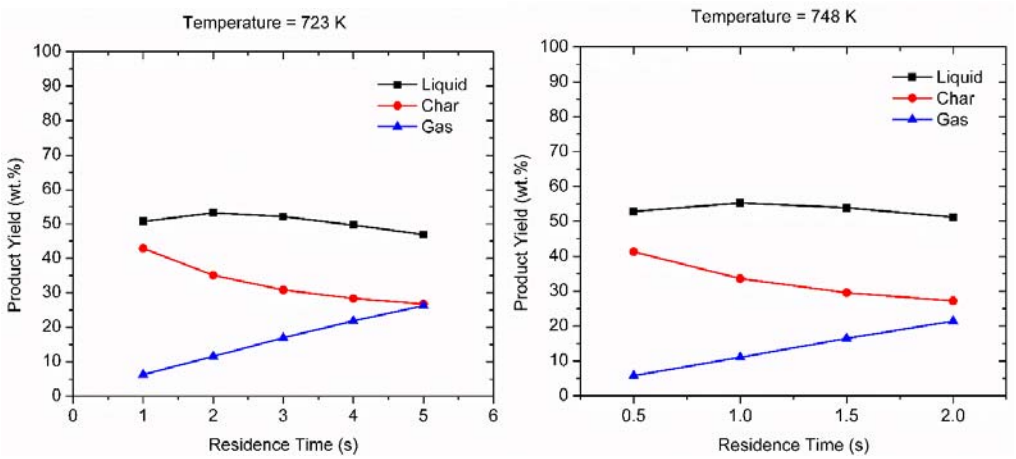

(a) 723 K

(b) 748 K

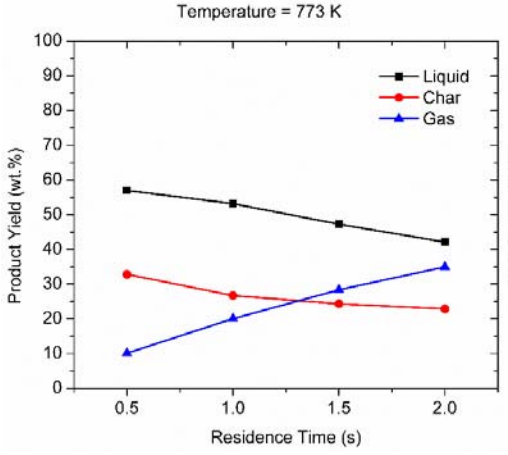

(c) 773 K

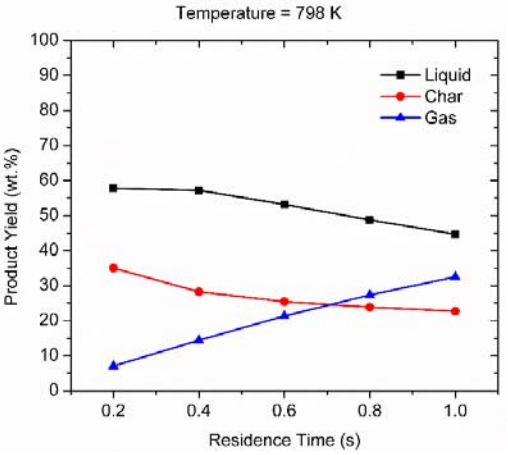

(d) 798 K

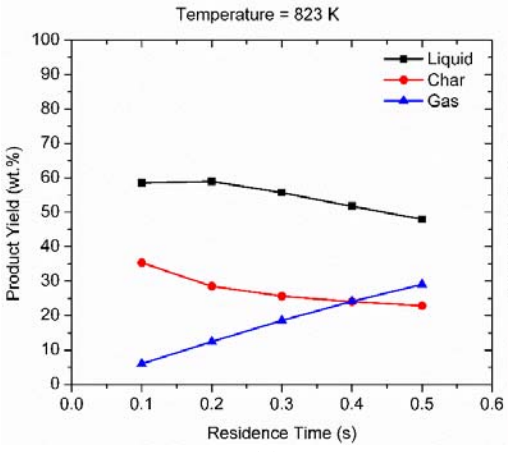

(e) 823 K

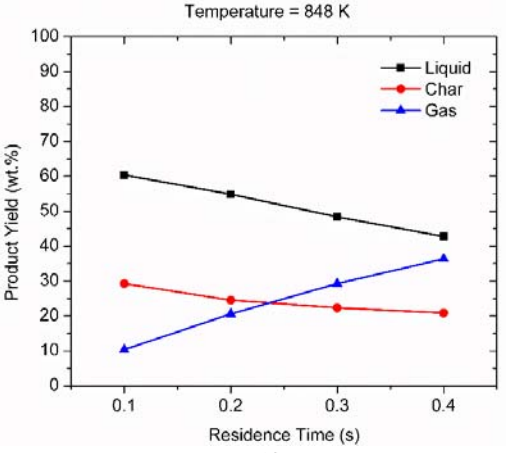

(f) 848 K

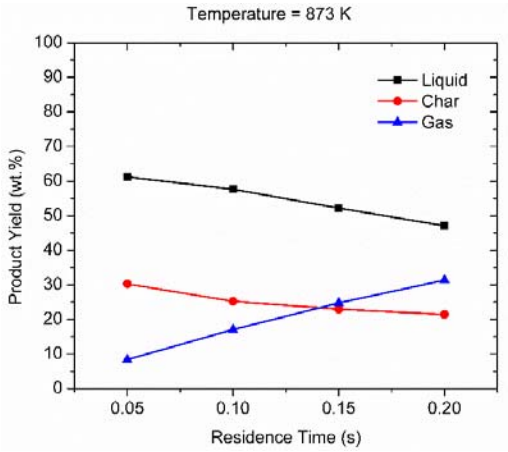

(g) 873 K

Figure 4.10. Simulated product yields of EFB biomass fast pyrolysis at the temperature in the range of 723-873 K and residence time range of 0.2-5 s

Table 4.3. Product yields at temperature 723 K

Residence Time (s)	Liquid (wt.%)	Char (wt.%)	Gas (wt.%)
1	50.72	42.91	6.26
2	53.23	35.11	11.56
3	52.13	30.84	16.93
4	49.68	28.35	21.87
5	46.92	26.76	26.22

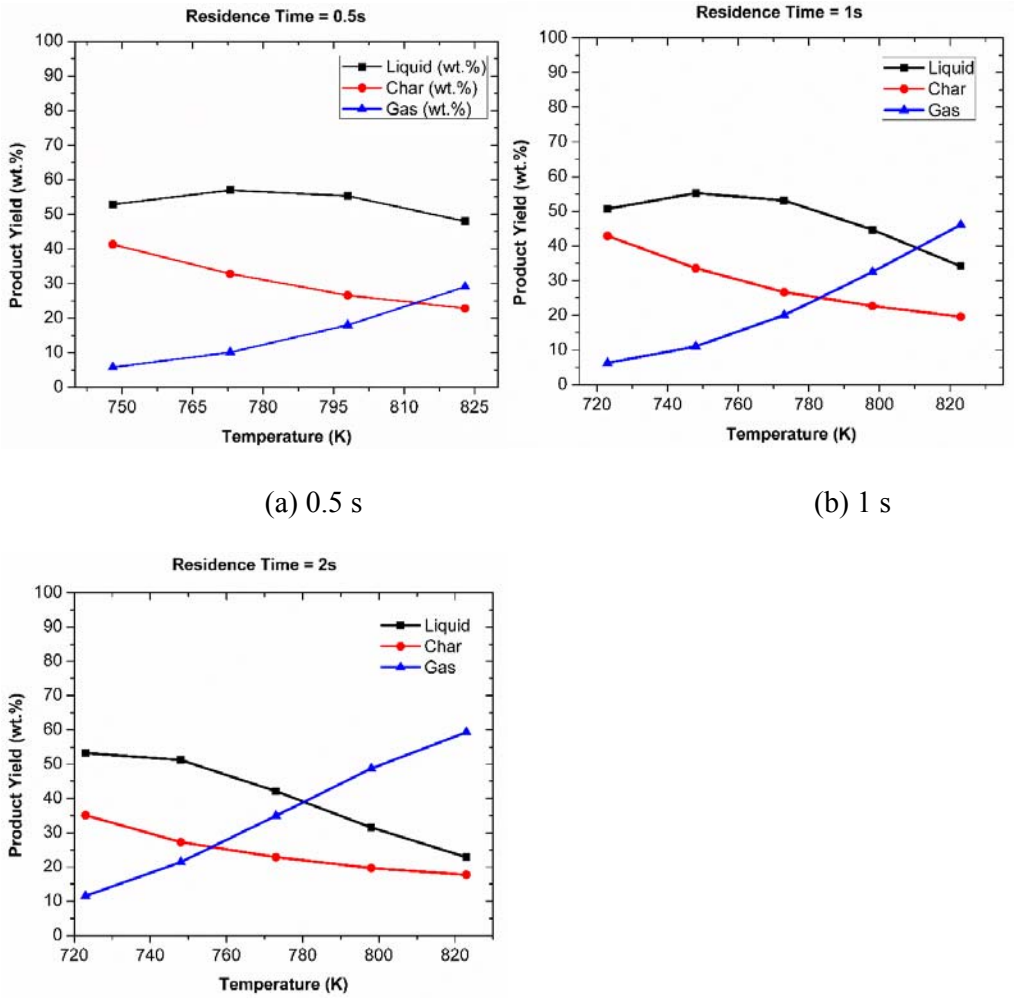

(a) 0.5 s (b) 1 s

(c) 2 s

Figure 4.11. Simulated product yields of EFB biomass fast pyrolysis at residence time (a) 0.5 s, (b) 1 s and (c) 2 s at the temperature in the range 723-823 K

4.3.2 Effect of residence time on product yields

Figure 4.11 shows the simulated liquid product yield of empty fruit bunch fast pyrolysis at reaction temperature in the range 723-823 K with different vapor residence time. The short vapor residence time of 0.5 s obtained the highest yield of liquid and char products at 723 K. The higher char product happens at short residence time of vapor because of unreacted fraction of biomass inside of the reactor. Therefore, the long vapor residence time need to avoid incomplete reaction mechanisms inside the reactor at lower temperature. The optimum liquid yield gave when an increase of vapor

residence time from 0.5 s to 2 s at 723 K. The short vapor residence time need to obtain optimum liquid product yield at high temperature. When the vapor residence time increase from 1 s to 2 s, the simulated liquid yield slightly decreased from 53.14 wt.% to 42.08 wt.% at 773 K (in Figure 4.12 (b)). Sulaiman et al., (2011) have studied product yields from fast pyrolysis of EFB biomass at optimum vapor residence time of 1.03 s and at 773 K. The simulated highest liquid product yield obtained about 47.99 wt.% at vapor residence time 0.5 s and 823 K. Mabrouki et al., (2015) studied the product yields from fast pyrolysis of EFB biomass at optimum vapor residence time 0.5 and at 823 K. The simulated optimum vapor residence time at 723 K, 773 K and 823 K occurred at 2 s, 1 s and 0.5 s, respectively. Therefore, the optimum liquid product yield from EFB fast pyrolysis was obtained either at long vapor residence time with lower temperature or short vapor residence time with higher temperature.

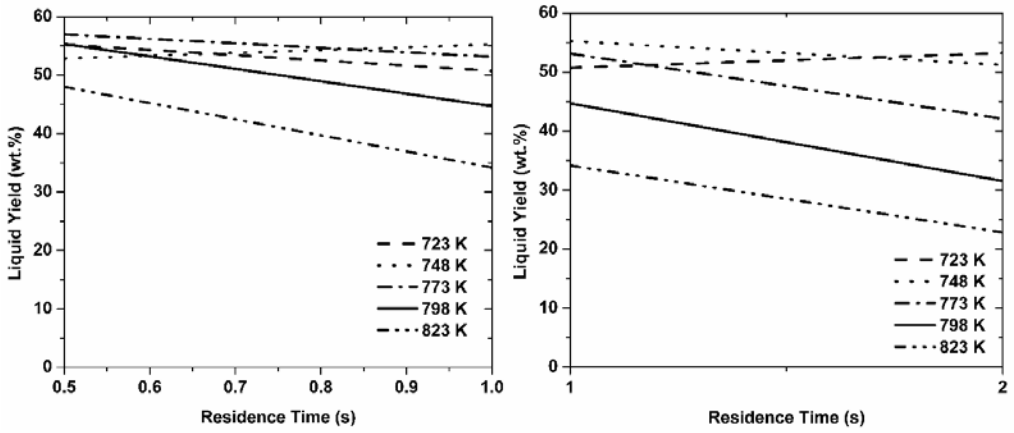

(a) 0.5-1 s (b) 1-2 s

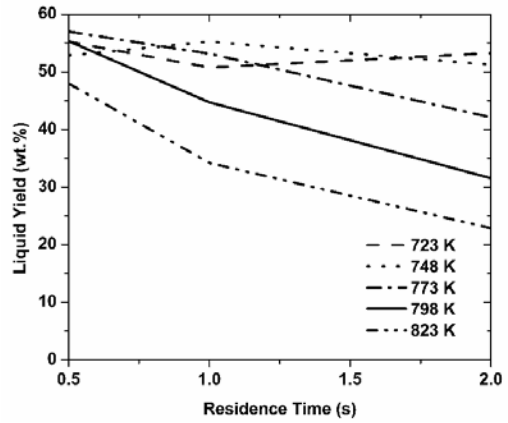

(c) 0.5-2 s

Figure 4.12. Liquid yield on EFB fast pyrolysis at vapor residence time in the range (a) 0.5-1 s, (b) 1-2 s and (c) 0.5-2 s with temperature range of 723-823 K

4.4 Model validation

Figure 4.13 shows the valid comparison between the simulated liquid, char, and gas product yields and reported experiment data of Sulaiman et al., (2011). The comparison maximum liquid product yields were 55.1 wt.% in reported experiment at 1.03 s and 55.4 wt.% at 0.79 s, respectively. The simulated liquid yield of 52.77 wt.% at 1.03 s was close to the maximum reported experimental liquid yield. The experimental liquid yield was increased from 50.58 wt.% to 55.14 wt.% at 0.79 s to 1.03 s and then it was decreased to 45. 32 s at 1.32 s. The simulated liquid yield was slightly decreased from 55.4 wt.% to 45.32 wt.% when an increase of vapor residence time 0.79 s to 1.32 s. The simulated liquid yields are good in agreement with reported experimental data at vapor residence time in the range 0.79-1.32 s as shown in Figure 4.13 (a). The short vapor residence time of 0.79 s was caused the higher char yield about 27.2 wt.% in reported experiment and 28.48 wt.% in simulation because of incomplete reaction mechanisms. The lower char yields occur at medium vapor residence time than short and long vapor residence time in reported experiment data. But char yield was decreased from 28.48 wt.% to 25.01 wt.% when an increase of vapor residence time from 0.79 to 1.32 s in simulation (Table 4.4). At 0.96 s, the simulation char yield was good agreement with reported experiment char yield nearly about 27 wt.% as shown in Figure 4.13 (b). The highest gas yields in both reported experiment and simulation were

found about 25.1 wt.% and 25.26 wt.% at the vapor residence time of 1.32 s. The longer vapor residence time cause the higher gas yield because volatile products converted into gas in secondary reaction. Therefore, the gas yield was higher than char and liquid yields at the longer vapor residence time in both reported experimental data and simulation data. Otherwise, lower gas product yield was found at the short vapor residence time. The simulated gas yield was slightly higher than the reported experiment gas yield when an increase of vapor residence time in the range 0.79-1.32 s, but the trend was consistent as shown in Figure 4.13 (c). According to the above facts, the comparison between simulated and reported experiment values were good in agreement on product yields of empty fruit bunch fast pyrolysis at 773 K.

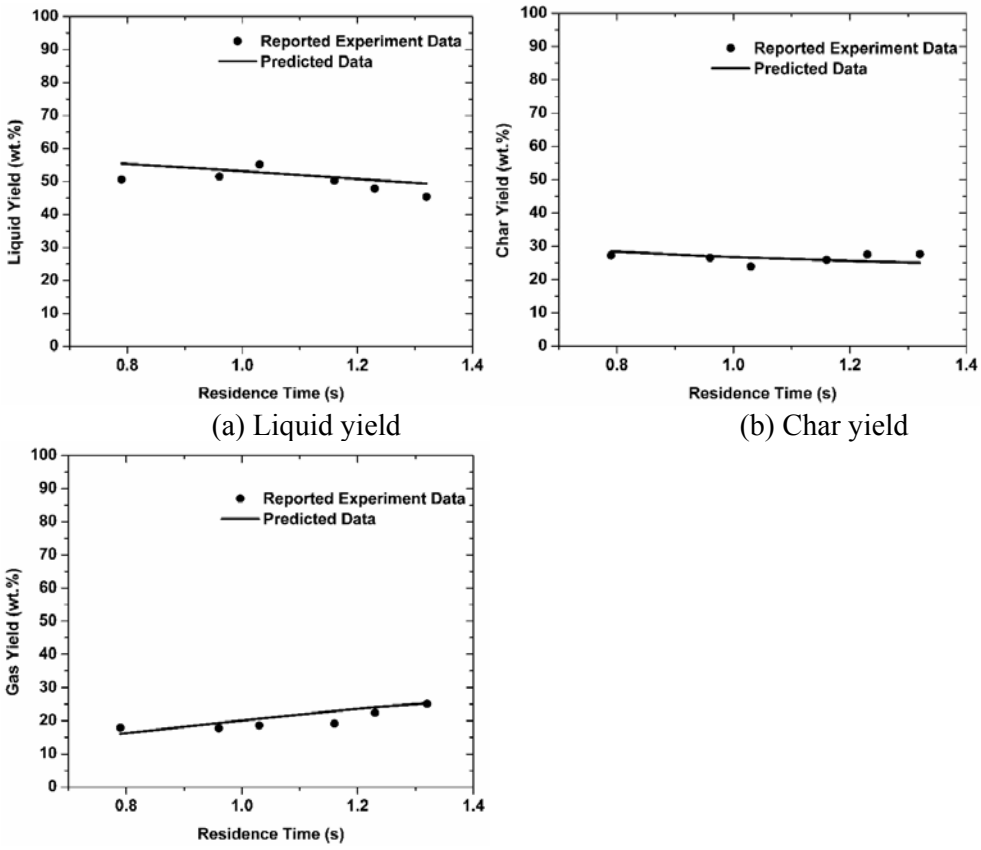

(a) Liquid yield (b) Char yield

(c) Gas yield

Figure 4.13. Valided comparison between reported experimental and simulated product yields of (a) liquid, (b) char and (c) gas

Table 4.4. Comparison between reported experimental and simulated product yields at the vapor residence time range of 0.79-1.32 s and at the reaction temperature of 773 K

Vapor residence time (s)	Reported liquid data	Simulated liquid data	Reported char data	Simulated char data	Reported gas data	Simulated gas data
0.79	50.6	55.40	27.2	28.48	17.9	16.02
0.96	51.5	53.61	26.5	26.99	17.7	19.03
1.03	55.1	52.77	23.9	26.53	18.6	20.60
1.16	50.2	51.24	25.9	25.76	19.1	22.90
1.23	47.8	50.39	27.5	25.41	22.4	24.10
1.32	45.3	49.32	27.6	25.01	25.1	25.57

CHAPTER 5

Conclusion

In this work, modeling of heat transfer and kinetic mechanisms are studied the effects of reaction parameters on the product yields for fast pyrolysis of empty fruit bunch biomass. The effects of minimum fluidization velocity, heat transfer coefficient, particle size, reaction temperature, and time parameters are studied on the heat transfer of biomass particle in heat transfer model. The minimum fluidization velocities for mixture of sand and EFB were predicted by using four authors correlations of Geldart Group B. The values of minimum fluidization velocity (U_{mf}) are estimated in the range over 0.086-0.153 m/s by four correlations at temperature in the range 723-873 K. The higher minimum fluidization velocity happened the higher heat transfer coefficient on small particle than large particle. Therefore, the high U_{mf} effected the excellent fluidization between sand and EFB particles that causes the good heat transfer of particle in EFB fast pyrolysis process. As a result, the heat transfer rate of EFB particle mainly depends on the U_{mf}. Collier et al., (2004) and Ranz et al., (1952) correlations are applied to calculate the heat transfer coefficient along the radius of the particle in the heat transfer conduction model. The average heat transfer coefficient of 550, 515 and 460 W/m^2K were applied for prediction on heat transfer of particle size in the range 150-500 μm, 250-355 μm and 300-355 μm, respectively. The small particle size of EFB biomass heat transfer are needed to complete for heat conduction along the radius of particle at lower reaction temperature and short vapor residence time. But, the complete heat transfer on large particle size happened at the higher reaction temperature and long vapor residence time. Therefore, the minimum fluidization velocity, heat transfer coefficient, particle size, reaction temperature and vapor residence time were affected mainly on the heat transfer for EFB fast pyrolysis process.

The effects of reaction kinetics parameters are studied to predict the product yields from fast pyrolysis of empty fruit bunch biomass in kinetics model. The prediction of product yields for EFB fast pyrolysis was simulated by using global kinetics scheme. The activation energy and preexponential factor for first-order irreversible reactions of the cellulose, hemicellulose, and lignin fast pyrolysis were found from academic works of literature for the global kinetic scheme (Diebold, 1994, Miller et al., 1996). The Arrhenius equation was chosen for each kinetic reaction

mechanisms of the cellulose, hemicellulose, and lignin. The model validation was performed the product yields between simulated and Sulaiman et al., (2011) data at 773 K reaction temperature and vapor residence time in the range 0.79-1.32 s. As well as, at 723 K, the optimal liquid yield from EFB fast pyrolysis has a simulation of vapor residence time around 2 s which is in a good agreement from many literatures (Agblevor et al., 2010, Tao et al., 2016 and Xiaoquan et al., 2005). The maximum simulated liquid yields of 773 K occur at vapor residence time 1 s. When the temperature increase to 873 K, the maximum liquid yields obtained at 0.5 s. The long vapor residence time gave lower liquid product yield and higher gas yields because of secondary reactions at the higher temperature. Therefore, the optimum liquid product yield from EFB fast pyrolysis was obtained either at long vapor residence time with lower temperature or short vapor residence time with higher temperature. Finally, the simulated results show that the maximum liquid product yields of reaction temperature at 723 K, 773 K and 873 K obtained at the vapor residence time of 2 s, 1 s and 0.5 s, respectively.

References

Abdullah, N., and Gerhauser, H., 2008. Bio-oil derived from empty fruit bunches. Fuel 87, 2606–2613.

Abdullah, N., and Bridgwater, A.V., 2006. Pyrolysis liquid derived from oil palm empty fruit bunches. Journal of Physical Science 17, 117–129.

Abdullah, N., Gerhauser, H., and Sulaiman, F., 2010. Fast pyrolysis of empty fruit bunches. Fuel 89, 2166–2169.

Agblevor, F.A., Beis, S., Kim, S.S., Tarrant, R., and Mante, N.O., 2010. Biocrude oils from the fast pyrolysis of poultry litter and hardwood. Waste Management 30, 298–307.

Asadieraghi, M., and Daud, W.M.A.W., 2015. In-depth investigation on thermochemical characteristics of palm oil biomasses as potential biofuel sources. Journal of Analytical Applied Pyrolysis 115, 379–391.

Asadullah, M., Rasid, N.S.A., Kadir, S.A.S.A., and Azdarpour, A., 2013. Production and detailed characterization of bio-oil from fast pyrolysis of palm kernel shell. Biomass and Bioenergy 59, 316- 324.

Basu, P., 2004. Biomass gasification and pyrolysis: Practical design and theory.

Bin, A.K., 1994. Prediction of the minimum fluidization velocity. Powder Technology 81, 197–199.

Blasi, C.D., 1993a. Modeling and simulation of combustion processes of charring and non-charring solid fuels. Progress in Energy and Combustion Science 19, 71–104.

Blasi, C.D., 1993b. Analysis of convection and secondary reaction effect effects within porous solid fuels undergoing pyrolysis. Combustion Science Technology 90, 315–339.

Bourgeois, P., and Grenier, P., 1968. The ratio of terminal velocity to minimum fluidizing velocity for spherical particles. The Canadian Journal of Chemical Engineering 46, 325–334.

Chan, W.R., Kelbon, M., and Krieger, B.B., 1985. Modelling and experimental verification of physical and chemical processes during pyrolysis of large biomass particle. Fuel 64, 1505–1513.

Choi, G.G., Oh S.J., Lee, S.J., and Kim, J.S., 2015. Production of bio-based phenolic resin and activated carbon from bio-oil and biochar derived from fast pyrolysis of palm kernel shells. Bioresource Technology 178, 99–107.

Collier, A.R., Hayhurst, A.N., Richardson, J.L., and Scott, S.A., 2004. The heat transfer coefficient between a particle and a bed (packed or fluidised) of much larger particles. Chemical Engineering Scienc 59, 4613–4620.

COMSOL Group., 2008. COMSOL Multiphysics.

Demirbas, A., 2000. Mechanisms of liquefaction and pyrolysis reactions of biomass. Energy Conversion Management 41, 633-646.

Diebold, J.P., 1994. Unified A. Global model for the pyrolysis of cellulose. Biomass and Bioenergy 7, 75-85.

Dong, N.H., Luo, K.H., and Wang, Q., 2017. Modeling of biomass pyrolysis in a bubbling fluidized bed reactor: Impact of intra-particle heat conduction. Fuel Processing Technology 161, 199–203.

Dupont, C., Chiriac, R., Gauthier, G., and Toche, F., 2014. Heat capacity measurements of various biomass types and pyrolysis residues. Fuel 115, 644–651.

Eri, Q., Zhao, X., Ranganathan, P., and Gu, S., 2017. Numerical simulations on the effect of potassium on the biomass fast pyrolysis in fluidized bed reactor. Fuel 197, 290–297.

Erik, O., Franklin, D.J., Holbrook, L.H., and Henry, H.R., 2012. Machinery's handbook 29th edition. Industrial press. New York.

Gupta, M., Yang, J., and Roy, C., 2003. Specific heat and thermal conductivity of softwood bark and softwood char particles. Fuel 82, 919–927.

Hilal, N., Ghannam, M.T., and Anabtawi, M.Z., 2001. Effect of bed diameter, distributor and inserts on minimum fluidization velocity. Chemical Engineering Technology 24, 161.

Humbird, D., Trendewicz, A., Braun, R., and Dutta, A., 2017. One-dimensional biomass fast pyrolysis model with reaction kinetics integrated in an aspen plus biorefinery process model. ACS Sustainable Chemistry and Engineering 5, 2463−2470.

Jahirul, M.I., Rasul, M.G., Chowdhury, A.A., and Ashwath, N., 2012. Biofuels production through biomass pyrolysis. Energies 5, 4952-5001.

Jeong, J.Y., Lee, U.D., Chang, W.S., and Jeong, S.H., 2016. Production of bio-oil rich in acetic acid and phenol from fast pyrolysis of palm residues using a fluidized bed reactor: Influence of activated carbons. Bioresource Technology 219, 357–364.

Kim, S.J., Jung, S.H., and Kim, J.S., 2010. Fast pyrolysis of palm kernel shells: Influence of operation parameters on the bio-oil yield and the yield of phenol and phenolic compounds. Bioresource Technology 101, 9294–9300.

Kim, S., and Kim, C.H., 2013. Bioethanol production using the sequential acid/alkali-pretreated empty palm fruit bunch fiber. Renewable Energy 54, 150–155.

Kim, S.W., Koo, B.S., Ryu J.W., Lee, J.S., Kim, C.J., Lee, D.H., Kim, G.R, Choi, S., 2013. Bio-oil from the pyrolysis of palm and Jatropha wastes in a fluidized bed. Fuel Processing Technology 108, 18–124.

Kim, S.W., Koo, B.S., and Lee, D.H., 2014. Catalytic pyrolysis of palm kernel shell waste in a fluidized bed. Bioresource Technology 167, 425–432.

Liden, A.G., Berruti, F., and Scott, D.S., 1988. A kinetic model for the production of liquids from the flash pyrolysis of biomass. Chemical Engineering Communications 65, 207–221.

Liu, B., Papadikis, K., Gu, S., Fidalgo, B., Longhurst, P., Li, Z., and Kolios, A., 2017. CFD modelling of particle shrinkage in a fluidized bed for biomass fast pyrolysis with quadrature method of moment. Fuel Processing Technology 164, 51–68.

Lv, P.M., Xiong, Z.H., Chang, J., Wu, C.Z., Chen, Y., and Zhu, J.X., 2004. An experimental study on biomass air-stem gasification in a fluidized bed. Bioresource Technology 95, 95-101.

Mabrouki, J., Abbassi, M.A., Guedri, K., Omeri, A., and Jeguirim, M., 2015. Simulation of biofuel production via fast pyrolysis of palm oil residues. Fuel 159, 819-827.

Matta, J., Bronson, B., Gogolek, P.E.G., Mazerolle, D., Thibault, J., and Mehrani, P., 2017. Comparison of multi-component kinetic relations on bubbling fluidized-bed woody biomass fast pyrolysis reactor model performance. Fuel 210, 625–638.

Miller, R.S., and Bellan, J.A., 1996. A generalized biomass pyrolysis model based on superimposed cellulose, hemicellulose and lignin kinetics. Combustion Science and Technology 126, 97-137.

Mohamed, A.R., Hamzah, Z., Daud, M.Z.M., and Zakaria, Z., 2013. The effects of holding time and the sweeping nitrogen gas flowrates on the pyrolysis of efb using a fixed bed reactor. Procedia Engineering 53, 185–191.

Ngo, T.A., Kim, J., and Kim, S.S., 2013. Fast pyrolysis of palm kernel cake using a fluidized bed reactor: Design of experiment and characteristics of bio-oil. Journal of Industrial and Engineering Chemistry 19, 137–143.

Papadikis, K., Gu, S., Bridgwater, A.V., and Gerhauser, H., 2009a. Application of CFD to model fast pyrolysis of biomass. Fuel Processing Technology 90, 504–512.

Papadikis, K., Gu, S., and Bridgwater, A.V., 2009b. CFD modelling of the fast pyrolysis of biomass in fluidised bed reactors. Part B Heat, momentum and mass transport in bubbling fluidised beds. Chemical Engineering Science 64, 1036–1045.

Papadikis, K., Gu, S., Bridgwater, A.V., and Gerhauser, H., 2010. Computational modelling of the impact of particle size to the heat transfer coefficient between biomass particles and a fluidised bed. Fuel Processing Technology 91, 68–79.

Prasentsan, S., and Prasentsan, P., 1996. Biomass residues from palm oil mills in Thailand: An overview on quantity and potential usage. Biomass and Bioenergy 11, 387-395.

Ranz, W.E., and W.R. Marshall, W.R., 1952. Evaporation from drops - Part 1. Chemical Engineering Progress 48, 141–148.

Ranzi, E., Cuoci, A., Faravelli, T., Frassoldati, A., Migliavacca, G., Pierucci, S., and Sommariva, S., 2008. Chemical kinetics of biomass pyrolysis. Energy Fuels 22, 4292–4300.

Ranzi, E., Corbetta, M., Manenti, F., and Pierucci, S., 2014. Kinetic modeling of the thermal degradation and combustion of biomass. Chemical Engineering Science 110, 2–12.

Salema, A.A., and Afzal, M.T., 2015. Numerical simulation of heating behaviour in biomass bed and pellets under multimode microwave system. International Journal of Thermal Science 91, 12–24.

Sembiring, K.C., Rinaldi, N., and Simanungkalit, S.P., 2015. Bio-oil from fast pyrolysis of empty fruit bunch at various temperature. Energy Procedia 65, 162–169.

Shafizadeh, F., and Bradbury, A.G., 1979. Thermal degradation of cellulose in air and nitrogen at low temperature. Journal of Applied Polymer Science 23, 1432–1442.

Silalertruksa, T., Gheewala, S.H., Pongpat, P., Kaenchan, P., Permpool, N., Lecksiwilai, N., and Mungkung, R., 2016. Environmental sustainability of oil palm cultivation in different regions of Thailand: Greenhouse gases and water use impact. Journal of Cleaner Production 167, 1009-1019.

Sulaiman, F., and Abdullah, N., 2011. Optimum conditions for maximising pyrolysis liquids of oil palm empty fruit bunches. Energy 36, 2352–2359.

Tao, K., Vladimir, S., and Tim, J.E., 2016. Lignocellulosic biomass pyrolysis: A review of product properties and effects of pyrolysis parameters. Renewable and Sustainable Energy Reviews 57, 1126–1140.

Vaid, R.P., and Gupta, P.S., 1978. Minimum fluidization velocities in beds of mixed solids. The Canadian Journal of Chemical Engineering 56, 292–296.

Velden, M.V.D., Baeyens, J., Brems, A., Janssens, B., and Dewil, R., 2010. Fundamentals, kinetics and endothermicity of the biomass pyrolysis reaction. Renewable Energy 35, 232–242.

Wen, C.Y., and Yu, Y.H., 1966. A generalized method for predicting the minimum fluidization velocity. AICHE Journal 12.

Xue, Q., Heindel, T.J., and Fox, R.O., 2011. A CFD model for biomass fast pyrolysis in fluidized-bed reactors. Chemical Engineering Science 66, 2440–2452.

Xue, Q., Dalluge, D., Heindel, T.J., Fox, R.O., and Brown, R.C., 2012. Experimental validation and CFD modeling study of biomass fast pyrolysis in fluidized-bed reactors. Fuel 97, 757–769.

Xiaoquan, W., Sascha, R.A.K., Wolter, P., and Wim, P.M.S., 2005. Biomass Pyrolysis in a Fluidized Bed Reactor. Part 2: Experimental Validation of Model Results. Industrial and Engineering Chemistry Research 44, 8786-8795.

Xiong, Q., and Kong, S.C., 2014a. Modeling effects of interphase transport coefficients on biomass pyrolysis in fluidized beds. Powder Technology 262, 96–105.

Xiong, Q., Aramideh, S., Passalacqua, A., Kong, S.C., 2014b. BIOTC: An open-source CFD code for simulating biomass fast pyrolysis. Computer Physics Communications 185, 1739–1746.

Yaman, S., 2004. Pyrolysis of biomass to produce fuels and chemical feedstocks. Energy Conversion and Management 45, 651-671.

Appendix A

Parameters estimation for heat transfer model

A.1. Minimum Fluidization Velocity (U_{mf})

A.1.1. U_{mf} calculation at 723 K

$\mu_g = 3.275\times10^{-5}$ kg/ms, $\rho_g = 0.478$ kg/m^3, $\rho_s = 2500$ kg/m^3, $d_s = 427.5$ μm, $g = 9.81$ m/s^2

$$U_{mf} = \frac{Re_{mf}\times\mu_g}{\rho_g\times d_s}$$

$$Ar = \frac{g\times\rho_g\times(\rho_s-\rho_g)\times d_s^3}{\mu_g^2}$$

$$Ar = \frac{9.81\times0.478\times(2500-0.478)\times(427.5\times10^{-6})^3}{(3.275\times10^{-5})^2} = 853.77$$

(a) Bin correlation

$Re_{mf} = (27.31^2+0.0386Ar)^{0.5}-27.31 = 0.597$

$$U_{mf} = \frac{0.597\times3.275\times10^{-5}}{0.478\times427.5\times10^{-6}} = 0.096 \text{ m/s}$$

(b) Bourgies correlation

$Re_{mf} = (25.46^2+0.0382Ar)^{0.5}-25.46=0.633$

$$U_{mf} = \frac{0.633\times3.275\times10^{-5}}{0.478\times427.5\times10^{-6}} = 0.101 \text{ m/s}$$

(c) Halal correlation

$Re_{mf} = (13.07^2+0.0263Ar)^{0.5}-13.07 = 0.832$

$$U_{mf} = \frac{0.832\times3.275\times10^{-5}}{0.478\times427.5\times10^{-6}} = 0.133 \text{ m/s}$$

(d) Vaid correlation

$Re_{mf} = (24^2+0.0546Ar)^{0.5}-24 = 0.952$

$$U_{mf} = \frac{0.952 \times 3.275 \times 10^{-5}}{0.478 \times 427.5 \times 10^{-6}} = 0.153 \text{ m/s}$$

Table A1. Estimated U_{mf} at 723 K

Correlations	Ar	Re_{mf}	U_{mf} (m/s)
Bin	853.77	0.597	0.096
Bourgies	853.77	0.633	0.101
Hilal	853.77	0.832	0.133
Vaid	853.77	0.952	0.153

A.1.2. U_{mf} calculation at 748 K

$\mu_g = 3.343 \times 10^{-5}$ kg/ms, $\rho_g = 0.462$ kg/m^3, $\rho_s = 2500$ kg/m^3, $d_s = 427.5$ μm, $g = 9.81$ m/s^2

$$U_{mf} = \frac{Re_{mf} \times \mu_g}{\rho_g \times d_s}$$

$$Ar = \frac{g \times \rho_g \times (\rho_s - \rho_g) \times d_s^3}{\mu_g^2}$$

$$Ar = \frac{9.81 \times 0.462 \times (2500 - 0.462) \times (427.5 \times 10^{-6})^3}{(3.343 \times 10^{-5})^2} = 791.97$$

(a) Bin correlation

$Re_{mf} = (27.31^2+0.0386Ar)^{0.5}-27.31 = 0.554$

$$U_{mf} = \frac{0.554 \times 3.343 \times 10^{-5}}{0.462 \times 427.5 \times 10^{-6}} = 0.094 \text{ m/s}$$

(b) Bourgies correlation

$Re_{mf} = (25.46^2+0.0382Ar)^{0.5}-25.46 = 0.587$

$$U_{mf} = \frac{0.587 \times 3.343 \times 10^{-5}}{0.462 \times 427.5 \times 10^{-6}} = 0.099 \text{ m/s}$$

(c) Halal correlation

$Re_{mf} = (13.07^2+0.0263Ar)^{0.5}-13.07 = 0.774$

$$U_{mf} = \frac{0.774 \times 3.343 \times 10^{-5}}{0.462 \times 427.5 \times 10^{-6}} = 0.131 \text{ m/s}$$

(d) Vaid correlation

$Re_{mf} = (24^2+0.0546Ar)^{0.5}-24 = 0.885$

$$U_{mf} = \frac{0.885 \times 3.343 \times 10^{-5}}{0.462 \times 427.5 \times 10^{-6}} = 0.150 \text{ m/s}$$

Table A2. Estimated U_{mf} at 748 K

Correlations	Ar	Re_{mf}	U_{mf} (m/s)
Bin	791.97	0.554	0.094
Bourgies	791.97	0.587	0.099
Hilal	791.97	0.774	0.131
Vaid	791.97	0.885	0.150

A.1.3. U_{mf} calculation at 773 K

$\mu_g = 3.411 \times 10^{-5}$ kg/ms, $\rho_g = 0.445$ kg/m^3, $\rho_s = 2500$ kg/m^3, $d_s = 427.5$ μm, $g = 9.81$ m/s^2

$$U_{mf} = \frac{Re_{mf} \times \mu_g}{\rho_g \times d_s}$$

$$Ar = \frac{g \times \rho_g \times (\rho_s - \rho_g) \times d_s^3}{\mu_g^2}$$

$$Ar = \frac{9.81 \times 0.445 \times (2500 - 0.445) \times (427 \times 10^{-6})^3}{(3.411 \times 10^{-5})^2} = 732.72$$

(a) Bin correlation

$Re_{mf} = (27.31^2 + 0.0386Ar)^{0.5} - 27.31 = 0.513$

$$U_{mf} = \frac{0.513 \times 3.411 \times 10^{-5}}{0.445 \times 427.5 \times 10^{-6}} = 0.092 \text{ m/s}$$

(b) Bourgies correlation

$Re_{mf} = (25.46^2 + 0.0382Ar)^{0.5} - 25.46 = 0.544$

$$U_{mf} = \frac{0.544 \times 3.411 \times 10^{-5}}{0.445 \times 427.5 \times 10^{-6}} = 0.098 \text{ m/s}$$

(c) Halal correlation

$Re_{mf} = (13.07^2 + 0.0263Ar)^{0.5} - 13.07 = 0.718$

$$U_{mf} = \frac{0.718 \times 3.411 \times 10^{-5}}{0.445 \times 427.5 \times 10^{-6}} = 0.129 \text{ m/s}$$

(d) Vaid correlation

$Re_{mf} = (24^2 + 0.0546Ar)^{0.5} - 24 = 0.819$

$$U_{mf} = \frac{0.819 \times 3.411 \times 10^{-5}}{0.445 \times 427.5 \times 10^{-6}} = 0.147 \text{ m/s}$$

Table A3. Estimated U_{mf} at 773 K

Correlations	Ar	Re_{mf}	U_{mf} (m/s)
Bin	732.72	0.513	0.092
Bourgies	732.72	0.544	0.098
Hilal	732.72	0.718	0.129
Vaid	732.72	0.819	0.147

A.1.4. U_{mf} calculation at 798 K

$\mu_g = 3.479\times10^{-5}$ kg/ms, $\rho_g = 0.429$ kg/m^3, $\rho_s = 2500$ kg/m^3, $d_s = 427.5$ μm, $g = 9.81$ m/s^2

$$U_{mf} = \frac{Re_{mf} \times \mu_g}{\rho_g \times d_s}$$

$$Ar = \frac{g \times \rho_g \times (\rho_s - \rho_g) \times d_s^3}{\mu_g^2}$$

$$Ar = \frac{9.81 \times 0.429 \times (2500 - 0.429) \times (427.5\times10^{-6})^3}{(3.479\times10^{-5})^2} = 679.03$$

(a) Bin correlation

$Re_{mf} = (27.31^2+0.0386Ar)^{0.5}-27.31 = 0.476$

$$U_{mf} = \frac{0.476\times3.479\times10^{-5}}{0.429\times427.5\times10^{-6}} = 0.090 \text{ m/s}$$

(b) Bourgies correlation

$Re_{mf} = (25.46^2+0.0382Ar)^{0.5}-25.46 = 0.504$

$$U_{mf} = \frac{0.504\times3.479\times10^{-5}}{0.429\times427.5\times10^{-6}} = 0.096 \text{ m/s}$$

(c) Halal correlation

$Re_{mf} = (13.07^2+0.0263Ar)^{0.5}-13.07 = 0.666$

$$U_{mf} = \frac{0.666 \times 3.479 \times 10^{-5}}{0.429 \times 427.5 \times 10^{-6}} = 0.126 \text{ m/s}$$

(d) Vaid correlation

$Re_{mf} = (24^2 + 0.0546Ar)^{0.5} - 24 = 0.760$

$$U_{mf} = \frac{0.760 \times 3.479 \times 10^{-5}}{0.429 \times 427.5 \times 10^{-6}} = 0.144 \text{ m/s}$$

Table A4. Estimated U_{mf} at 798 K

Correlations	Ar	Re_{mf}	U_{mf} (m/s)
Bin	679.03	0.476	0.090
Bourgies	679.03	0.504	0.096
Hilal	679.03	0.666	0.126
Vaid	679.03	0.760	0.144

A.1.5.U_{mf} calculation at 823 K

$\mu_g = 3.545 \times 10^{-5}$ kg/ms, $\rho_g = 0.417$ kg/m^3, $\rho_s = 2500$ kg/m^3, $d_s = 427.5$ μm, $g = 9.81$ m/s^2

$$U_{mf} = \frac{Re_{mf} \times \mu_g}{\rho_g \times d_s}$$

$$Ar = \frac{g \times \rho_g \times (\rho_s - \rho_g) \times d_s^3}{\mu_g^2}$$

$$Ar = \frac{9.81 \times 0.417 \times (2500 - 0.417) \times (427.5 \times 10^{-6})^3}{(3.545 \times 10^{-5})^2} = 635.69$$

(a) Bin correlation

$Re_{mf} = (27.31^2 + 0.0386Ar)^{0.5} - 27.31 = 0.446$

$$U_{mf} = \frac{0.446 \times 3.545 \times 10^{-5}}{0.417 \times 427.5 \times 10^{-6}} = 0.089 \text{ m/s}$$

(b) Bourgies correlation

$Re_{mf} = (25.46^2 + 0.0382Ar)^{0.5} - 25.46 = 0.473$

$$U_{mf} = \frac{0.473 \times 3.545 \times 10^{-5}}{0.417 \times 427.5 \times 10^{-6}} = 0.094 \text{ m/s}$$

(c) Halal correlation

$Re_{mf} = (13.07^2 + 0.0263Ar)^{0.5} - 13.07 = 0.625$

$$U_{mf} = \frac{0.625 \times 3.545 \times 10^{-5}}{0.417 \times 427.5 \times 10^{-6}} = 0.124 \text{ m/s}$$

(d) Vaid correlation

$Re_{mf} = (24^2 + 0.0546Ar)^{0.5} - 24 = 0.713$

$$U_{mf} = \frac{0.713 \times 3.545 \times 10^{-5}}{0.417 \times 427.5 \times 10^{-6}} = 0.142 \text{ m/s}$$

Table A5. Estimated U_{mf} at 823 K

Correlations	Ar	Re_{mf}	U_{mf} (m/s)
Bin	635.69	0.446	0.089
Bourgies	635.69	0.473	0.094
Hilal	635.69	0.625	0.124
Vaid	635.69	0.713	0.142

A.1.6.U_{mf} calculation at 848 K

$\mu_g = 3.611 \times 10^{-5}$ kg/ms, $\rho_g = 0.405$ kg/m^3, $\rho_s = 2500$ kg/m^3, $d_s = 427.5$ μm, $g = 9.81$ m/s^2

$$U_{mf} = \frac{Re_{mf} \times \mu_g}{\rho_g \times d_s}$$

$$Ar = \frac{g \times \rho_g \times (\rho_s - \rho_g) \times d_s^3}{\mu_g^2}$$

$$Ar = \frac{9.81 \times 0.405 \times (2500 - 0.405) \times (427.5 \times 10^{-6})^3}{(3.611 \times 10^{-5})^2} = 595.04$$

(a) Bin correlation

$Re_{mf} = (27.31^2 + 0.0386Ar)^{0.5} - 27.31 = 0.417$

$$U_{mf} = \frac{0.417 \times 3.611 \times 10^{-5}}{0.405 \times 427.5 \times 10^{-6}} = 0.087 \text{ m/s}$$

(b) Bourgies correlation

$Re_{mf} = (25.46^2 + 0.0382Ar)^{0.5} - 25.46 = 0.443$

$$U_{mf} = \frac{0.443 \times 3.611 \times 10^{-5}}{0.405 \times 427.5 \times 10^{-6}} = 0.092 \text{ m/s}$$

(c) Halal correlation

$Re_{mf} = (13.07^2 + 0.0263Ar)^{0.5} - 13.07 = 0.586$

$$U_{mf} = \frac{0.586 \times 3.611 \times 10^{-5}}{0.405 \times 427.5 \times 10^{-6}} = 0.122 \text{ m/s}$$

(d) Vaid correlation

$Re_{mf} = (24^2 + 0.0546Ar)^{0.5} - 24 = 0.668$

$$U_{mf} = \frac{0.668 \times 3.611 \times 10^{-5}}{0.405 \times 427.5 \times 10^{-6}} = 0.139 \text{ m/s}$$

Table A6. Estimated U_{mf} at 848 K

Correlations	Ar	Re_{mf}	U_{mf} (m/s)
Bin	595.04	0.417	0.087
Bourgies	595.04	0.443	0.092
Hilal	595.04	0.586	0.122
Vaid	595.04	0.668	0.139

A.1.7. U_{mf} calculation at 873 K

$\mu_g = 3.677\times10^{-5}$ kg/ms, $\rho_g = 0.393$ kg/m^3, $\rho_s = 2500$ kg/m^3, $d_s = 427.5$ μm, $g = 9.81$ m/s^2

$$U_{mf} = \frac{Re_{mf}\times\mu_g}{\rho_g\times d_s}$$

$$Ar = \frac{g\times\rho_g\times(\rho_s-\rho_g)\times d_s^3}{\mu_g^2}$$

$$Ar = \frac{9.81\times0.393\times(2500-0.393)\times(427.5\times10^{-6})^3}{(3.677\times10^{-5})^2} = 556.87$$

(a) Bin correlation

$Re_{mf} = (27.31^2+0.0386Ar)^{0.5}-27.31 = 0.391$

$$U_{mf} = \frac{0.391\times3.677\times10^{-5}}{0.393\times427.5\times10^{-6}} = 0.086 \text{ m/s}$$

(b) Bourgies correlation

$Re_{mf} = (25.46^2+0.0382Ar)^{0.5}-25.46 = 0.414$

$$U_{mf} = \frac{0.414\times3.677\times10^{-5}}{0.393\times427.5\times10^{-6}} = 0.091 \text{ m/s}$$

(c) Halal correlation

$Re_{mf} = (13.07^2+0.0263Ar)^{0.5}-13.07= 0.545$

$$U_{mf} = \frac{0.545\times3.677\times10^{-5}}{0.393\times427.5\times10^{-6}} = 0.119 \text{ m/s}$$

(d) Vaid correlation

$Re_{mf} = (24^2+0.0546Ar)^{0.5}-24= 0.625$

$$U_{mf} = \frac{0.625\times3.677\times10^{-5}}{0.393\times427.5\times10^{-6}} = 0.137 \text{ m/s}$$

Table A7. Estimated U_{mf} at 873 K

Correlations	Ar	Re_{mf}	U_{mf} (m/s)
Bin	556.87	0.391	0.086
Bourgies	556.87	0.414	0.091
Hilal	556.87	0.545	0.119
Vaid	556.87	0.625	0.137

Table A8. Estimated U_{mf} by four correlations at 723-873 K

Temperature (K)	U_{mf} by Bin Correlation	U_{mf} by Bourgies Correlation	U_{mf} by Hilal Correlation	U_{mf} by Vaid Correlation
723	0.096	0.101	0.133	0.153
748	0.094	0.099	0.131	0.15
773	0.092	0.098	0.129	0.147
798	0.09	0.096	0.126	0.144
823	0.089	0.094	0.124	0.142
848	0.087	0.092	0.122	0.139
873	0.086	0.091	0.119	0.137

Table A9. Relationship between Ar and Re_{mf} by four correlations

Ar	Re_{mf} by Bin Correlation	Re_{mf} by Bourgies Correlation	Re_{mf} by Hilal Correlation	Re_{mf} by Vaid Correlation
853.77	0.597	0.633	0.832	0.952
791.97	0.554	0.587	0.774	0.885
732.72	0.513	0.544	0.718	0.819
679.03	0.476	0.504	0.666	0.76
635.69	0.446	0.473	0.625	0.713
595.04	0.417	0.443	0.586	0.668
556.87	0.391	0.414	0.545	0.625

A.2. Heat Transfer Coefficient

Table A10. Two types of correlation for heat transfer coefficient (h) calculation

Case	Correlation	Equation
$d_p < d_s$	Collier	$h = (k_g/d_p) \times (2+0.9Re^{0.62}(d_p/d_s)^{0.2})$
$d_p > d_s$	Ranz-Marshall	$h = (k_g/d_p) \times (2+0.6Re_d^{1/2}Pr^{1/3})$

$$Re = \frac{(\rho_g \times U_{mf} \times d_b)}{\mu_g}, \quad Pr = \frac{\mu_g \times Cp_g}{k_g}$$

Table A11. Estimated h at 723 K

Correlations and U_{mf}	Particle Size (μm)	Re	Pr	h(W/m^2K)
Bin (0.096 m/s)	150	0.210	-	789.45
	250	0.350	-	503.71
	300	0.420	-	431.54
	355	0.497	-	375.30
	500	0.701	0.695	254.28
Baurgies (0.101 m/s)	150	0.221	-	792.58
	250	0.369	-	506.63
	300	0.442	-	434.27
	355	0.523	-	377.94
	500	0.737	0.695	255.45
Hilal (0.133 m/s)	150	0.291	-	811.04

	250	0.485	-	523.37
	300	0.582	-	450.57
	355	0.689	-	393.78
	500	0.971	0.695	262.47
Vaid (0.153 m/s)	150	0.335	-	821.78
	250	0.558	-	533.17
	300	0.670	-	460.04
	355	0.793	-	402.97
	500	1.117	0.695	266.42

Table A12. Estimated h at 748 K

Correlations and U_{mf}	Particle Size (μm)	Re	Pr	h(W/m^2K)
Bin (0.094 m/s)	150	0.195	-	815.37
	250	0.325	-	518.99
	300	0.390	-	444.18
	355	0.461	-	385.84
	500	0.650	0.687	262.10
Baurgies (0.099 m/s)	150	0.205	-	818.37
	250	0.342	-	521.78
	300	0.410	-	446.83
	355	0.486	-	388.56
	500	0.684	0.687	263.29

Hilal (0.131 m/s)	150	0.272	-	837.22
	250	0.453	-	538.88
	300	0.543	-	463.35
	355	0.643	-	404.54
	500	0.905	0.687	270.39
Vaid (0.150 m/s)	150	0.301	-	844.82
	250	0.501	-	545.76
	300	0.601	-	470.07
	355	0.711	-	410.99
	500	1.002	0.687	273.23

Table A13. Estimated h at 773 K

Correlations and U_{mf}	Particle Size (μm)	Re	Pr	h(W/m^2K)
Bin (0.092 m/s)	150	0.184	-	827.03
	250	0.307	-	525.52
	300	0.368	-	449.37
	355	0.436	-	390.16
	500	0.614	0.692	265.74
Baurgies (0.098 m/s)	150	0.196	-	830.77
	250	0.327	-	528.94
	300	0.392	-	452.68
	355	0.464	-	393.32

	500	0.654	0.692	267.21
Hilal (0.129 m/s)	150	0.258	-	848.88
	250	0.430	-	545.39
	300	0.516	-	468.66
	355	0.611	-	408.85
	500	0.860	0.692	274.14
Vaid (0.147 m/s)	150	0.294	-	858.62
	250	0.490	-	554.28
	300	0.588	-	477.26
	355	0.696	-	417.17
	500	0.980	0.692	277.79

Table A14. Estimated h at 798 K

Correlations and U_{mf}	Particle Size (μm)	Re	Pr	h(W/m^2K)
Bin (0.090 m/s)	150	0.166	-	836.17
	250	0.222	-	519.22
	300	0.333	-	452.49
	355	0.394	-	392.28
	500	0.555	0.697	268.17
Baurgies (0.096 m/s)	150	0.178	-	840.13
	250	0.296	-	533.13
	300	0.355	-	455.69

	355	0.420	-	395.38
	500	0.592	0.697	269.62
Hilal (0.126 m/s)	150	0.233	-	857.11
	250	0.388	-	548.69
	300	0.466	-	470.82
	355	0.552	-	410.13
	500	0.777	0.697	276.27
Vaid (0.144 m/s)	150	0.266	-	866.56
	250	0.444	-	557.46
	300	0.533	-	479.29
	355	0.630	-	418.21
	500	0.888	0.697	279.88

Table A15. Estimated h at 823 K

Correlations and U_{mf}	Particle Size (μm)	Re	Pr	h(W/m^2K)
Bin (0.089 m/s)	150	0.157	-	848.01
	250	0.262	-	536.34
	300	0.314	-	457.68
	355	0.372	-	396.55
	500	0.523	0.701	271.65
Baurgies (0.094 m/s)	150	0.166	-	851.10
	250	0.276	-	538.97

	300	0.332	-	460.42
	355	0.393	-	399.16
	500	0.553	0.701	272.88
Hilal (0.124 m/s)	150	0.219	-	868.18
	250	0.365	-	554.67
	300	0.438	-	475.49
	355	0.518	-	413.73
	500	0.729	0.701	279.53
Vaid (0.142 m/s)	150	0.251	-	877.72
	250	0.418	-	563.33
	300	0.501	-	483.78
	355	0.593	-	421.83
	500	0.835	0.701	283.15

Table A16. Estimated h at 848 K

Correlations and U_{mf}	Particle Size (μm)	Re	Pr	h(W/m^2K)
Bin (0.087 m/s)	150	0.146	-	858.94
	250	0.244	-	542.22
	300	0.293	-	462.39
	355	0.346	-	400.13
	500	0.488	0.706	274.90
Baurgies (0.092 m/s)	150	0.155	-	862.17

	250	0.258	-	544.97
	300	0.310	-	465.09
	355	0.366	-	402.73
	500	0.516	0.706	276.12
Hilal (0.122 m/s)	150	0.205	-	878.99
	250	0.342	-	560.43
	300	0.410	-	479.93
	355	0.486	-	417.34
	500	0.684	0.706	282.79
Vaid (0.139 m/s)	150	0.234	-	888.02
	250	0.390	-	568.61
	300	0.468	-	487.90
	355	0.553	-	424.89
	500	0.799	0.706	286.90

Table A17. Estimated h at 873 K

Correlations and U_{mf}	Particle Size (μm)	Re	Pr	h(W/m^2K)
Bin (0.086 m/s)	150	0.138	-	870.76
	250	0.230	-	548.71
	300	0.276	-	467.56
	355	0.326	-	404.33
	500	0.460	0.710	278.84
Baurgies (0.091 m/s)	150	0.146	-	873.75

	250	0.243	-	551.37
	300	0.292	-	470.20
	355	0.345	-	406.90
	500	0.486	0.710	280.03
Hilal (0.119 m/s)	150	0.191	-	889.53
	250	0.318	-	565.77
	300	0.382	-	484.13
	355	0.452	-	420.48
	500	0.636	0.710	286.37
Vaid (0.137 m/s)	150	0.220	-	898.96
	250	0.366	-	574.31
	300	0.439	-	492.31
	355	0.520	-	428.48
	500	0.732	0.710	290.04

Appendix B

Product yields at different reaction temperature (K) and various residence time (s)

Table B1. Product compositions at temperature 723 K

Residence time (s)	Vapor (wt. %)	Active Cellulose (wt. %)	Active Lignin (wt. %)	Char (wt. %)	Gas (wt. %)	Water (wt. %)	Tar (wt. %)
0.5	27.38	42.03	17.09	6.80	3.98	1.88	0.74
1	33.91	29.42	16.02	9.24	6.26	3.22	1.83
2	38.22	14.42	14.06	12.40	11.56	4.81	4.43
3	36.62	7.07	12.34	14.26	16.93	5.59	7.09
4	32.78	3.47	10.84	15.43	21.87	5.97	9.54
5	28.38	1.69	9.52	16.23	26.22	6.16	11.70

Table B2. Product yields at temperature 723 K

Residence Time (s)	Liquid (wt.%)	Char (wt.%)	Gas (wt.%)
0.5	55.22	40.70	3.98
1	50.72	42.91	6.26
2	53.23	35.11	11.56
3	52.13	30.84	16.93
4	49.68	28.35	21.87
5	46.92	26.76	26.22

Table B3. Product compositions at temperature 748 K

Residence time (s)	Vapor (wt. %)	Active Cellulose (wt. %)	Active Lignin (wt. %)	Char (wt. %)	Gas (wt. %)	Water (wt. %)	Tar (wt. %)
0.5	36.95	27.21	16.00	8.97	5.77	3.59	1.41
1	41.68	12.36	14.02	12.15	11.06	5.23	3.40
1.5	40.25	5.62	12.28	13.90	16.44	5.97	5.44
2	36.53	2.55	10.76	14.96	21.44	6.32	7.34

Table B4. Product yields at temperature 748 K

Residence Time (s)	Liquid (wt.%)	Char (wt.%)	Gas (wt.%)
0.5	52.83	41.30	5.77
1	55.25	33.59	11.06
1.5	53.91	29.55	16.44
2	51.21	27.25	21.44

Table B5. Product compositions at temperature 773 K

Residence time (s)	Vapor (wt. %)	Active Cellulose (wt. %)	Active Lignin (wt. %)	Char (wt. %)	Gas (wt. %)	Water (wt. %)	Tar (wt. %)
0.5	44.42	11.38	14.12	11.85	10.12	5.54	2.47
1	40.28	2.17	10.91	14.50	20.05	6.59	5.40
1.5	32.40	0.42	8.43	15.62	28.36	6.79	7.88
2	25.39	0.08	6.51	16.32	34.94	6.83	9.83

Table B6. Product yields at temperature 773 K

Residence Time (s)	Liquid (wt.%)	Char (wt.%)	Gas (wt.%)
0.5	56.98	32.80	10.12
1	53.14	26.71	20.05
1.5	47.24	24.30	28.36
2	42.08	22.88	34.94

Table B7. Product compositions at temperature 798 K

Residence time (s)	Vapor (wt. %)	Active Cellulose (wt. %)	Active Lignin (wt. %)	Char (wt. %)	Gas (wt. %)	Water (wt. %)	Tar (wt. %)
0.2	45.00	15.75	15.07	10.49	7.08	5.21	1.30
0.4	45.97	4.15	12.40	13.36	14.44	6.58	3.00
0.5	43.83	2.13	11.25	14.07	17.98	6.82	3.82
0.6	41.17	1.09	10.21	14.56	21.32	6.95	4.60
0.8	35.58	0.29	8.40	15.26	27.32	7.04	6.01
1	30.40	0.08	6.91	15.74	32.50	7.06	7.21
2	13.42	0	2.61	17.06	48.71	7.08	11.02

Table B8. Product yields at temperature 798 K

Residence Time (s)	Liquid (wt.%)	Char (wt.%)	Gas (wt.%)
0.2	57.81	35.01	7.08
0.4	57.21	28.25	14.44
0.5	55.32	26.60	17.98
0.6	53.16	25.42	21.32
0.8	48.75	23.83	27.32
1	44.70	22.70	32.50
2	31.52	19.67	48.71

Table B9. Product compositions at temperature 823 K

Residence time (s)	Vapor (wt. %)	Active Cellulose (wt. %)	Active Lignin (wt. %)	Char (wt. %)	Gas (wt. %)	Water (wt. %)	Tar (wt. %)
0.1	45.80	16.53	15.35	10.07	6.00	5.28	0.87
0.2	48.36	4.57	12.85	12.95	12.4	6.74	2.03
0.3	44.88	1.26	10.76	14.14	18.55	7.14	3.17
0.4	40.18	0.35	9.01	14.79	24.12	7.25	4.20
0.5	35.56	0.10	7.54	15.24	29.07	7.28	5.11
1	18.6	0.00	3.10	16.50	46.13	7.29	8.28
2	4.78	0.00	0.53	17.20	59.34	7.29	10.76

Table B10. Product yields at temperature 823 K

Residence Time (s)	Liquid (wt.%)	Char (wt.%)	Gas (wt.%)
0.1	58.56	35.34	6.00
0.2	58.96	28.54	12.40
0.3	55.69	25.66	18.55
0.4	51.77	24.01	24.12
0.5	47.99	22.84	29.07
1	34.17	19.60	46.13
2	22.83	17.73	59.34

Table B11. Product compositions at temperature 848 K

Residence time (s)	Vapor (wt. %)	Active Cellulose (wt. %)	Active Lignin (wt. %)	Char (wt. %)	Gas (wt. %)	Water (wt. %)	Tar (wt. %)
0.1	50.00	5.50	13.41	12.52	10.33	6.81	1.33
0.2	44.36	0.51	9.80	14.37	20.59	7.44	2.83
0.3	36.73	0.05	7.15	15.13	29.23	7.5	4.11
0.4	30.07	0	5.22	15.63	36.32	7.50	5.16

Table B12. Product yields at temperature 848 K

Residence Time (s)	Liquid (wt.%)	Char (wt.%)	Gas (wt.%)
0.1	60.34	29.23	10.33
0.2	54.83	24.48	20.59
0.3	48.36	22.31	29.23
0.4	42.73	20.85	36.32

Table B13. Product compositions at temperature 873 K

Residence time (s)	Vapor (wt. %)	Active Cellulose (wt. %)	Active Lignin (wt. %)	Char (wt. %)	Gas (wt. %)	Water (wt. %)	Tar (wt. %)
0.05	50.76	7.05	14.03	12.03	8.40	6.79	0.84
0.1	47.85	0.83	10.71	14.00	17.07	7.59	1.85
0.15	41.70	0.10	8.18	14.72	24.76	7.68	2.76
0.2	35.84	0.01	6.25	15.19	31.38	7.70	3.53

Table B14. Product yields at temperature 873 K

Residence Time (s)	Liquid (wt.%)	Char (wt.%)	Gas (wt.%)
0.05	61.21	30.29	8.40
0.1	57.62	25.21	17.07
0.15	52.18	22.96	24.76
0.2	47.07	21.45	31.38

B.2 Validation simulated data at 773 K and at 0.79-1.32 s

Table B15. Product compositions at 0.79-1.32s and 773 K

Residence time (s)	Vapor (wt. %)	Active Cellulose (wt. %)	Active Lignin (wt. %)	Char (wt. %)	Gas (wt. %)	Water (wt. %)	Tar (wt. %)
0.79	43.11	4.35	12.16	13.71	16.02	6.34	4.21
0.96	40.87	2.47	11.14	14.37	19.30	6.55	5.20
1.03	39.82	1.96	10.75	14.60	20.60	6.61	5.56
1.16	37.78	1.28	10.05	14.94	22.90	6.70	6.25
1.23	36.66	1.02	9.70	15.10	24.10	6.72	6.60
1.32	35.22	0.76	9.25	15.30	25.57	6.75	7.05

Table B16. Product yields at temperature 873 K

Residence Time (s)	Liquid (wt.%)	Char (wt.%)	Gas (wt.%)
0.79	55.40	28.48	16.02
0.96	53.61	26.99	19.03
1.03	52.77	26.53	20.60
1.16	51.24	25.76	22.90
1.23	50.39	25.41	24.10
1.32	49.32	25.01	25.57

Appendix C

Manuscript 1

Authors : Kyaw Thu, Taweesak Reungpeerakul, Chayanoot Sangwichien.

Title : Simulation of Heat Transfer and Reaction Kinetics Effects on Product Yields from Fast Pyrolysis of Oil Palm Empty Fruit Bunch Biomass in Fluidized Bed Reactor.

Journal Name : Biomass Conversion and Biorefinery

Simulation of Heat Transfer and Reaction Kinetics Effects on Product Yields from Fast Pyrolysis of Oil Palm Empty Fruit Bunch Biomass in Fluidized Bed Reactor

Kyaw Thu[1], Taweesak Reungpeerakul[2], Chayanoot Sangwichien[1]

[1]Department of Chemical Engineering, Faculty of Engineering, Prince of Songkla University, Hat Yai, Thailand

[2]Department of Computer Engineering, Faculty of Engineering, Prince of Songkla University, Hat Yai, Thailand

Correspondence: chayanoot.sangwichien@gmail.com

Abstract

This present work aimed to study the modeling of biofuel production from the empty fruit bunch (EFB) biomass by fast pyrolysis. The heat diffusion equation and global chemical kinetic scheme were used to model the heat conduction along the radius of an isotropic EFB particle and to predict yields of three products (bio-oil, gas and char) over the EFB particle size range 300-355 μm at the reaction temperature range of 748-798 K. The heat transfer in solids and chemical reaction engineering module were chosen to predict the effects of reaction parameters in finite element based COMSOL Multiphysics 4.3b software. The results show that the surface and center reaction temperatures of isotropic EFB particles gave a suitable reaction time across the particle sizes. The predicted pyrolysis product yields for various vapor residence times were compared with reported experiment yields. The heat transfer and product yield simulations for fast pyrolysis of EFB were in good agreement with reported experimental data.

Keywords: empty fruit bunch (EFB), fast pyrolysis, heat transfer, kinetic, mathematical modeling

INTRODUCTION

Palm oil is the most widely cultivated as a source of oil around the world. The world largest cultivation of palm oil is found in the South East Asia countries [1]. Thailand is the world's third-largest country of palm oil plantation. An increase of the global oil palm plantation area occurred from 10 to 17 million hectares between 2000 and 2012 [2]. In Thailand, palm oil plantation area increased from 0.4 to 0.7 million hectares between 2006 and 2012. This plantation area produced 10.94 million tons of fresh fruit bunches in 2012 [3]. The oil plantation area will be increased up to 1.5 million hectares in 2050 according to the Ministry of Agriculture and Cooperatives (MOAC)'s plan [4]. As a result, oil palm mills are significantly increased about 36% from 2007 to 2012 [3].

Palm press fiber (PPF), palm kernel shell (PKS), decanter cakes, empty fruit bunch (EFB) and palm oil mill effluent are produced as five type of wastes at oil palm mill. Among these waste, large quantities of EFB waste are openly dumped in the oil palm mill area and emitted methane [5]. In the past, solid wastes from palm oil mills are disposed by the landfilling method, which is very difficult to store and costly to manage. In some factories, these wastes are burnt in the furnaces, which causes air pollution. Many local people in Thailand are against an EFB combustion project because of relatively high costs of investment and operation [4]. The conversion of wastes into renewable energy is an effective way to solve this problem. EFB can be converted into renewable energy. The two alternatives of renewable energy production from biomass are biochemical and thermochemical processes. Thermochemical process has been popular in the last decades, helping to reduce the need of landfills and producing energy. Pyrolysis is the popular thermochemical process for liquid fuel production from biomass and takes place at ambient pressure in the absence of oxygen.

The main three types of pyrolysis processes are slow (conventional), fast and flash, differing in operating conditions such as reaction temperature, heating rate, nitrogen flow rate, residence time and particle size [6]. The reactor also plays an important role in any pyrolysis process. Fluidized bed reactors are most widely used in pyrolysis process because of its advantages.

Modeling of the design and operating parameters of these reactor have been widely studied in the past. A kinetic model with heat transfer equations are modeled to evaluate the effect of operating parameters in the yield of the process. Simple, global and advanced kinetic models have been applied to reaction kinetics modeling in the fast pyrolysis of lignocellulose biomass. In simple kinetic model, a single type of biomass is decomposed to the three main products tar, char, and non-condensable gas. The tar product degrades to char and gas products in the secondary pyrolysis reactions. Many authors have been studied to predict the yield of products by coupling a simple kinetic model with a heat transfer model in the bed [7, 8]. Chan *et al.* [9] and Blasi [10] studied kinetic rate parameters in a first-order reaction model of the simple kinetic scheme.

Shafizadeh and Bradbury [11] proposed a global kinetic model. In this developed kinetic model, the three major constituents of biomass (cellulose, hemicellulose, and lignin) degrade to solid active intermediate products in the primary pyrolysis reactions, and then these active intermediate products decompose to the final pyrolysis products (tar, char and non-condensable gas) in secondary pyrolysis reactions**.** Diebold [12] proposed degradation reaction mechanisms in the pyrolysis of cellulose. The feedstock cellulose decomposed via two reactions: scission of active cellulose polymers to low degree of polymerization (DP) cellulose and forming char and gas products. This low DP cellulose product would then react to produce secondary gas, primary vapor and dehydrated products. The primary vapor was permitted to form secondary gas and tar products. Miller and Bellan [13] reported degradation reaction mechanisms in hemicellulose and lignin pyrolysis. The virgin feedstock of hemicellulose and lignin would form active materials. To form vapor and char with gas, two reactions were would crack the active material. In a secondary reaction, vapor would be converted to gas products. Several authors have been studied to predict the formation of final products by coupling a global kinetic model with a heat transfer model in the fluidized bed reactor [14-16]. Ranzi *et al.* [17] developed the detail pyrolysis reactions for fast pyrolysis of cellulose, hemicellulose, and lignin in an advanced kinetic model. The main purpose of this model is to predict the pyrolysis product species [18-20].

In this work, the global kinetics model with heat diffusion model are used to optimize the effects of operating parameters (such as minimum fluidization velocity, heat transfer coefficient, particle size, reaction temperature and vapor residence time) for fast pyrolysis of EFB particles for the fluidized bed reactor. The simulation results are compared with reported experimental data.

METHODOLOGY

Simulation Model and Parameters

EFB biomass was used as feedstock material in this study. The EFB particles were assumed to be spherical in shape. In the simulation, the particle size was kept in the range from 300 to 355 μm, and the reaction temperature was kept in the range of 748-798 K, while various vapor residence times were tested. The simulation utilized heat transfer in solids and reaction engineering modules in COMSOL Multiphysics 4.3b software. The heat transfer inside a particle was by diffusion from surface to center. Both heat transfer and reaction kinetics of fast EFB pyrolysis were considered transient. The simulation parameters are shown in Table 1.

TABLE 1 Simulation parameters

No.	Name	Symbol	Value	References
1.	Density of EFB	ρ_b	800 kg/m^3	[21]
2.	Thermal conductivity of EFB	k_b	0.03 W/mK	[21]
3.	Specific heat capacity of EFB	C_b	1150 J/kgK	[21]
4.	Density of sand	ρ_p	2500 kg/m^3	[22]
5.	Specific heat capacity of char	C_{pc}	1004 J/kgK	[23]
6.	Thermal conductivity of char	k_c	0.062 W/mK	[24]
7.	Heat of reaction	$-\Delta H$	410800 J/kg	[25]
8.	Diameter of EFB particle	D_b	300-355 μm	[26]
9.	Nitrogen viscosity	μ_g	3.411×10^{-5} kg/ms	At 773K
10.	Nitrogen density	ρ_g	0.445 kg/m^3	At 773K
11.	Nitrogen thermal conductivity	k_g	0.0563 W/mK	At 773K

Literature Experimental Procedure

Sulaiman *et al.* [26] studied the bio-oil production from EFB by fast pyrolysis in a fluidized bed bench-scale reactor. In their work, the length and diameter of the stainless-steel (type 316) cylinder reactor were 260 mm and 40 mm, respectively. The sand used as a fluidization inert particle with the size in the range of 355-500 μm and filled the reactor to a depth of approximately 8 cm. Nitrogen gas was not only applied for the fluidization of sand and biomass particles but also as a carrier of hot gases during fast pyrolysis process. A cyclone was used to separate the char from the product stream. The condensable vapor from the product stream were collected by using two cooled condensers, an electrostatic precipitator and a cotton wool filter in the liquid collection system. The non-condensable gases were passed through a gas meter and were then sampled by gas chromatography to evaluate the quality and type of gas produced. Figure 1 shows a schematic diagram of the fluidized bed pyrolysis system.

Kinetic Scheme for EFB Fast Pyrolysis

The reaction kinetics for fast pyrolysis of biomass constituents were modeled using the global scheme as shown in Figure 2. Diebold [12] studied seven global reaction mechanisms in the pyrolysis of cellulose (Figure 2A). Miller and Bellan [13] reported on multi-component global reaction mechanisms in the pyrolysis of hemicellulose (Figure 2B) and lignin (Figure 2C). The reaction kinetics parameters of first-order irreversible reactions by cellulose, hemicellulose, and lignin were found from literature for the global kinetic scheme [12,13]. Each reaction kinetics mechanism of cellulose, hemicellulose, and lignin pyrolysis was assumed to follow the Arrhenius Equation (1). Table 2 shows the activation energies and pre-exponential factors for cellulose, hemicellulose, and lignin, for use in a global kinetic scheme to model fast EFB pyrolysis. Table 3 shows the mass fraction contents of cellulose, hemicellulose, and lignin in different oil palm residues. The reaction rate equations for the fast pyrolysis of cellulose, hemicellulose and lignin are shown in Equations (2-18).

$$K_i = A_i \exp(-E_i / RT) \quad (1)$$

Here K_i, A_i, and E_i are reaction rate, pre-exponential factor, and activation energy. The

gas constant and reaction temperature are represented by R and T, respectively.

$$\frac{dC_{cellulose}}{dt} = -(k_1 + k_2)C_{cellulose} \quad (2)$$

$$\frac{dC_{active-cellulose}}{dt} = k_1 C_{cellulose} - (k_3 + k_4 + k_5)C_{active-cellulose} \quad (3)$$

$$\frac{dC_{vapor}}{dt} = k_4 C_{active-cellulose} - k_6 C_{gas} - k_7 C_{tar} \quad (4)$$

$$\frac{dC_{gas}}{dt} = k_3 C_{active-cellulose} + k_6 C_{vapor} \quad (5)$$

$$\frac{dC_{tar}}{dt} = k_7 C_{vapor} \quad (6)$$

$$\frac{dC_{H_2O}}{dt} = 0.4k_2 C_{cellulose} + 0.4k_5 C_{active-cellulose} \quad (7)$$

$$\frac{dC_{char}}{dt} = 0.6k_2 C_{cellulose} + 0.6k_5 C_{active-cellulose} \quad (8)$$

$$\frac{dC_{hemicellulose}}{dt} = -k_8 C_{hemicellulose} \quad (9)$$

$$\frac{dC_{active-hemicellulose}}{dt} = k_8 C_{hemicellulose} - (k_9 + k_{10})C_{active-hemicellulose} \quad (10)$$

$$\frac{dC_{vapor}}{dt} = k_9 C_{active-hemicellulose} - k_{11} C_{vapor} \quad (11)$$

$$\frac{dC_{gas}}{dt} = 0.4k_{10} C_{active-hemicellulose} + k_{11} C_{vapor} \quad (12)$$

$$\frac{dC_{char}}{dt} = 0.6k_{10} C_{active-hemicellulose} \quad (13)$$

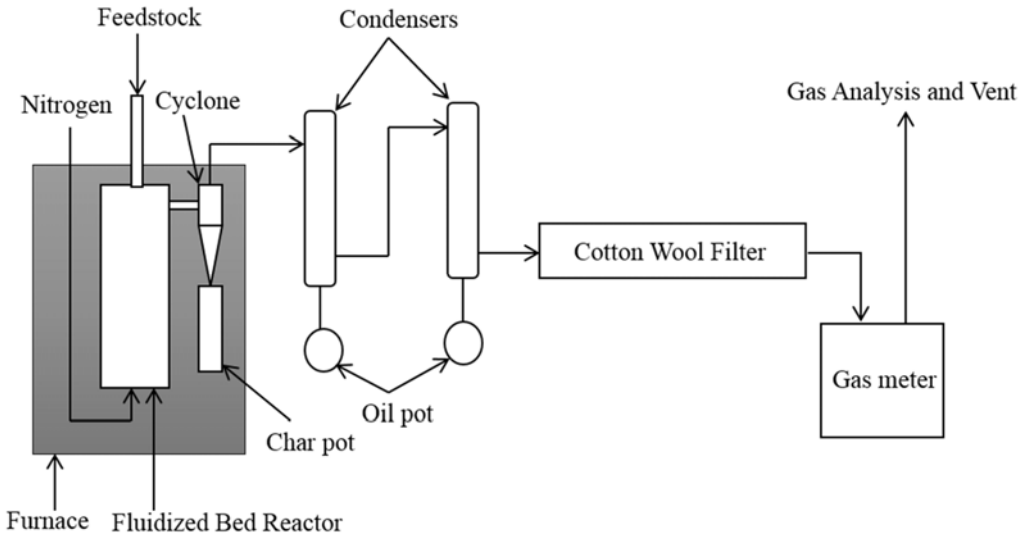

FIGURE 1 Diagram of the fluidized bed pyrolysis system from the work of Sulaiman *et al.*[26]

TABLE 2 Reaction kinetics parameters for fast pyrolysis [12,13]

Pyrolysis reactions	Pre-exponential factor (s^{-1})	Activation energy (kJ mol^{-1})
Cellulose to active cellulose	2.8×10^{19}	240
Cellulose to 0.6Char + 0.4H_2O	6.7×10^{5}	110
Active cellulose to Gas	3.6×10^{11}	200
Active cellulose to Vapors	6.8×10^{9}	140
Active cellulose to 0.6Char + 0.4H_2O	1.3×10^{10}	150
Vapors to Gas	3.6×10^{11}	200
Vapors to Tar	1.8×10^{3}	61
Hemicellulose to Active Hemicellulose	2.1×10^{16}	186.7

Active Hemicellulose to Vapors	8.75×10^{15}	202.4
Active Hemicellulose to 0.6Char + 0.4Gas	2.6×10^{11}	145.7
Vapors to Gas	4.28×10^{6}	108.0
Lignin to Active Lignin	9.6×10^{8}	107.6
Active Lignin to Vapors	1.5×10^{9}	143.8
Active Lignin to 0.75Char + 0.25Gas	7.7×10^{6}	111.4
Vapors to Gas	4.28×10^{6}	108.0

TABLE 3 The linocellulosic contents of different part of the oil palm [26-28]

z	EFB	Mesocarp fiber	Palm shell	Oil palm fronds
Cellulose	59.7	23.7	27.7	44
Hemicellulose	22.1	30.5	21.6	30.4
Lignin	18.1	27.3	44	15.4

$$\frac{dC_{lignin}}{dt} = -k_{12}C_{lignin} \quad (14)$$

$$\frac{dC_{active-lignin}}{dt} = k_{12}C_{lignin} - (k_{13}+k_{14})C_{active-lignin} \quad (15)$$

$$\frac{dC_{vapor}}{dt} = k_{13}C_{active-lignin} - k_{15}C_{vapor} \quad (16)$$

$$\frac{dC_{gas}}{dt} = 0.25k_{14}C_{active-lignin} + k_{15}C_{vapor} \quad (17)$$

$$\frac{dC_{char}}{dt} = 0.75k_{14}C_{active-lignin} \quad (18)$$

Where C is the mass concentration of species.

Heat Transfer Model for EFB Fast Pyrolysis

The heat transfer in EFB particles was simulated with the heat diffusion equation. Equation (19) was applied for heat conduction along the radius of an isotropic spherical EFB particle.

$$\frac{\partial}{\partial t}(\rho Cp_{eff}T) = \frac{1}{r^2}\frac{\partial}{\partial r}(k_{eff}r^2\frac{\partial T}{\partial r}) + (-\Delta H)(\frac{\partial \rho}{\partial r}) \quad (19)$$

where the effective thermal conductivity (k_{eff}) and effective specific heat capacity (Cp_{eff}) are given by Equations (20) and (21),

$$k_{eff} = k_c + |k_b - k_c|\alpha_b \quad (20)$$

$$Cp_{eff} = Cp_c + |Cp_b - Cp_c|\alpha_b \quad (21)$$

where k_c, k_b, Cp_c, Cp_b and α_b were the char thermal conductivity, biomass thermal conductivity, char specific heat capacity, biomass specific heat capacity and biomass mass fraction.

The boundary conditions on surface and at center of the EFB particle were set as follows,

$$-k_{eff}\left.\frac{\partial T}{\partial r}\right|_{r=R} = h(T_i - T_s) \quad (22)$$

$$\left.\frac{\partial T}{\partial r}\right|_{r=0} = 0 \quad (23)$$

where T_i, T_s, and h are ambient temperature, surface temperature and the film heat transfer coefficient.

The heat transfer coefficient for biomass particle size (d_b) below the sand particle size (d_s) was estimated from a modified Nusselt number, by using a well-known correlation of Collier *et al.* [29]. Equation (24) enables estimating the heat transfer coefficient based on biomass and sand particle diameters.

$$h = (\frac{k_g}{d_b}) \times (2 + 0.9\,Re^{0.62}(\frac{d_b}{d_s})^{0.2}) \quad (24)$$

where the dimensionless Reynold number (Re) is defined as,

$$Re = \frac{(\rho_g \times U_{mf} \times d_b)}{\mu_g} \quad (25)$$

Where μ_g, ρ_g, and U_{mf} are viscosity of gas, density of gas and minimum fluidization velocity, respectively.

Wan and Yu [30] developed an Ergun equation for calculation the minimum fluidization velocity (U_{mf}), shown in Equations (26) to (28). Equation (29-32) show four correlations of the Geldart B group to estimate the dimensionless Reynolds (Re_{mf}) according to the properties of fluidization inert particle [31-34].

$$U_{mf} = \frac{Re_{mf} \times \mu_g}{\rho_g \times d_s} \quad (26)$$

$$Re_{mf} = (K_1^2 + K_2 Ar)^{0.5} - K_1 \quad (27)$$

$$Ar = \frac{(g \times \rho_g \times (\rho_s - \rho_g) \times d_s^3)}{\mu_g^2} \quad (28)$$

$$Re_{mf} = (27.31^2 + 0.0386Ar)^{0.5} - 27.31 \quad (29)$$

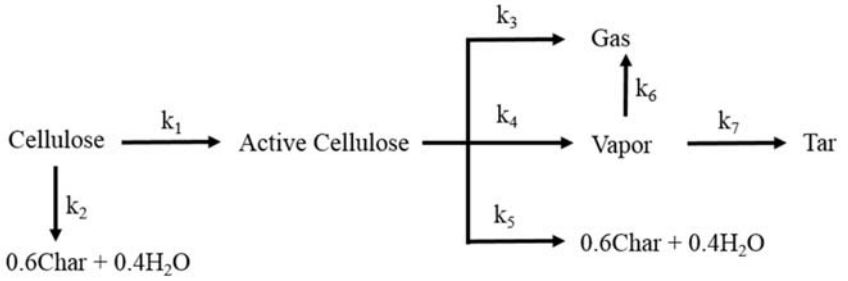

(A)

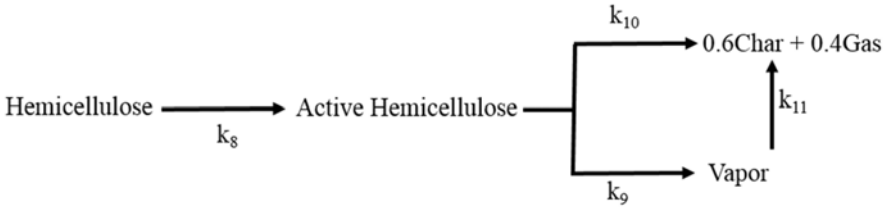

(B)

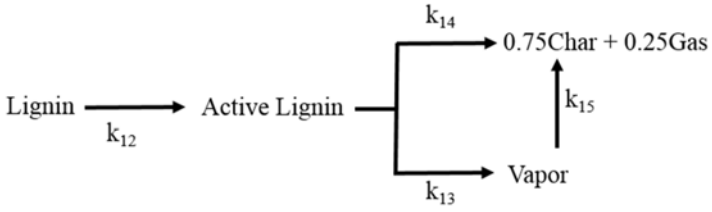

(C)

FIGURE 2 Degradation pathways for fast pyrolysis of (A) Cellulose (B) Hemicellulose and (C) Lignin [11, 12]

$$Re_{mf} = (25.46^2 + 0.0382Ar)^{0.5} - 25.46 \quad (30)$$

$$Re_{mf} = (13.07^2 + 0.0263Ar)^{0.5} - 13.07 \quad (31)$$

$$Re_{mf} = (24.00^2 + 0.0546Ar)^{0.5} - 24.00 \quad (32)$$

where K_1, K_2, ρ_s, d_s and g are empirical constant 1, and 2, sand particle density, sand particle diameter and gravitational acceleration constant, respectively.

RESULTS AND DISCUSSION

Effect of Minimum Fluidization Velocity (U_{mf}) on Heat Transfer in EFB Pyrolysis

The minimum fluidization velocity is important to the heat transfer in fast pyrolysis of EFB biomass. It depends on the particle size and the reaction temperature. Chiou et al. [35] studied the effects of temperature and particle size distribution on minimum fluidization velocity estimates for silica sand in the particle size range 400-1100 µm. A higher minimum fluidization velocity was required with narrow particle size distribution at temperatures below 473 K. Fluidization facilities provided an increased heat transfer on the particle surface, through which heat diffuses towards the center on the particle. The minimum fluidization velocity decreased with an increase in temperature up to 1073 K, and the particle size had a strong effect on U_{mf}. Basu and Zhi [36] mentioned a relationship of Archimedes number (in the range of 100-1000) and Reynolds number (in the range of 0.1-1). In

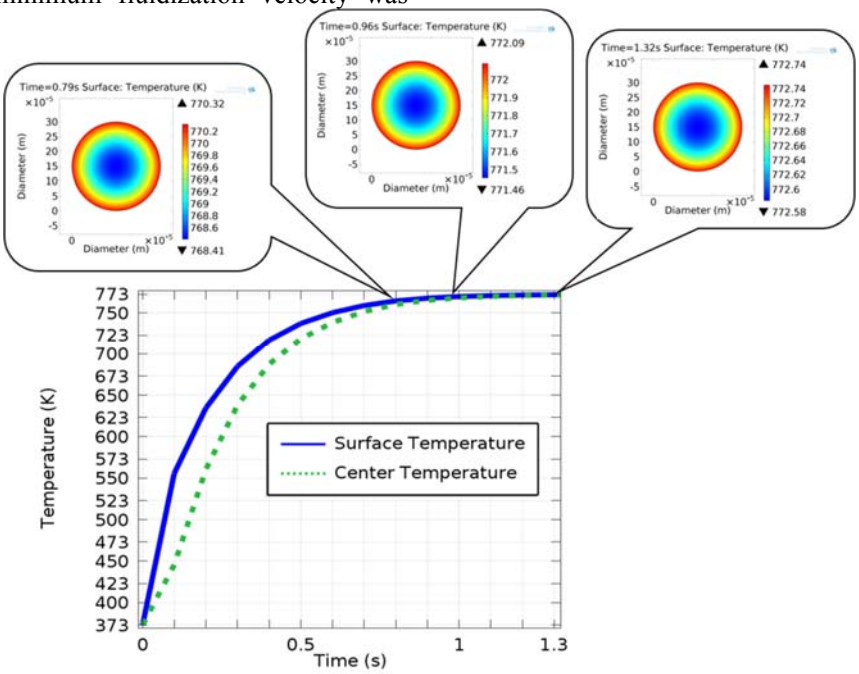

FIGURE 3 Simulated time profiles of temperature in a 300 µm sized EFB particle during pyrolysis

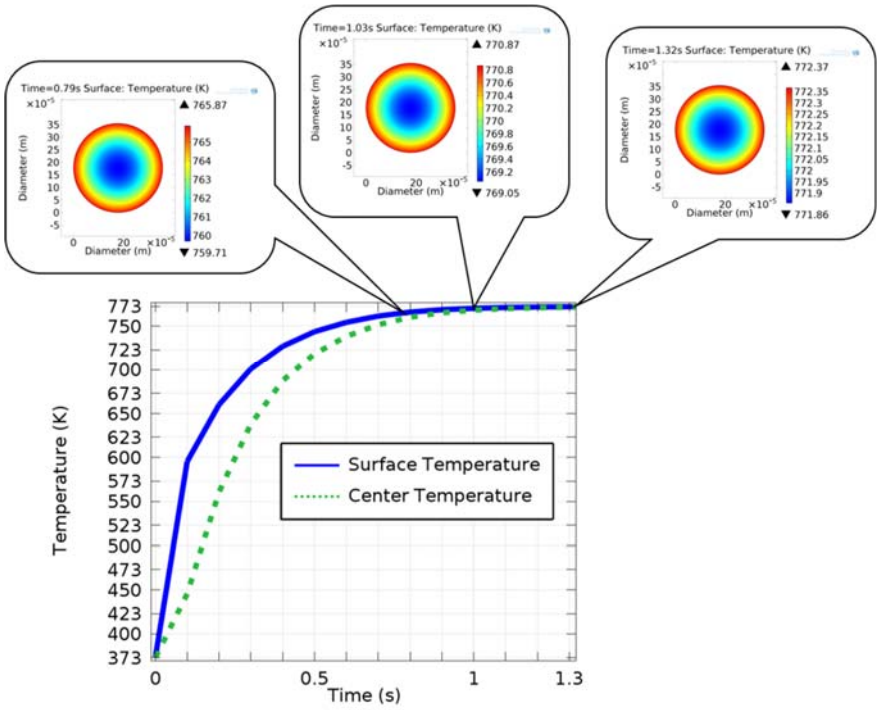

FIGURE 4 Simulated time profiles of temperature in a 355 µm sized EFB particle during pyrolysis

this current work, the Archimedes number is 733 and the Reynolds number is in the range of 0.5-0.85, for sand with 427.5 µm average particle size and EFB particles of size 300-355 µm, and four correlations were used for these. The U_{mf} estimates from the four correlations were about 0.09, 0.10, 0.13 and 0.15 m/s, respectively.

Effect of Heat Transfer Coefficient (h) on EFB Particle Heat Transfer

During the turbulent flow of the fluidization bed particles, the heat transfer coefficient largely depends on the interaction between biomass and fluidized bed material. In addition, the particle size and minimum fluidization velocity (U_{mf}) affect that heat transfer coefficient. The calculated heat transfer coefficients for EFB particles of sizes 300 µm and 355 µm were in the ranges 486.37-458.00 W/m^{2}K and 397.52-425.14 W/m^{2}K, respectively, when estimates were based on the minimum fluidization velocity range 0.09-0.15 m/s at 773 K. Several hundreds of heat transfer coefficient estimates have been applied in models of fast biomass pyrolysis in a fluidized bed reactor. In Papadikis and Bridgwater [37] work, the estimated heat transfer coefficient range 190-475 W/m^{2}K was used for spherical wood biomass particles size with 500 µm in fast pyrolysis at 773 K. In their work, minimum fluidization velocity 0.08 m/s was applied to the fluidization for the average sand particle diameter of 440 µm Geldart B group. The heat transfer coefficient is larger for the smaller particle according to convective effects from the higher velocity of carrier gas in the freeboard of the reactor. On the other hand, heat transfer coefficient is smaller for large particle due to dominant conductive effects in that area. Collier *et al.* [29] studied that the heat transfer coefficient rises to a maximum value when superficial velocity slightly exceeds minimum fluidization velocity and when the bed was fluidized well above the minimum fluidization velocity. In this current work, the average heat transfer coefficient 460 W/m^{2}K and minimum fluidization velocity 0.12 m/s were used to study heat transfer effects over the EFB particle size range 300-355 µm at 773 K.

Effects of Reaction Temperature and Time on Heat Transfer in EFB Pyrolysis

The heat transfer in EFB particles of 300-355 µm size was simulated up to 1.32 s maximum reaction time by using the heat diffusion model in COMSOL Multiphysics 4.3b software. This section describes the conduction mode of heat transfer of the particle from the surface towards its center during pyrolysis process, which depends on reaction time. The initial temperature of the particle was set at 373 K. The surface and center temperatures of a 300 µm particle increased from initial to 770.32 K and 768.4 K respectively, in 0.79 s. In Figure 3, stable surface and center temperatures of a 300 µm particle were in the range of 772.09-772.74 K and 771.45-772.58 K, respectively, in the time range of 0.96-1.32 s, while stable temperatures were reached at 1.03 s by 355 µm size particles. The highest simulated surface and center temperatures for 355 µm particles were about 772.37 K and 771.86 K, respectively at 1.32 s (see Figure 4). Therefore, less time was needed by the heat transfer in the smaller sized particles. Later in sub-section, the particle size effects on heat transfer will be discussed in more detail, in relation to the reaction temperature and time. The simulated time profiles of temperature for 300-355 µm sizes are in good agreement with the reported experimental data of Sulaiman *et al.* [26].

Effect of Particle Size on Heat Transfer in EFB Pyrolysis

Particle size has a large effect on biomass pyrolysis. In this work, the range of the EFB particle size chosen was in the range of 300-355 µm. The simulated surface temperature on 300 and 355 µm particles were in the ranges of 770.32-772.74 K and 765.87-772.34 K, respectively, in time range of 0.79-1.32 s (see Figure 3 and 4). The highest center temperatures 772.58 K and 771.86 K for these were reached at 1.32 s. According to these simulation results, heat transfer was better (more rapid) for small particle than for large ones, as would be expected. Therefore, biomass particle size is important operating parameter in a pyrolysis reactor.

Decompositions of Cellulose, Hemicellulose and Lignin in EFB Biomass at 773 K

According to literature, the two main processes in fast lignocellulosic biomass are dehydration and constituent degradation. The removal of moisture from biomass happens at temperatures below 393 K. Then the degradation of hemicellulose, cellulose and lignin occur in this order, in the temperature ranges 493-588 K, 588-673 K and above 723 K, respectively [38, 39]. Asadieraghi and Daud [25] studied moisture removal and constituent decomposition of EFB biomass, and these were observed below 423 K and over 423-673 K, respectively. The decomposition of cellulose in various types of oil palm biomass (empty fruit bunches (EFB), palm mesocarp fiber (PMF), and palm kernel shell (PKS)) took place above 573 K. The hemicellulose in PMF and PKS was decomposed below 573 K [25, 40]. The slow decomposition of lignin in oil palm biomass happens at a wide range of temperatures, 410-940 K [25].

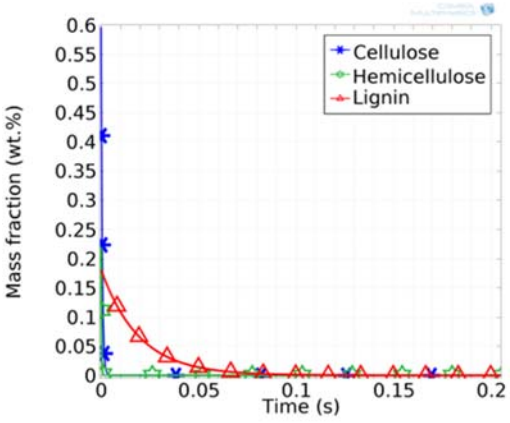

FIGURE 5 Decomposition of lignocellulosic components in EFB biomass at 773 K

In this work, the product yields from fast pyrolysis of EFB biomass were estimated based on decomposition during pyrolysis at 773 K. Figure 5 shows simulations of decomposition of cellulose, hemicellulose and lignin in EFB biomass, during fast pyrolysis at 773 K. The hemicellulose and cellulose were completely degraded into pyrolytic products at 773 K because they have less thermal stability than lignin. The degradation of lignin in EFB biomass

occurred at residence times of up to 0.2 s, at 773 K. This is because lignin is a rigid polymer and it is more difficult to degrade than cellulose and hemicellulose. The desired pyrolytic products from hemicellulose, cellulose, and lignin in EFB were obtained after 0.2 s of fast pyrolysis at 773 K.

Effect of Vapor Residence Time on Product Yields

Figure 6 shows the simulated product yields from fast pyrolysis of empty fruit bunch particles at 773 K, for vapor residence times from 0.79 to 1.32 s. More vapor, active cellulose and active lignin products were found at 0.79 s than at 1.32 s. Conversion to gas, char, water, and tar products occurred on increasing vapor residence time from 0.79 to 1.32 s. Active cellulose and active lignin were intermediate products. Diebold [12] has demonstrated that active cellulose is a fraction of cellulose with low degree of polymerization (DP), which acts as a solvent during pyrolysis. Therefore, active cellulose was mainly liquid with char products. Active lignin was in the unreacted solid fractions of mostly char products according to Miller and Bellan [13]. In our model assumptions, the combination of vapor (condensable) and tar was considered bio-oil products. The unreacted fraction, ash, and carbon were considered char products. The unreacted gas was the non-condensable gas products [25].

The simulated liquid, char and gas product yields were compared with experimental data by Abdullah *et al.* [41, 42]. The maximum liquid product yield was experimentally about 55.1 wt.%, but it was 52.77 wt.% in the simulation at 1.03 s (Table 4). The maximum liquid yield was about 55.4 wt.% at 0.79 s in the simulation, but the simulated liquid yield was close to the reported experimental data at 1.03 s. The short 0.79 s residence time gave much char products, about 27.2 wt.% in the reported experiments and 28.48 wt.% in the simulation, because of incomplete reactions. Char yield was lower at medium vapor residence time than at short and long vapor residence times, experimentally, but char yield decreased as the vapor residence time increased from 0.79 to 1.32 s in the simulation. At 0.96 s, the simulated about 27 wt.% char yield was in good agreement with experiments. The highest gas yields in the experimental and simulation were 25.1 wt.% and 25.57 wt.% at 1.32 s vapor residence time, respectively. Extending the vapor residence time increased gas yield because the volatile products were converted to gas in secondary reactions consuming the liquid product. Ogunsina *et al.* [43] have studied that the gas yield from experimental fast pyrolysis of EFB biomass obtained about 42.83 wt.% at a residence time 2 s and 773 K reaction temperature. Therefore, the gas yield was higher than char and liquid yields at long residence times, both experimental and in simulation. Otherwise, low gas product yield was found at short residence times. The simulated gas yield was higher than experimental at long residence time but in a consistent manner. In summary, vapor residence

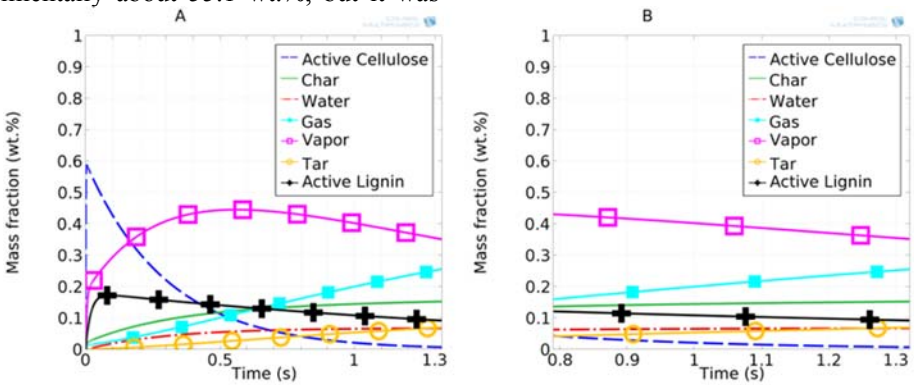

FIGURE 6 Simulated product yields at vapor residence times (A) up to 1.32 s, and (B) 0.79-1.32 s

TABLE 4 Product yields comparison between reported experimental [26] and simulation by vapor residence time

Case	Vapor Residence Time (s)					
	0.79	0.96	1.03	1.16	1.23	1.32
Reported Experimental Liquid (wt.%)	50.6	51.5	55.1	50.2	47.8	45.3
Simulation Liquid (wt.%)	55.40	53.59	52.77	51.24	50.39	49.32
Reported Experimental Char (wt.%)	27.2	26.5	23.9	25.9	27.5	27.6
Simulation Char (wt.%)	28.48	26.99	26.53	25.82	25.41	25.01
Reported Experimental Gas (wt.%)	17.9	17.7	18.6	19.1	22.4	25.1
Simulation Gas (wt.%)	16.02	19.30	20.60	22.90	24.10	25.57
Reported Experimental Liquid (wt.%)	0.79	0.96	1.03	1.16	1.23	1.32

time affects product yield from fast pyrolysis of empty fruit bunch biomass and the simulation results are in good agreement with experimental data [26, 41, 42] over the vapor residence time range from 0.79 s to 1.32 s at 773 K. The following section discusses in detail the effects of vapor residence time at optimal conditions.

Optimal Vapor Residence Time for Maximal Product Yields at 773 K

Table 5 summarizes the simulated product yields from fast pyrolysis of EFB at 773 K over the residence time range of 1.02-1.05 s. Simulation gave more char yield at the shorter 1.02 s time. On the other hand, at 1.05 s the gas yield had increased because of the secondary reactions. To avoid increasing of char and gas yields, the optimum vapor residence time in the range of 1.02-1.05 s can be sought. The simulated average yields of liquid, char and gas products were about 52.8 wt.%, 26.5 wt.%, and 20.7 wt.%, over 1.02-1.05 s. These averages from simulated data are close to the simulated product yields at 1.03 s. Sulaiman *et al.* [26] mentioned that 1.03 s vapor residence time maximizes product yields from fast pyrolysis of empty fruit bunches at 773 K. Therefore, the simulated product yields at 1.03 s are in good agreement with the experimental data of Sulaiman *et al.* [26]. The differences between average simulated yields and reported experiments in liquid, char, and gas yields were about 2.9 wt.%, 2.0 wt.% and -1.6 wt.%, respectively.

TABLE 5 Comparison of simulated data with reported experimental [26] data at vapor residence time range 1.02-1.05 s

Case	Vapor residence time (s)	Liquid (wt.%)	Char (wt.%)	Gas (wt.%)
Reported experiment data	1.02-1.05	49.9	24.5	22.3
Simulation data	1.02	52.9	26.6	20.4
Simulation data	1.03	52.8	26.5	20.6
Simulation data	1.04	52.7	26.4	20.8
Simulation data	1.05	52.6	26.3	21.0
Simulation data (average)	1.02-1.05	52.8	26.5	20.7
Difference (Simulation data - Reported experiment data)	1.02-1.05	2.9	2.0	-1.6

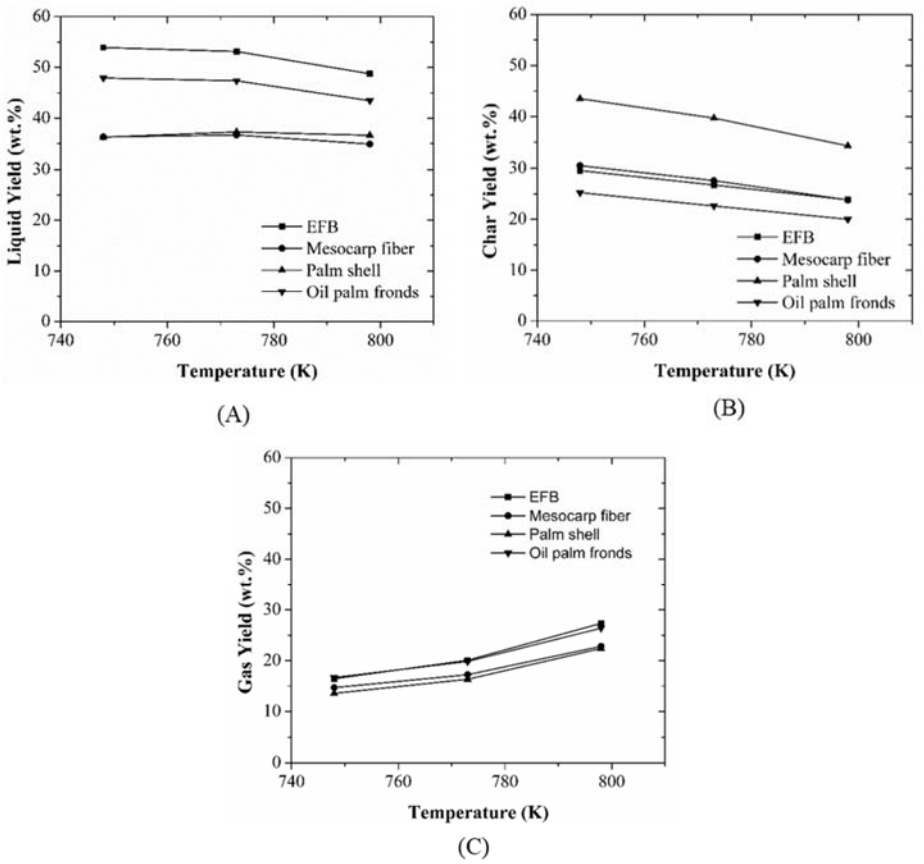

FIGURE 7 Effect of temperature on (A) liquid yield, (B) char yield and (C) gas yield

Effect of Reaction Temperature on Product Yields

Figure 7 shows the product yields of different palm oil (EFB, mesocarp fiber, palm shell and oil palm fronds) residues at the reaction temperature in the range 748-798 K and vapor residence time in the range over 0.8-1.5 s. The liquid product yield in EFB biomass decreases from 53.91 wt.% to 48.75 wt.% reaction temperature between 748 K and 798 K (Figure 7A). Similarly, Sulaiman *et al.* [26] have obtained that the experimental liquid product yield decreased from 50.5 wt.% to 49.3 wt.% at that temperature range. Therefore, the higher reaction temperature causes a decrease of liquid yield. In fact, the higher liquid product yields occur in EFB biomass than other residues because of not only the higher composition of cellulose but also lower composition of lignin that produce more condensable gas. The char product yield of palm shell biomass gives 43.49 wt.% at the reaction temperature 748 K (Figure 7B). The higher char yield in palm shell occurs than other residues according to the higher content of lignin which is difficult to degrade. In Sukiran *et al.* [44] work, the highest char product yield was obtained about 55.3 wt.% from palm shell compare than EFB and oil palm fronds. The char product yield from fast pyrolysis of palm oil residues significantly decreased when the reaction temperature increased. The gas yield in oil palm residues significantly increased from about 15 wt.% to 27 wt.% when the temperature increase in the range from 748 K to 798 K (Figure 7C). Therefore, the higher temperature prefers to increase the gas product because of secondary reactions formations as a result in decrease of liquid and char products.

Effect of Reaction Temperature on Product Quality

The influence of reaction temperature plays a significant role in the product quality. The effects of reaction temperature on water content, elemental compositions (C, H, N, and O), ash content in char product, high heating value (HHV) and composition of phenols are important on the product quality in biomass fast pyrolysis. Water is the most abundant compound in pyrolysis oil [45]**.** The water comes from dehydration of carbohydrates during pyrolysis, namely, pyrolytic water. Most pyrolytic water is produced from the decomposition of the cellulose and hemicellulose. Some additional water is also produced from lignin degradation [46]. The water from EFB pyrolysis in simulation shows a nearly yield about 6.5 wt.% at temperatures between 748 K and 798 K, which are in a good agreement with experimental results of Sulaiman *et al.* [26]. The low water content in product oil occurred at the lower reaction temperature below 723 K but it decreased the yield of organics of the oil [45]. Therefore, lower reaction temperature is not recommended for the high-quality bio-oil production in fast pyrolysis. On the other hand, higher reaction temperature above 773 K produced high water content in product oil because secondary cracking of bio-oil produced pyrolytic water. The reaction temperature affects elemental compositions (C, H, N, and O) of the bio-oil and char products. The carbon content tended to increase at higher reaction temperature while hydrogen and oxygen contents are significantly decreased. The reaction temperature effects on maximum carbon content and minimum oxygen content was important to yield high-quality product while hydrogen and oxygen contents remained almost constant. The ash content in char product increased at higher reaction temperature due to the volatile part of the solid phase decreased. The reaction temperature plays a significant role in the high heating value of bio-oil product. The maximum high heating value for bio-oil was observed at the reaction temperature around 773 K, at which bio-oil yield peaked [46]. The main products from decomposition of lignin are phenols and oligomers [47]. The maximum phenol content of the bio-oil gave at reaction temperature between 723 K and 773 K. Above 773 K, lower phenol content of the bio-oil happened due to the higher rates of secondary thermochemical reactions [46]. The reaction temperature played vital roles in the phenolics concentrations of bio-oil product quality. Therefore, reaction temperature is important to obtain not only maximum yield but also high quality in bio-oil.

CONCLUSIONS

The operating parameters on the fast pyrolysis of EFB were optimized using heat diffusion and a global kinetic model with finite element based COMSOL Multiphysics simulation. The good heat transfer effect on EFB small particle size (300 μm) was occurred than larger particle size (355 μm) using average heat transfer coefficient 460 W/m^2K with minimum fluidization velocity 0.12 m/s. Therefore, heat transfer coefficient, the minimum fluidization velocity and the particle size play significantly a role in the EFB particles heat transfer.

The reaction temperature was significantly affected by both yield and quality of the liquid product than the vapor residence time. The maximum liquid yield from fast pyrolysis of EFB was obtained about 53 wt.% in both reported experimental and simulation at reaction temperature between 748 K and 773 K. The high-quality liquid product from fast pyrolysis of oil palm residues was yielded at that temperature range because of lower water content, maximum carbon content, high heating value, and high phenol content. The influences of reaction temperature and vapor residence time from model predictions can be useful for the optimization of product yields on EFB fast pyrolysis without performing heavy experimental investigations.

ACKNOWLEDGMENTS

The authors acknowledge the financial support from the Higher Education Research Promotion and the Thailand's Education Hub for Southern Region of ASEAN Countries Project Office of the Higher Education Commission. In addition, we are also

thankful to Research and Development office (RDO), Prince of Songkla University and to Associate Professor Dr. Seppo Karrila, Faculty of Science and Industrial Technology, Prince of Songkla University for the valuable comments on the manuscript.

LITERATURE CITED

1. Beaudry, G., Macklin, C., Roknich, E., Sears, L., Wiener, M., & Gheewala, S.H. (2018). Greenhouse gas assessment of palm oil mill biorefinery in Thailand from a life cycle perspective, Biomass Conversion and Biorefinery, 8, 43–58.
2. Pirker, J., Mosnier, A., Kraxner, F., Havlík, P., & Obersteiner, M. (2016). What are the limits to oil palm expansion?, Global Environmental Change, 40, 73–81.
3. Chavananand, K. (2013). Palm Oil Residue Waste Potential and Waste Utilization in Thailand, Clean Power Asia Conference and Expo 2013.
4. Saswattecha, K., Kroeze, C., Jawjit, W., & Hein, L. (2017). Improving environmental sustainability of Thai palm oil production in 2050, Journal of Cleaner Production, 147, 572–588.
5. Saswattecha, K., Kroeze, C., Jawjit, W., & Hein, L. (2015). Assessing the environmental impact of palm oil produced in Thailand, Journal of Cleaner Production, 100, 150–169.
6. Prabir, B. (2010). Biomass gasification and pyrolysis: Practical Design and Theory. Oxford, Elsevier Inc.
7. Sharma, A., Wang, S., Pareek, V., Yang, H., & Zhang, D. (2015). Multi-fluid reactive modeling of fluidized bed pyrolysis process, Chemical Engineering Science, 123, 311–321.
8. Blanco, A., & Chejne, F. (2016). Modeling and simulation of biomass fast pyrolysis in a fluidized bed reactor, Journal of Analytical and Applied Pyrolysis, 118, 105–114.
9. Chan, W.R., Kelbon, M., & Krieger, B.B. (1985). Modelling and experimental verification of physical and chemical processes during pyrolysis of large biomass particle, Fuel, 64, 1505–1513.
10. Blasi, C.D. (1996). Kinetic and heat transfer control in the slow and flash pyrolysis of solids, Industrial and Engineering Chemistry Research, 35, 37–46.
11. Shafizadeh, F., & Bradbury, A.G. (1979). Thermal degradation of cellulose in air and nitrogen at low temperature, Journal of Applied Polymer Science, 23, 1432–1442.
12. Diebold, J.P. (1994). Global model for the pyrolysis of cellulose, Biomass Bioenergy, 7, 75-85.
13. Miller, R.S., & Bellan, J.A. (1996). A generalized biomass pyrolysis model based on superimposed cellulose, hemicellulose and lignin kinetics,

Combustion Science and Technology, 126, 97-137.

14. Xiong, Q., & Kong S.C. (2014). Modeling effects of interphase transport coefficients on biomass pyrolysis in fluidized beds, Powder Technology, 262, 96–105.
15. N.H. Dong, N.H. Luo, K.H. & Wang, Q. (2017). Modeling of biomass pyrolysis in a bubbling fluidized bed reactor: Impact of intra-particle heat conduction, Fuel Processing Technology, 161, 199–203.
16. Liu, B., Papadikis, K., Gu, S., Fidalgo, B., Longhurst, P., Li, Z., & Kolios, A. (2017). CFD modelling of particle shrinkage in a fluidized bed for biomass fast pyrolysis with quadrature method of moment, Fuel Processing Technology, 164, 51–68.
17. Ranzi, E., Cuoci, A., Faravelli, T., Frassoldati, A., Migliavacca, G., Pierucci, S., & Sommariva, S. (2008). Chemical kinetics of biomass pyrolysis, Energy Fuels, 22, 4292–4300.
18. Mellin, P., Kantarelis, E., & Yang, W. (2014). Computational fluid dynamics modeling of biomass fast pyrolysis in a fluidized bed reactor, using a comprehensive chemistry scheme, Fuel, 117, 704–715.
19. Ranganathan, P., & Gu, S. (2016). Computational fluid dynamics modelling of biomass fast pyrolysis in fluidised bed reactors, focusing different kinetic schemes, Bioresource Technology, 213, 333–341.
20. Matta, J., Bronson, B., Gogolek, P.E.G., Mazerolle, D., Thibault, J., & Mehrani, J. (2017). Comparison of multi-component kinetic relations on bubbling fluidized-bed woody biomass fast pyrolysis reactor model performance, Fuel, 210, 625–638.
21. Salema, A.A., & Afzal, M.T. (2015). Numerical simulation of heating behaviour in biomass bed and pellets under multimode microwave system, International Journal of Thermal Sciences, 91, 12–24.
22. Papadikis, K., Gu, S., & Bridgwater, A.V. (2009). CFD modelling of the fast pyrolysis of biomass in fluidised bed reactors, Part B, Heat, momentum and mass transport in bubbling fluidised beds, Chemical Engineering Science, 64, 1036–1045.
23. Dupont, C., Chiriac, R., Gauthier, G., & Toche, F. (2014). Heat capacity measurements of various biomass types and pyrolysis residues, Fuel, 115, 644–651.
24. Gupta, M., Yang, J., & Roy, C. (2003). Specific heat and thermal conductivity of softwood bark and softwood char particles, Fuel, 82, 919–927.
25. Asadieraghi, M., & Daud, W.M.A.W. (2015). In-depth investigation on

thermochemical characteristics of palm oil biomasses as potential biofuel sources, Journal of Analytical and Applied Pyrolysis, 115, 379–391.

26. Sulaiman, F., & Abdullah, N. (2011). Optimum conditions for maximising pyrolysis liquids of oil palm empty fruit bunches, Energy, 36, 2352–2359.
27. Abnisa, F., Arash, A.N., Daud W.M.A.W., & Sahu, J.N. (2013). Characterization of Bio-oil and Bio-char from Pyrolysis of Palm Oil Wastes, BioEnergy Research, 6, 830–840.
28. Hanim, S.S., Noor, M.A.M., & Rosma, A. (2011). Effect of autohydrolysis and enzymatic treatment on oil palm (Elaeis guineensis Jacq.) frond fibres for xylose and xylooligosaccharides production, Bioresource Technology, 102, 1234–1239.
29. Collier, A.R., Hayhurst, A.N., Richardson, J.L., & Scott, S.A. (2004). The heat transfer coefficient between a particle and a bed (packed or fluidised) of much larger particles, Chemical Engineering Science, 59, 4613–4620.
30. Wen & Yu. (1966). A generalized method for predicting the minimum fluidization velocity, AIChE Journal, 12.
31. Bin, A.K. (1994). Prediction of the minimum fluidization velocity, Powder Technology, 81, 197–199.
32. Bourgeois, P., & Grenier, P. (1968). The ratio of terminal velocity to minimum fluidizing velocity for spherical particles, The Canadian Journal of Chemical Engineering, 46, 325–334.
33. Hilal, N., Ghannam, M.T., & Anabtawi, M.Z. (2001). Effect of bed diameter, distributor and inserts on minimum fluidization velocity, Chemical Engineering Technology, 24, 161.
34. Vaid, R.P., & Sen, G.P. (1978). Minimum fluidization velocities in beds of mixed solids, The Canadian Journal of Chemical Engineering, 56, 292–296.
35. Chiou, L.L., Ming, Y.W., & Shr, D.Y. (2002). The effect of particle size distribution on minimum fluidization velocity at high temperature, Powder Technology, 126, 297– 301.
36. Basu, P., & Zhi, G.F. (2013). Prediction of minimum fluidization velocity for binary mixtures of biomass and inert particles, Powder Technology, 237, 134–140.
37. Papadikis, K., Gu, S., & Bridgwater, A.V. (2009). CFD modelling of the fast pyrolysis of biomass in fluidised bed reactors, Part B, Heat, momentum and mass transport in bubbling fluidised beds, Chemical Engineering Science, 64, 1036–1045.
38. Sanchez, S.L., López, G.D., Villaseñor, J., Sánchez, P., & Valverde, J.L. (2012). Thermogravimetric mass spectrometric analysis of lignocellulosic and marine

biomass pyrolysis, Bioresource Technology, 109, 163–172.

39. Haiping, Y., Rong, Y., Hanping, C., Dong, H.L., & Chuguang, Z. (2007). Characteristics of hemicellulose, cellulose and lignin pyrolysis, Fuel, 86, 1781–1788.

40. Haiping, Y., Rong, Y., Terence, C., David, T.L., Hanping, C., & Chuguang, Z. (2004). Thermogravimetric analysis-fourier transform infrared analysis of palm oil waste pyrolysis. Energy & Fuels, 18, 1814-1821.

41. Abdullah, N., & Bridgwater, A.V. (2006). Pyrolysis liquid derived from oil palm empty fruit bunches, Journal of Physical Science, 17, 117–129.

42. Abdullah, N., Gerhauser, H., & Sulaiman, F. (2010). Fast pyrolysis of empty fruit bunches, Fuel, 89, 2166–2169.

43. Ogunsina, B.S., Ojolo S.J., Ohunakin, O.S., Oyedeji, O.A., Matanmi, K.A., & Bamgboye. (2012). Potentials for generating alternative fuels from empty palm fruit bunches by Pyrolysis, Procedia ICCEM, 185–190.

44. Sukiran, M.A., Loh, S.K., & Bakar, N.A. (2016). Production of Bio-oil from Fast Pyrolysis of Oil Palm Biomass using Fluidised Bed Reactor, Journal of Energy Technologies and Policy, 6, 2225-0573.

45. Westerhof, R.J.M., Brilman, D.W.F., Swaaij, W.P.M., & Kersten, S.R.A. (2010). Effect of temperature in fluidized bed fast pyrolysis of biomass: oil quality assessment in test units, Industrial and Engineering Chemistry Research, 49, 1160–1168.

46. Salehi, E., Abedi, J., & Harding, T. (2011). Bio-oil from sawdust: effect of operating parameters on the yield and quality of pyrolysis products, Energy Fuels, 25, 4145–4154.

47. Bai, X., Kim, K.H., Brown, R.C., Dalluge, E., Hutchinson, C., Lee, Y.J., & Dalluge, D. (2014). Formation of phenolic oligomers during fast pyrolysis of lignin, Fuel, 128, 170–179.

Appendix D

Manuscript 2

Authors : Kyaw Thu, Taweesak Reungpeerakul, Ram Yamsaengsung, Chayanoot Sangwichien.

Title : Modeling of oil palm empty fruit bunch biomass fast pyrolysis in fluidized bed reactor: Optimization of reaction kinetics parameters influence on the yield and quality of pyrolysis products

Journal Name : Waste and Biomass Valorization

Modeling of oil palm empty fruit bunch biomass fast pyrolysis in fluidized bed reactor: Optimization of reaction kinetics parameters influence on the yield and quality of pyrolysis products

Kyaw Thu[1], Taweesak Reungpeerakul[2], Ram Yamsaengsung[1], Chayanoot Sangwichien[1]

[1]Department of Chemical Engineering, Faculty of Engineering, Prince of Songkla University, Hat Yai, Thailand

[2]Department of Computer Engineering, Faculty of Engineering, Prince of Songkla University, Hat Yai, Thailand

Corresponding author: chayanoot.sangwichien@gmail.com

Abstract

The purpose of this work is to study the relationship between reaction temperature and vapor residence time on product yields of empty fruit bunch (EFB) by fast pyrolysis in a fluidized bed reactor. A global chemical kinetic model was applied to simulate the fast pyrolysis of three constituents of the EFB biomass (cellulose, hemicellulose and lignin) by using finite element based COMSOL Multiphysics software. The fifteen pyrolysis reactions mechanism were simulated to predict the pyrolytic products (such as bio-oil, gas and char) at the reaction temperature range of 450-550 ˚C. The model validation was performed with the reported experimental data from fast pyrolysis of EFB at 500 ˚C. The simulated higher liquid yield for reaction temperature in the range of 450-550 ˚C occurs at vapor residence time range of 0.5-2 s. The model predictions can be applied to the experimental work for fast pyrolysis of biomass in a fluidized bed reactor.

Keywords: Empty fruit bunch (EFB), Fast pyrolysis, Reaction kinetics, Modeling

1. Introduction

The world's third-largest palm oil production accounting country is Thailand. The increments of oil palm cultivated areas in Thailand have grown 9% annually over the past decade. As a result, the expansion of the palm oil industry in Thailand is continuously increasing because of not only the consumption of edible oil but also renewable energy production (Silalertruksa et al., 2017). In Thailand, most of the renewable energy were obtained from biomass, followed by biogas, solar, municipal solid waste and wind, respectively. Oil palm waste from oil palm industry provides a strong reason for selecting biomass as the foremost renewable energy source (Prasentsan et al., 1996).

In most oil palm mill in Southern Thailand, large amount of empty palm fruit bunch solid wastes is manufactured as a by-product. In the past, empty fruit bunches and the shells are disposed by landfilling, which is very difficult to store and costly to manage. In some factories, the empty fruit bunches are burnt in the furnaces which causes air pollution. An effective way to solve this problem is to convert it into useful alternative energy. Biochemical and thermochemical routes are used to convert biomass into fuel, gases and chemicals. In thermochemical route, pyrolysis process takes place in the absence of oxygen. The main three types of pyrolysis can be classified as slow (conventional), fast and flash according to the operating conditions, such as heating rate, reaction temperature, feedstock size and vapor residence time (Prabir, 2010).

Many authors (Sulaiman et al., 2011; Sembiring et al., 2015; Kim et al., 2013; Abdullah et al., 2006; Sukiran et al., 2016; Ogunsina et al., 2012) have studied the biofuel energy conversion from empty fruit bunch biomass using the fast pyrolysis process in fluidized bed reactors. The oil palm empty fruit bunch (OPEFB) was pyrolyzed in a bench scale fluidized bed system for a maximum product yield of liquids at 450 ˚C reaction temperature and at residence time of 1.03 s by Sulaiman et

al., (2011). The maximum liquid product yield of 55.14 wt.% was found at vapor residence time of 1.03 s and at 500 ˚C (Sulaiman et al., 2011). Sembiring et al., (2015) produced their highest bio-oil yield of about 27 wt.% from EFB using fast pyrolysis at an optimum pyrolysis temperature of 500 ˚C. Kim et al., (2013) studied the production of pyrolysis oil from Jatropha seed shell cake (JSC), palm kernel shell (PKS) and empty palm fruit bunches (EFB) wastes. Moreover, a comparison of maximum liquids yield produced from washed and unwashed EFB at reactor temperature range from 425 ˚C to 550 ˚C and vapor residence time range of 1.01–1.04 s was done by Abdullah et al., (2006). In a work by Sukiran et al., (2016), four types of oil palm biomasses (EFB, trunk, front and palm kernel shell) were used to produce bio-oil by fast pyrolysis in fluidized bed reactor. The maximum bio-oils of 47.4 wt.% was obtained at 500 ˚C. The bio-oils yield of 29.98 wt.% from EFB fast pyrolysis was performed at 2 s and 500 ˚C by Ogunsina et al., (2012). According to these experimental literatures, reaction temperature and vapor residence time parameters were mainly affected on product yields from fast pyrolysis of oil palm biomass.

With rapid advancement of computation techniques in the last decades, various computational simulation tools have been widely employed for understanding inner conditions (such as hydrodynamics, heat transfer and chemical reaction) of fluidized bed for biomass fast pyrolysis. Euler-Euler and Euler-Lagrangian models with various kinetic mechanism have been used to study the effect of reactor hydrodynamics, product yields and reaction parameters by computational fluid dynamics (CFD) (Qitai et al., 2017). Papadikis et al., (2009a; 2009b; 2010a; 2010b) chose a two-stage, semi-global model to predict the product yield of wood biomass pyrolysis using the Eulerian CFD method in Fluent software. Many authors have applied multi-stage global kinetic mechanism for reaction kinetic on different biomass fast pyrolysis using CFD with Euler-Euler model in Fluent software (Bo et al., 2017; Dong et al., 2017; Xue et al., 2011; Xue et al., 2012; Qingang et al., 2014a; Qingang et al., 2014b; Johnny et al., 2017). Mabrouki et al., (2015) simulated a multi-component global mechanism model to maximize the liquid yield from fast pyrolysis of three palm oil residues using SuperPro Designer (SPD) software. In this work, the global kinetic mechanism applied for prediction the effects of reaction temperature and vapor residence time on product yields from fast pyrolysis of EFB using the finite element based COMSOL Multiphysics 4.3b software. A comparison between the simulated and reported experimental data were in good agreement.

2. Methodology

2.1. Kinetic model for EFB fast pyrolysis

Three types of kinetic model for prediction of product yields have been applied to fast pyrolysis of biomass. They are simple, global and advance models. For the simple kinetic model, biomass is decomposed into bio-oil, char and gas in the primary reaction, and then, bio-oil is broken down into char and gas products in the secondary reaction. Therefore, the main three pyrolytic products are decomposed in both the primary and secondary reactions. From previous works, Papadikis et al., (2009a; 2009b; 2010a; 2010b) studied the bio-oil production from fast pyrolysis of wood biomass using the simple kinetic model, while Blasi, (1996) and Chan et al., (1985) also proposed the kinetic parameters of each reaction using the simple kinetic model.

In another work, Shafizadeh et al., (1979) published the global kinetic model for fast pyrolysis of biomass. They considered the feedstock biomass consisting of cellulose, hemicellulose and lignin. This consideration is the main difference between simple and global kinetic models. The other main difference between simple and global models is that the active materials have low degree of polymerization (DP) stage. Therefore, constituents of biomass are decomposed into intermediate products in the primary reaction and then they are broken down into bio-oil, char and gas products in the secondary reaction. In fact, primary vapor can be decomposed into non-condensable gas in secondary reaction. In 1994, the global kinetic

model for fast pyrolysis of cellulose was published by Diebold, (1994). In his work, cellulose decomposed into active cellulose in the first stage and then they were broken down into pyrolytic products in the second stage (Figure 1A). The kinetic mechanism of these two stages were studied by a seven reactions pathway. Miller et al., (1996) studied the kinetic mechanisms for fast pyrolysis of hemicellulose and lignin using the pathway of Shafizadeh et al., (1979) as shown in Figure 1B and 1C. The constituents of the biomass allowed the formation of active material before decomposing into three pyrolytic products. The vapor product was permitted to convert into the gas product in the secondary reaction. The Arrhenius equation was chosen for each kinetic reaction mechanisms of the cellulose, hemicellulose and lignin as shown in Eqs. 1. The activation energy and pre-exponential factor for first-order irreversible reactions of the cellulose,

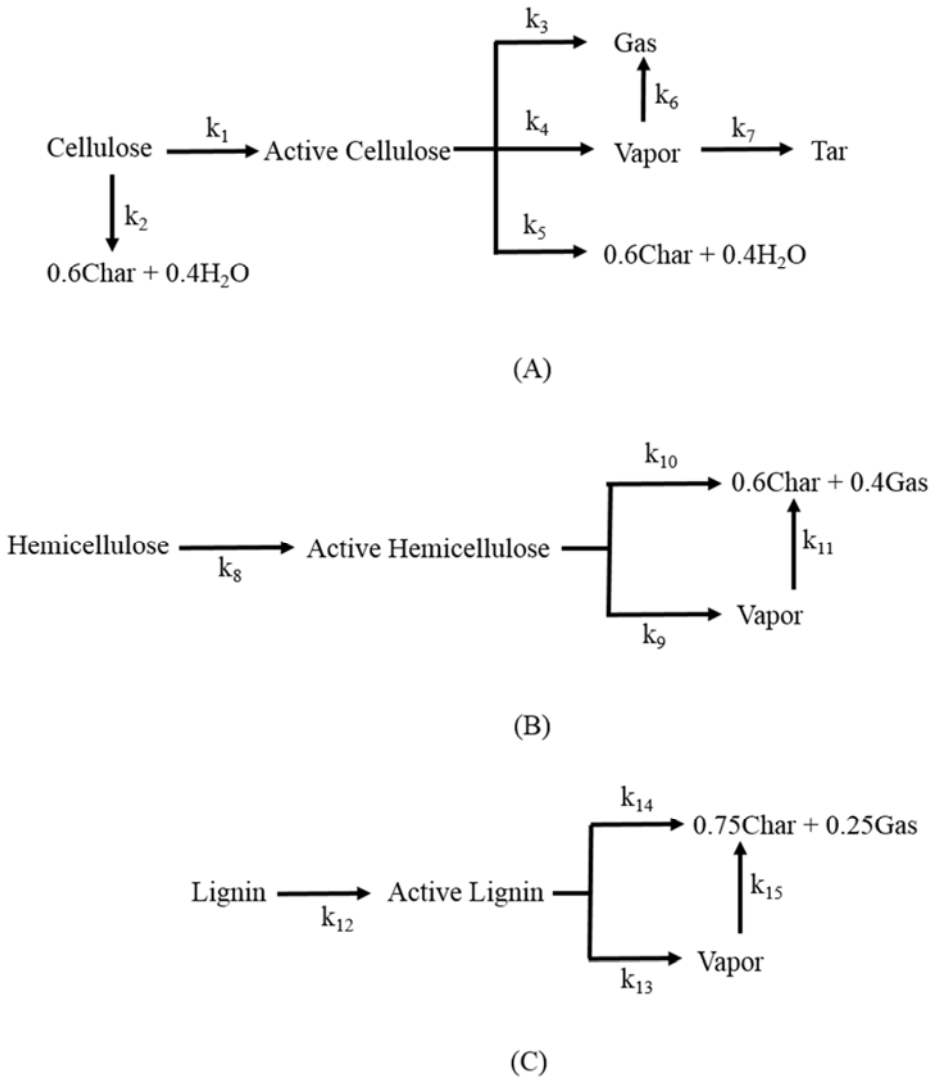

Figure 1. Degradation pathways for fast pyrolysis of (A) cellulose (B) hemicellulose and (C) lignin in the modified Shafizadeh et al., (1979) and Diebold, (1994) mechanisms

hemicellulose and lignin were found from academic literatures for global kinetic scheme (Diebold, 1994; Miller et al., 1996). Table 1 shows kinetic reaction parameters of the cellulose, hemicellulose and lignin for the EFB fast pyrolysis in the global kinetic scheme. The chemical compositions of cellulose, hemicellulose and lignin of empty fruit bunch are shown in Table 2. Table 3 shows the rate equations for cellulose, hemicellulose and lignin fast pyrolysis.

The detail reaction mechanisms of biomass fast pyrolysis using the advance model was published in 2008 by Ranzi et al., (2008). The main reason for the advance model is to predict the pyrolysis product species. Sixteen reactions mechanism were listed in the feedstock constituent's fast pyrolysis in the advance model.

$$K_i = A_i \exp(-E_i / RT) \qquad \text{Eq. (1)}$$

Here K_i, A_i and E_i are reaction rate, pre-exponential factor and activation energy of each reaction, respectively. The gas constant and reaction temperature are represented by R and T.

2.2. Model Assumptions

Active cellulose and active lignin are intermediate products of biomass for fast pyrolysis**.** Diebold, (1994) illustrated that the active cellulose for unreacted cellulose have low degree of polymerization (DP) fractions which acts as the solvent during pyrolysis. Therefore, the compositions of the unreacted active cellulose were assumed to be forty percent water and sixty percent char products.

Table 1. Kinetic parameters for EFB fast pyrolysis (Diebold, 1994; Miller et al., 1996)

Pyrolysis reactions	A (s^{-1})	E (kJ mol^{-1})
Cellulose to Active Cellulose	2.8×10^{19}	240
Cellulose to 0.6Char + 0.4H_2O	6.7×10^{5}	110
Active Cellulose to Gas	3.6×10^{11}	200
Active Cellulose to Vapors	6.8×10^{9}	140
Active Cellulose to 0.6Char + 0.4H_2O	1.3×10^{10}	150
Vapors to Gas	3.6×10^{11}	200
Vapors to Tar	1.8×10^{3}	61
Hemicellulose to Active Hemicellulose	2.1×10^{16}	186.7
Active Hemicellulose to Vapors	8.75×10^{15}	202.4
Active Hemicellulose to 0.6Char + 0.4Gas	2.6×10^{11}	145.7
Vapors to Gas	4.28×10^{6}	108
Lignin to Active Lignin	9.6×10^{8}	107.6
Active Lignin to Vapors	1.5×10^{9}	143.8
Active Lignin to 0.75Char + 0.25Gas	7.7×10^{6}	111.4
Vapors to Gas	4.28×10^{6}	108

Table 2. Chemical compositions of EFB (Sulaiman et al., 2011)

	Chemical composition (wt.%)
Cellulose	59.7
Hemicellulose	22.1
Lignin	18.1

The active lignin was the unreacted solid fractions according to Miller et al., (1996). In the model assumptions, the combination of vapor (condensable), water and tar were considered as the liquid products. The unreacted fraction, ash and carbon were assumed as the char products. The unreacted gas is the non-condensable gas products (Asadieraghi et al., 2015). In addition, the liquid product without water was noted as the bio-oil. Table 4 shows the assumptions of pyrolytic products in the simulation.

3. Results and Discussion

3.1. Decompositions of constituent in EFB biomass at 450-550 ˚C

The dehydration and constituent degradation are two main steps in lignocellulosic biomass pyrolysis. The moisture removal of biomass

Table 3. Rate equations for cellulose, hemicellulose and lignin fast pyrolysis

Reactions	Rate Equations
1	$\frac{dC_{cellulose}}{dt} = -(k_1 + k_2)C_{cellulose}$
2	$\frac{dC_{active-cellulose}}{dt} = k_1 C_{cellulose} - (k_3 + k_4 + k_5)C_{active-cellulose}$
3	$\frac{dC_{vapor}}{dt} = k_4 C_{active-cellulose} - k_6 C_{gas} - k_7 C_{tar}$
4	$\frac{dC_{gas}}{dt} = k_3 C_{active-cellulose} + k_6 C_{vapor}$
5	$\frac{dC_{tar}}{dt} = k_7 C_{vapor}$
6	$\frac{dC_{H_2O}}{dt} = 0.4k_2 C_{cellulose} + 0.4k_5 C_{active-cellulose}$
7	$\frac{dC_{char}}{dt} = 0.6k_2 C_{cellulose} + 0.6k_5 C_{active-cellulose}$
8	$\frac{dC_{hemicellulose}}{dt} = -k_8 C_{hemicellulose}$

9 $$\frac{dC_{active-hemicellulose}}{dt} = k_8 C_{hemicellulose} - (k_9 + k_{10}) C_{active-hemicellulose}$$

10 $$\frac{dC_{vapor}}{dt} = k_9 C_{active-hemicellulose} - k_{11} C_{vapor}$$

11 $$\frac{dC_{gas}}{dt} = 0.4 k_{10} C_{active-hemicellulose} + k_{11} C_{vapor}$$

12 $$\frac{dC_{char}}{dt} = 0.6 k_{10} C_{active-hemicellulose}$$

13 $$\frac{dC_{lignin}}{dt} = -k_{12} C_{lignin}$$

14 $$\frac{dC_{active-lignin}}{dt} = k_{12} C_{lignin} - (k_{13} + k_{14}) C_{active-lignin}$$

15 $$\frac{dC_{vapor}}{dt} = k_{13} C_{active-lignin} - k_{15} C_{vapor}$$

16 $$\frac{dC_{gas}}{dt} = 0.25 k_{14} C_{active-lignin} + k_{15} C_{vapor}$$

17 $$\frac{dC_{char}}{dt} = 0.75 k_{14} C_{active-lignin}$$

Table 4. Assumptions of three products in simulation

Composition species from simulation	Products
Vapor + Water + Tar	Liquid
Char + Active Lignin	Char
Unreacted Gas	Gas

happens at temperatures below 120 ˚C, while the degradation of hemicellulose, cellulose and lignin occur at the temperature ranges of 220-315 ˚C, 315-400 ˚C and above 450 ˚C, respectively (Sanchez et al., 2012; Haiping et al., 2007). Asadieraghi et al., (2015) studied moisture evolution and constituent decomposition of EFB biomass and observed of below 150 ˚C and over 150-400 ˚C, respectively. The cellulose decomposition of oil palm empty fruit bunch (EFB) biomass took place at 329 ˚C (Asadieraghi et al., 2015). The hemicelluloses in EFB biomass decomposed below 310 ˚C (Asadieraghi et al., 2015, Haiping et al., 2004, Rong et al., 2005). The lignin degradation of EFB biomass happens above 450 ˚C (Asadieraghi et al., 2015).

In this work, the product yields from fast pyrolysis of EFB biomass were considered after decomposition of three constituents in the EFB biomass. Figure 2 (A-C) show the simulation of the decomposition of cellulose, hemicellulose and lignin in the EFB biomass during fast pyrolysis at a reaction temperature range of 450-550 ˚C. The small amount of hemicellulose and cellulose degradation were found at 450 ˚C and at very short time of below 0.04 s. The degradation of lignin in EFB biomass occurred at a time of 0.7 s, at 450 ˚C

(Figure 2A). The lignin is difficult to degrade than cellulose and hemicellulose because it is rigid polymers. Therefore, lignin degradation happens at above 500 ˚C and at under 0.2 s when cellulose and hemicellulose were completely degraded. The complete degradation of three constituents for EFB biomass feedstock were started at up to 0.7 s and at temperature range of 450-550 ˚C. Above 0.7 s, the desired products from hemicellulose, cellulose and lignin in fast pyrolysis of EFB are yield at this temperature range.

3.2. Model validation with Sulaiman et al., (2011) experiment work

Figure 3 shows the simulated seven product compositions (such as active cellulose, active lignin, char, water, gas, tar and vapor) from fast pyrolysis of EFB biomass at a temperature of 500 ˚C and vapor residence time range from 0.79 to 1.32 s. The higher yields of vapor, char, water and tar and intermediate products (active cellulose and active lignin) happen an increase of liquid and char products. When an increase of vapor residence time from 0.79 to 1.32 s, the higher of unreacted gas product yield causes an increase of non-condensable gas product (Table 5).

Table 5. Product yields compositions in simulation at 0.79-1.32 s and 500 ˚C

Vapor residence time (s)	Vapor	Active cellulose	Active lignin	Char	Gas	Water	Tar
0.79	43.11	4.35	12.16	13.71	16.02	6.34	4.21
0.96	40.87	2.47	11.14	14.37	19.30	6.55	5.20
1.03	39.82	1.96	10.75	14.60	20.60	6.61	5.56
1.16	37.78	1.28	10.05	14.94	22.90	6.70	6.25
1.23	36.66	1.02	9.70	15.10	24.10	6.72	6.60
1.32	35.22	0.76	9.25	15.30	25.57	6.75	7.05

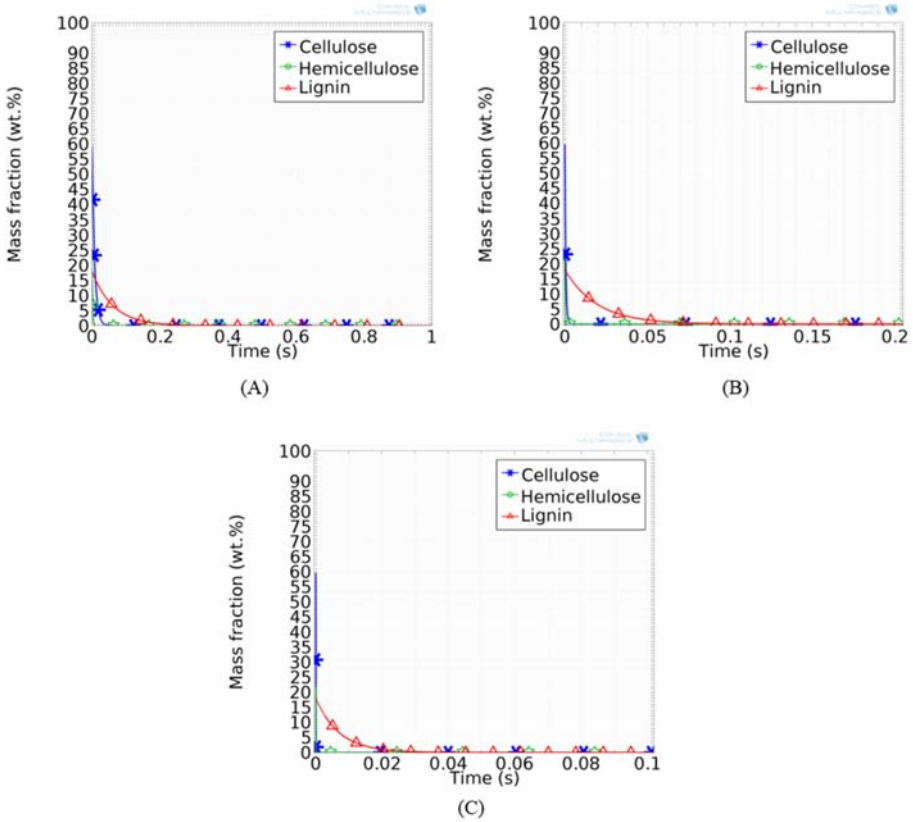

Figure 2. Simulated cellulose, hemicellulose and lignin decompositions in EFB biomass at (A) 450 ˚C, (B) 500 ˚C and (C) 550 ˚C

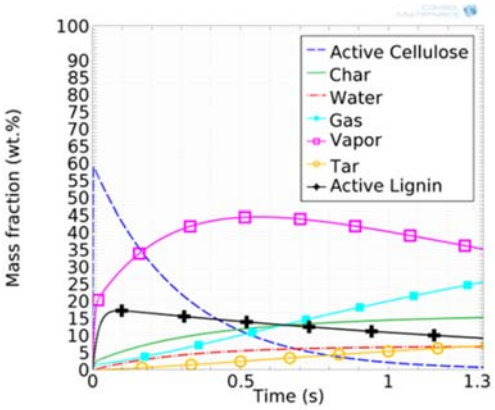

Figure 3. Simulated product yields of active cellulose, char, water, gas, vapor, tar and active lignin at reaction temperature of 500 ˚C and vapor residence time up to 1.32 s

The simulated liquid, char and gas product yields show good agreement with reported experiment data of Sulaiman et al., (2011) (Figure 4). The maximum liquid product yields were 55.1 wt.% in the reported experiments at 1.03 s and 55.4 wt.% in the simulation at 0.79 s, respectively. The simulated liquid yield of 52.77 wt.% at 1.03 s was close to the reported experimental data. The short 0.79 s vapor residence time gave much char yields about 27.2 wt.% in reported the experiments and 28.48 wt.% in the simulation because of incomplete reactions. The lower char yields occur at medium vapor residence time than at short and long vapor residence times, experimentally, but char yield decreased as the vapor residence time increased from 0.79 to 1.32 s in the simulation. At 0.96 s, the simulated char yield of about 26.99 wt.% was in good agreement with experimental char yield of about 26.5 wt.%. The highest gas yields in both reported experimental and simulation were found to be 25.1 wt.% and 25.26 wt.% at 1.32 s. The longer vapor residence time cause the higher gas yield because volatile products converted into gas in secondary reaction. Therefore, the gas yield was higher than char and liquid yields at the longer vapor residence

time in both reported experimental data and simulated data. Otherwise, lower gas product yield was found at the short vapor residence time. The simulated gas yield was slightly higher than experimental gas yield when an increase of vapor residence time, but the trend was consistent (Figure 4). According to the above facts, the simulated values are validated with experimental data of Sulaiman et al., (2011) on product yields of fast pyrolysis of empty fruit bunch biomass at 500 ˚C and over 0.79-1.32 s vapor residence time (Table 6).

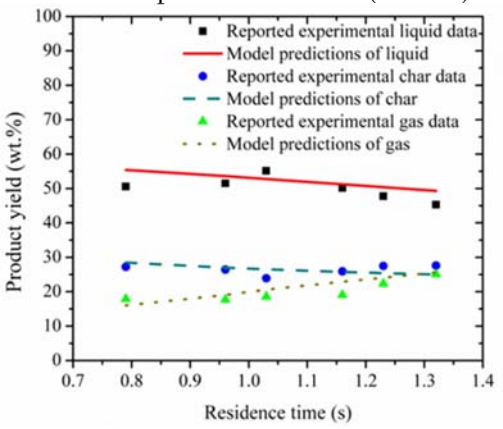

Figure 4. Model validation between simulated data and Sulaiman et al. [4] experimental data for product yield at reaction temperature of 500 ˚C and range of residence time 0.79-1.32 s

3.3. Model validation with Ogunsina et al., (2012) experiment work

Table 7 shows a good agreement in the yield of bio-oil, char and gas products comparison between simulated and experimental data by Ogunsina et al., (2012) at reaction temperature of 500 ˚C and at vapor residence time of 2 s, respectively. The values of simulated product yields were close to the Ogunsina et al., (2012) experiment work at 2 s. The highest bio-oil yield was found about 29.98 wt.% in the simulation and 25.35 wt.% in the experimental data. The gas yield was higher than bio-oil and char yields in both reported experimental and simulated data at vapor residence time of 2 s. Therefore, the longer vapor residence time was intended to the production of non-condensable gas product in EFB biomass fast pyrolysis process. The simulation results were validated with the literature experiment data at vapor residence time 2 s.

3.4. Influence of vapor residence time on product yield of EFB pyrolysis

In biomass fast pyrolysis, short vapor residence time favors the minimization of the secondary reactions which causes a decrease of liquid yield. Xiaoquan et al., (2005) found a highest bio-oil yield of 65 wt.% with minimal water

Table 6. Simulated product yields comparison with Sulaiman et al., (2011) experimental data at reaction temperature of 500 ˚C and vapor residence time in the range of 0.79-1.32 s

Vapor residence time (s)	Reported experimental liquid data	Model predictions of liquid	Reported experimental char data	Model predictions of char	Reported experimental gas data	Model predictions of gas
0.79	50.58	55.40	27.24	28.48	17.90	16.02
0.96	51.50	53.61	26.45	26.99	17.71	19.03
1.03	55.14	52.77	23.93	26.53	18.57	20.60
1.16	50.16	51.24	25.92	25.76	19.06	22.90
1.23	47.77	50.39	27.49	25.41	22.37	24.10
1.32	45.32	49.32	27.60	25.01	25.06	25.57

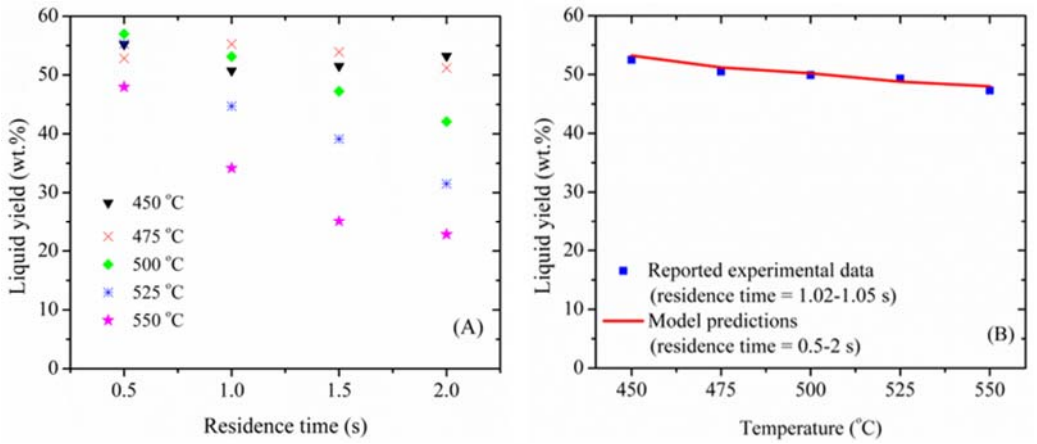

Figure 5. Effects of simulated (A) residence time (0.5-2 s) and (B) reaction temperature (450-550 ˚C) on liquid yield for fast pyrolysis of EFB

Table 7. Comparison of product yields between Ogunsina et al., (2012) experimental data and simulation data at vapor residence time 2 s and at temperature 500 ˚C

Case	Bio-oil	Char	Gas
Reported experimental data	29.98	27.19	42.83
Simulated data	25.35	22.88	34.94

of 30 wt.% by using various types of cylindrical biomass particles (pine, beech, bamboo, demolition wood) at vapor residence time range 0.25-6 s and at pyrolysis temperatures range of 450-550 ˚C. The simulated highest liquid yield for fast pyrolysis of EFB biomass at 450 ˚C and 475 ˚C were obtained to be 53.23 wt.% and 51.21 wt.% at 2 s. Bridgwater, (1999) stated that the fast pyrolysis of lignocellulose biomass takes place residence time less than 2 s. Abdullah et al., (2006) studied that the maximum liquid yield from fast pyrolysis of EFB biomass are obtained values of 55.14 wt.% at 500 ˚C and 1.03 s vapor residence time. The simulated maximum liquid yields at 500 ˚C occurred about 52.77 wt.% and at 1.03 s. The difference between reported experiment work and simulation were about 2.33 wt.% at 1.03 s. According to the comparison between reported experiment and simulation data, the optimum product yield for fast pyrolysis of EFB biomass occurred at vapor residence time around 1 s and at 500 ˚C. The liquid yield in simulation was decreased from 55.32 wt.% to 44.7 wt.% as the increase vapor residence time from 0.5 s to 1 s at 525 ˚C. For the pyrolysis of raw sorghum bagasse at 525 ˚C, Scott et al., (1999) observed that an increase in vapor residence time from 0.2 to 0.9 s resulted in a decrease in the bio-oil yields from 75 wt.% to 57 wt.%. So, the suitable vapor residence time for fast pyrolysis of EFB biomass occurs less than 1 s at 525 ˚C. At 550 ˚C, the liquid yield was sharply decreased from 47.99 wt.% to 22.83 wt.% when an increase of vapor residence time from 0.5 s to 2 s (Figure 5A). The longer residence time of vapor caused a decrease of liquid product yield resulting in an increase of gas product yield. The optimum simulated vapor residence time of 0.5 s gave the maximum liquid yield at 550 ˚C. Finally, Mabrouki et al., (2015) found that the highest bio-oil yields for EFB pyrolysis was obtained at 550 ˚C for a residence time equal to 0.5 s. Therefore, the simulated optimum vapor residence time of 2 s, 1 s and less than 1 s were obtained to be the highest liquid yield at the temperature of 450-475 ˚C, 500 ˚C and 525-550 ˚C, respectively.

3.5. Influence of reaction temperature on product yield of EFB pyrolysis

The reaction temperature significantly influences on the product yield of EFB fast pyrolysis. An increase of liquid yield in the simulation occurred from 50.72 wt.% to 53.23 wt.% at 450 ˚C with an increase of vapor residence time from 1 s to 2 s. At the simulated reaction temperature of 450 ˚C, the highest liquid products were found over the residence time range of 1 s to 2 s. Sulaiman et al., (2011) studied the maximum liquid yield of 52.5 wt.% from fast pyrolysis of empty fruit bunch at 450 ˚C and over 1.02-1.05 s. For 500 ˚C, the simulated product yield of liquid and char were decreased from 53.14 wt.% to 42.08 wt.% and from 26.71 wt.% to 22.88 wt.%, respectively and gas yield was increased from 20.05 wt.% to 34.94 wt.% at vapor residence time in the range of 1-2 s. In the reported experiments, the highest liquid yield range of 35-55.1 wt.% was obtained at an optimum temperature of 500 ˚C (Abdullah et al., 2006; Scott et al., 1999). At the higher temperature of 550 ˚C, the gas yield in the simulation was increased from 29.07 wt.% to 46.13 wt.% when the vapor residence time was increased from 0.5 s to 1 s. Sulaiman et al., (2011) obtained the gas yield of 27.6 wt.% at the residence time of vapor over the range 1.02-1.05 s. In addition, Sukiran et al., (2009) studied a similar trend of gas yield from EFB pyrolysis was increased to a maximum value in the range of 31-46 wt.% over the temperature range of 300-700 ˚C. The higher temperature causes the increase of gas product yield at longer vapor residence time because of secondary reactions formations as a resulted in decrease of liquid and char products. Therefore, the optimum reaction temperature in the range of 450-550 ˚C was found to be the maximum the liquid yield of the EFB biomass fast pyrolysis in both reported experiment and simulation results at vapor residence time range over 0.5-2 s. Figure 5B shows the comparison between simulated liquid yields and Sulaiman et al., (2011) experimental work of EFB fast pyrolysis at reaction temperature range of 450-550 ˚C.

3.6. Influence of vapor residence time and reaction temperature on product quality of EFB pyrolysis

The vapor residence time mainly affected on the product yield than the quality of the EFB fast pyrolysis. Salehi et al., (2011) concluded that the effect of vapor residence time on quality and elemental compositions of the bio-oil was negligible. On the other hand, reaction temperature obvious influence on the characteristics of the pyrolysis products. The influence of reaction temperature on the quality of the pyrolysis products determined by the water content, elemental compositions (carbon, hydrogen, nitrogen and oxygen), high heating value (HHV) and phenols and its derivatives compositions. The small amount of water content found at below 500 ˚C but it decreased the yield of organics of the oil. Besides, the large amount of water content occurred due to the secondary cracking of bio-oil at above 500 ˚C. Abdullah et al., (2008) studied the optimum water content of 11.01 wt.% from EFB fast pyrolysis at 500 ˚C. The higher carbon content and lower oxygen content favored to obtain high-quality of pyrolysis products. The highest carbon contents of 69.35 wt.% with oxygen contents of 20.02 wt.% from EFB fast pyrolysis obtained at 500 ˚C (Abdullah et al., 2010). The high heating value (HHV) play an important role in the quality of pyrolysis bio-oil. Salehi et al., (2011) observed the maximum heating value for the sawdust fast pyrolysis at the reaction temperature around of 500 ˚C. They found that high heating value was decreased at the reaction temperature below 500 ˚C and above 525 ˚C. The maximum heating value of 30.06 MJ/kg for EFB pyrolysis bio-oil obtained at 500 ˚C (Abdullah et al., 2010; Abdullah et al., 2008). The high content of phenol and its derivatives need to obtain high quality of bio-oil. Garcia-Perez et al., (2008) studied the maximum yield of phenol group from fast pyrolysis of woody biomass at the reaction temperature range of 450-500 ˚C. According to the higher rates of secondary thermochemical reactions, lower phenol content in bio-oil found at the reaction temperature above 500 ˚C (Garcia-Perez et al., 2008). The highest concentration of phenol (18.1 wt.%) and its derivatives (15.27 wt.%) in bio-oil from EFB

pyrolysis gave at 500 ˚C (Sukiran et al., 2009). Therefore, reaction temperature strongly affected on the quality of pyrolysis products.

4. Conclusion

A prediction of product yields for fast pyrolysis of EFB biomass was studied by using global kinetic scheme. The simulated product yields of liquid, gas and char were validated with the reported experiment data at vapor residence time range from 0.79 s to 1.32 s and at 500 ˚C. The high quality of bio-oil from fast pyrolysis EFB biomass obtained at the reaction temperature of 500 ˚C. The predicted highest liquid yield at reaction temperature of 450 ˚C, 500 ˚C and 550 ˚C were occurred at a vapor residence time of 2 s, 1 s and 0.5 s, respectively. A relationship between reaction temperature and vapor residence time influence of product yields on EFB fast pyrolysis from model predictions can be applied to the experimental work for fast pyrolysis of biomass in a fluidized bed reactor.

Acknowledgments

The authors acknowledge the financial support from the Higher Education Research Promotion and the Thailand's Education Hub for Southern Region of ASEAN Countries Project Office of the Higher Education Commission.

References

Abdullah, N. and Bridgwater, A.V. (2006) Pyrolysis liquid derived from oil palm empty fruit bunches. Journal of Physical Science 17,117–129.

Abdullah, N. and Gerhauser, H. (2008) Bio-oil derived from empty fruit bunches. Fuel 87, 2606- 2613.

Abdullah, N. Gerhauser, H. and Bridgwater, A.V. (2010) Fast pyrolysis of empty fruit bunches. Fuel 89, 2166-2169.

Asadieraghi, M. and Daud, W.M.A.W. (2015) In-depth investigation on thermochemical characteristics of palm oil biomasses as potential biofuel sources. Journal of Analytical and Applied Pyrolysis 115, 379–391.

Blasi, D.C. (1996) Kinetic and heat transfer control in the slow and flash pyrolysis of solids. Industrial and Engineering Chemistry Research 35, 37–46.

Bridgwater, A.V. (1999) Principles and practice of biomass fast pyrolysis processes for liquids. Journal of Analytical and Applied Pyrolysis 51, 3–22.

Bo, L., Papadikis, K., Gu, S., Beatriz, F., Philip, L., Zhongyuan, L. and Athanasios, K. (2017) CFD modelling of particle shrinkage in a fluidized bed for biomass fast pyrolysis with quadrature method of moment. Fuel Processing Technology 164, 51–68.

Chan, W.R, Kelbon, M. and Krieger, B.B. (1985) Modelling and experimental verification of physical and chemical processes during pyrolysis of large biomass particle. Fuel 64, 1505–1513.

Diebold, J.P. (1994) A unified, global model for the pyrolysis of cellulose. Biomass Bioenergy 7, 75-85.

Dong, N.H., Luo, K.H. and Wang, Q. (2017) Modeling of biomass pyrolysis in a bubbling fluidized bed reactor: Impact of intra-particle heat conduction. Fuel Processing Technology 161, 199–203.

Garcia-Perez, M., Wang, S., Shen, J., Rhodes, M., Lee, W. J. and Li, C. (2008) Effects of temperature on the formation of lignin-derived oligomers during the fast pyrolysis of mallee woody biomass. Energy Fuels 22, 2022–2032.

Haiping, Y., Rong, Y., Terence, C., David, T.L., Hanping, C. and Chuguang, Z. (2004) Thermogravimetric analysis-fourier transform infrared analysis of palm oil waste pyrolysis. Energy and Fuels 18, 1814-1821.

Haiping, Y., Rong, Y., Hanping, C., Dong, H. and Chuguang, Z. (2007) Characteristics of hemicellulose, cellulose and lignin pyrolysis. Fuel 86, 1781–1788.

Johnny, M., Benjamin, B., Peter, E.G., Gogolek, Dillon, M., Jules, T. and Poupak, M. (2017) Comparison of multi-component kinetic relations on bubbling fluidized-bed woody biomass fast pyrolysis reactor model performance.

Fuel 210, 625–638.

Kim, S.W., Bon, S.K., Jae, W.R., Joon, S.L., Cheol, J.K., Dong, H.L., Gyung, R.K. and Sun, C. (2013) Bio-oil from the pyrolysis of palm and Jatropha wastes in a fluidized bed. Fuel Processing Technology 108, 18–124.

Mabrouki, J., Mohamed, A.A., Kamel, G., Ahmed, O. and Mejdi, J. (2015) Simulation of biofuel production via fast pyrolysis of palm oil residues. Fuel 159, 819-827.

Miller, R.S. and Bellan, J.A. (1996) A generalized biomass pyrolysis model based on superimposed cellulose, hemicellulose and lignin kinetics. Combustion Science and Technology 126, 97-137.

Ogunsina, B.S., Ojolo, S.J., Ohunakin, O.S., Oyedeji, O.A., Matanmi, K.A. and Bamgboye, I.A. (2012) Potentials for generating alternative fuels from empty palm fruit bunches by pyrolysis. Proc ICCEM, 185–190.

Papadikis, K., Gu, S., Bridgwater, A.V. and Gerhauser, H. (2009a) Application of CFD to model fast pyrolysis of biomass. Fuel Processing Technology 90, 504–512.

Papadikis, K., Gu, S. and Bridgwater, A.V. (2009b) CFD modelling of the fast pyrolysis of biomass in fluidised bed reactors. Part B Heat, momentum and mass transport in bubbling fluidised beds. Chemical Engineering Science 64, 1036–1045.

Papadikis, K., Gu, S., Bridgwater, A.V. and Gerhauser, H. (2010a) Computational modelling of the impact of particle size to the heat transfer coefficient between biomass particles and a fluidised bed. Fuel Processing Technology 91, 68–79.

Papadikis, K., Gu, S. and Bridgwater, A.V. (2010b) Computational modelling of the impact of particle size to the heat transfer coefficient between biomass particles and a fluidised bed. Fuel Processing Technology 91, 68–79.

Prabir, B. (2010) Biomass gasification and pyrolysis: Practical Design and Theory. Oxford, Elsevier Inc.

Prasentsan, S. and Prasentsan, P. (1996) Biomass residues from palm oil mills in Thailand: An overview on quantity and potential usage. Biomass and Bioenergy 5, 387–395.

Qingang, X. and Song, C.K. (2014a) Modeling effects of interphase transport coefficients on biomass pyrolysis in fluidized beds. Powder Technology 262, 96–105.

Qingang, X., Soroush, A., Alberto, P. and Song, C.K. (2014b) BIOTC: An open-source CFD code for simulating biomass fast pyrolysis. Computer Physics Communications 185, 1739–1746.

Qitai, E., Xinjun, Z., Panneerselvam, R. and Sai, G. (2017) Numerical simulations on the effect of potassium on the biomass fast pyrolysis in fluidized bed reactor. Fuel 197, 290–297.

Ranzi, E., Cuoci, A., Faravelli, T., Frassoldati, A., Migliavacca, G., Pierucci, S. and Sommariva, S. (2008) Chemical kinetics of biomass pyrolysis. Energy Fuels 22, 4292–4300.

Rong, Y., Haiping, Y., Terence, C., David, T.L., Hanping, C. and Chuguang, Z. (2005) Influence of temperature on the distribution of gaseous products from pyrolyzing palm oil wastes. Combustion and Flame 142, 24–32.

Salehi, E., Abedi, J. and Harding, T. (2011) Bio-oil from Sawdust: Effect of operating parameters on the yield and quality of pyrolysis products. Energy and Fuel 25, 4145-4154.

Sanchez, S.L., Lopez, G.D., Villaseñor, J., Sánchez, P., Valverde, J.L. (2012) Thermogravimetric mass spectrometric analysis of lignocellulosic and marine biomass pyrolysis. Bioresource Technology 109, 163–172.

Scott, D.S., Majerski, P., Piskorz, J. and Radlein, D. (1999) A second look at fast pyrolysis of biomass -the RTI process. Journal of Analytical and Applied Pyrolysis 51, 23–37.

Sembiring, K.C., Rinaldi, N. and Simanungkalit, S.P. (2015) Bio-oil from

fast pyrolysis of empty fruit bunch at various temperature. Energy Procedia 65, 162–169.

Shafizadeh, F. and Bradbury, A.G. (1979) Thermal degradation of cellulose in air and nitrogen at low temperature. Journal of Applied Polymer Science 23, 1432–1442.

Silalertruksa, T., Shabbir, H.G., Patcharaporn, P., Piyanon, K., Napapat, P., Naruetep, L. and Rattanawan, M. (2017) Environmental sustainability of oil palm cultivation in different regions of Thailand: Greenhouse gases and water use impact. Journal of Cleaner Production 167, 1009–1019.

Sukiran, M.A., Chow, M.C. and Nor, K.A.B. (2009) Bio-oils from Pyrolysis of Oil Palm Empty Fruit Bunches. American Journal of Applied Sciences 6, 869-875.

Sukiran, M.A., Soh, K.L. and Nasrin, A.B. (2016) Production of bio-oil from fast pyrolysis of oil palm biomass using fluidised bed reactor. Journal of Energy Technologies and Policy 6, 9.

Sulaiman, F. and Abdullah, N. (2011) Optimum conditions for maximising pyrolysis liquids of oil palm empty fruit bunches. Energy 36, 2352–2359.

Xiaoquan, W., Sascha, R.A., Kersten, Wolter, P., Wim, P.M.S. (2005) Biomass Pyrolysis in a Fluidized Bed Reactor. Part 2: Experimental Validation of Model Results. Industrial and Engineering Chemistry Research 44, 8786–8795.

Xue, Q., Heindel, T.J. and Fox, R.O. (2011) A CFD model for biomass fast pyrolysis in fluidized-bed reactors. Chemical Engineering Science 66, 2440–2452.

Xue, Q., Dalluge, D., Heindel, T.J., Fox, R.O. and Brown, R.C. (2012) Experimental validation and CFD modeling study of biomass fast pyrolysis in fluidized-bed reactors. Fuel 97, 757–769.

VITAE

Name Mr. Kyaw Thu

Student ID 5910130039

Educational Attainment

Degree	Name of Institution	Year of Graduation
Master of Engineering (Chemical)	Mandalay Technological University	2016

Scholarship Awards during Enrolment

Thailand Education Hub (TEH-AC) Scholarship, Prince of Songkla University, Hatyai, Thailand.